UNIVERSITÀ DEGLI STUDI DI CATANIA

Department of Industrial Engineering

Doctorate of Philosophy

Scienza e Tecnologia dei Materiali

XXVIII Ciclo
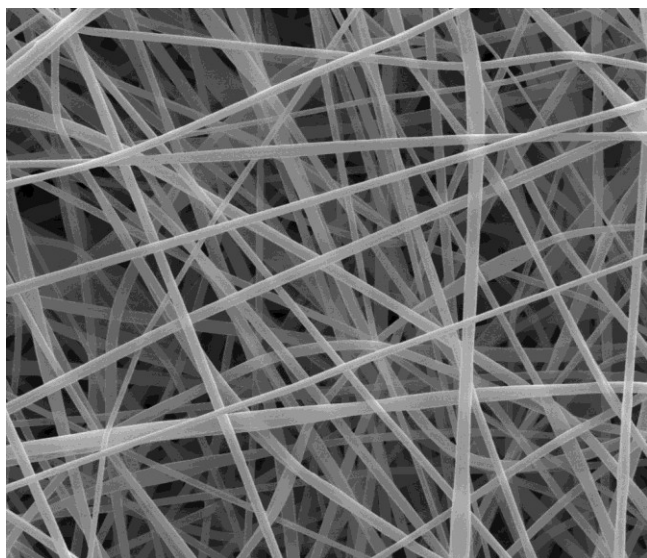
Salvatore Mannino

ELECTROSPUN NANOFIBRES
FOR MULTIFUNCTIONAL
COMPOSITES

PhD Supervisor: Prof. Gianluca Cicala

PhD Coordinator: Prof. Maria Grazia Grimaldi

2015

Dedication

The present work is dedicated to my two little nieces Giorgia and Giulia

who, day by day, have been filling my life with so much joy

and

to Claudia for fully supporting me through my choices.

Acknowledgements

Table of Contents

1.Polymer composites

The term *composite materials* refers to a class of materials having three main constituents: matrix, reinforcement, and interface. The matrix in composite materials transfers load to the reinforcement and protects it from environmental degradation. Composites can be classified according to their matrix type. When metal or ceramic matrix materials are used, composites are referred to as *metal matrix composites* (MMCs) or *ceramic matrix composites* (CMCs), respectively. When polymeric matrix materials is used, composites are referred to as *polymeric matrix composites* (PMCs). Composite classification is also made according to the reinforcement used. Three reinforcement types are usually considered: long continuous fibers, short fibers and particles (figure 1:1).
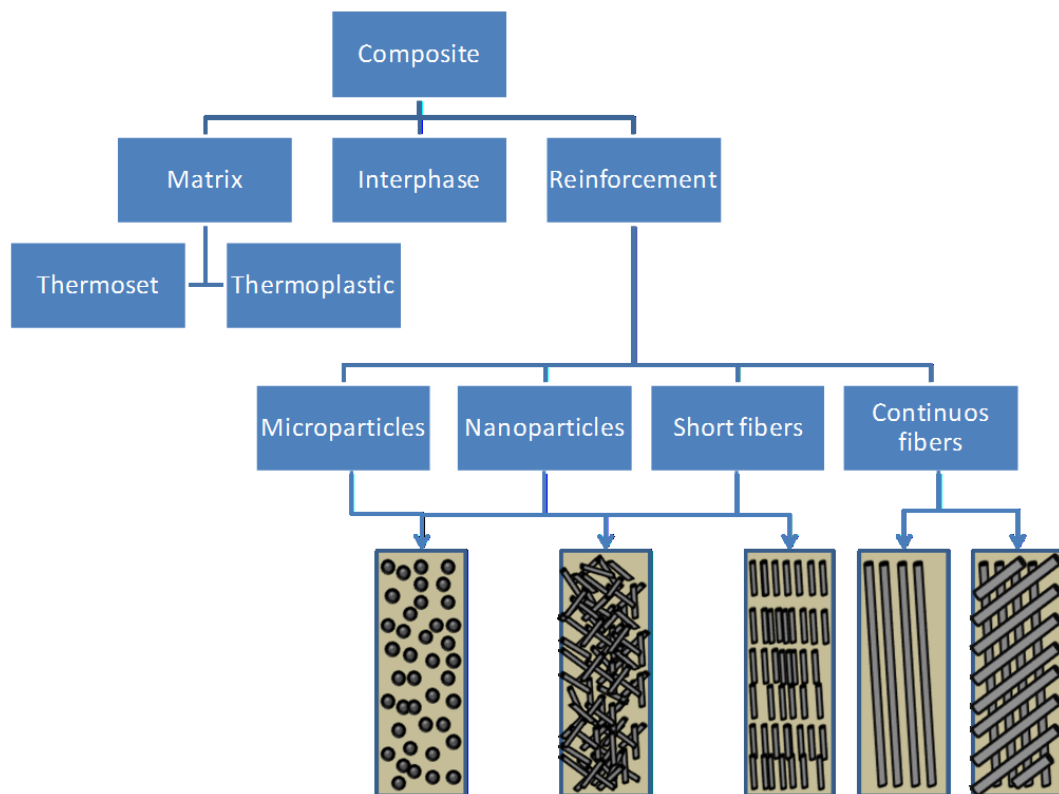
Figure 1:1 Composites classified according to reinforcement types

Polymeric matrix composites are the focus of this chapter. PMCs present several advantages compared to traditional materials as shown in figure 1:2 through figure 1:5.
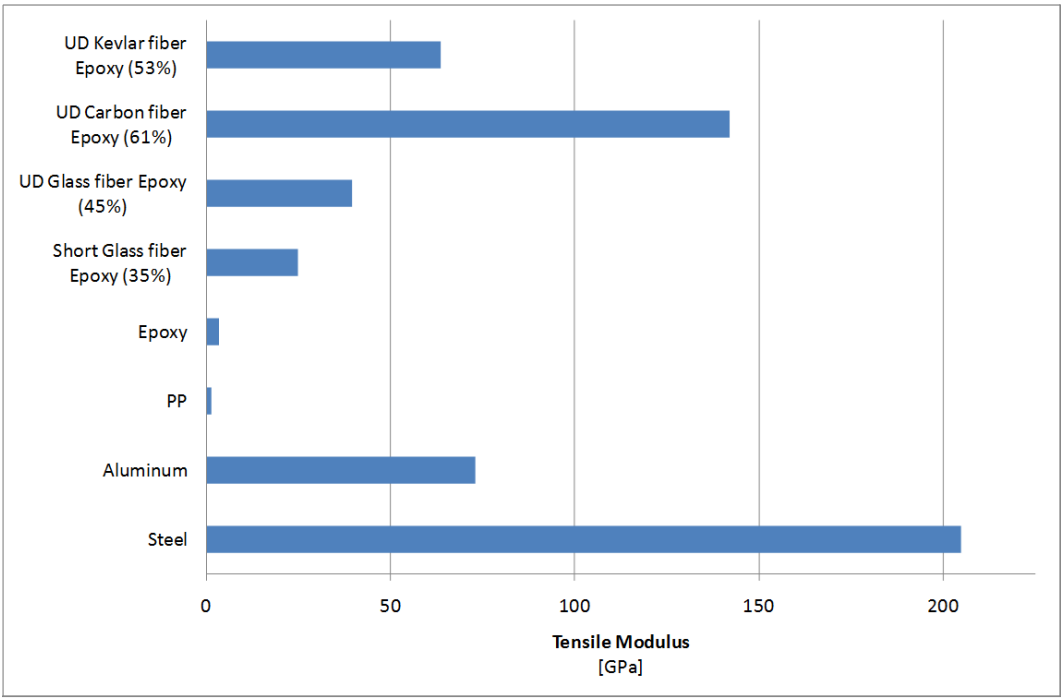
Figure 1:2 Modulus of elasticity
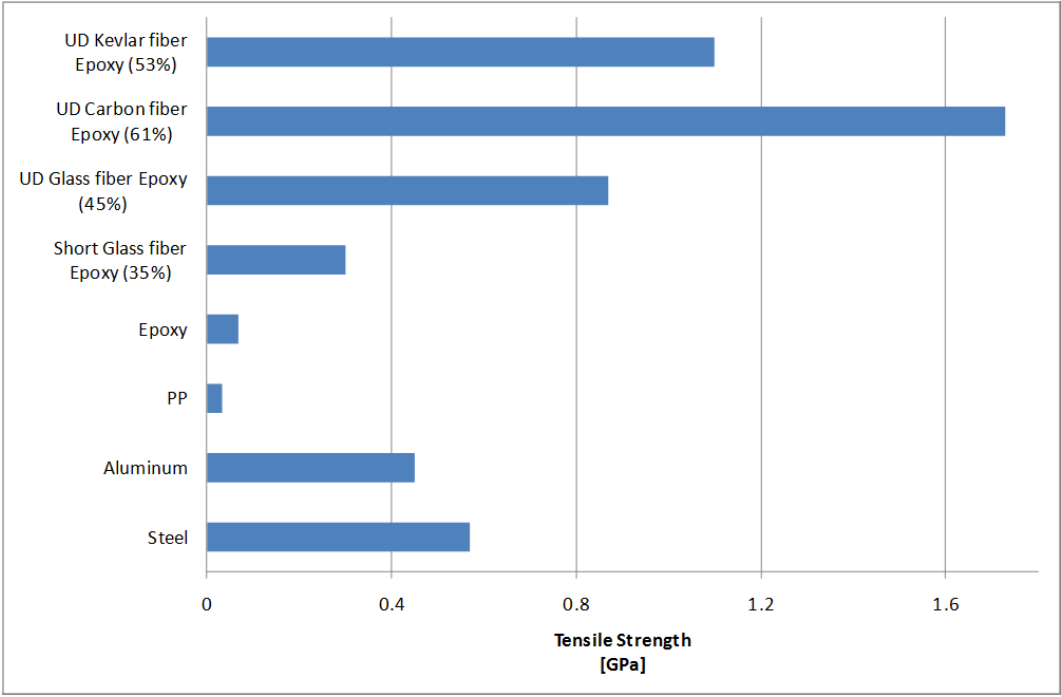
Figure 1:3 Tensile strength
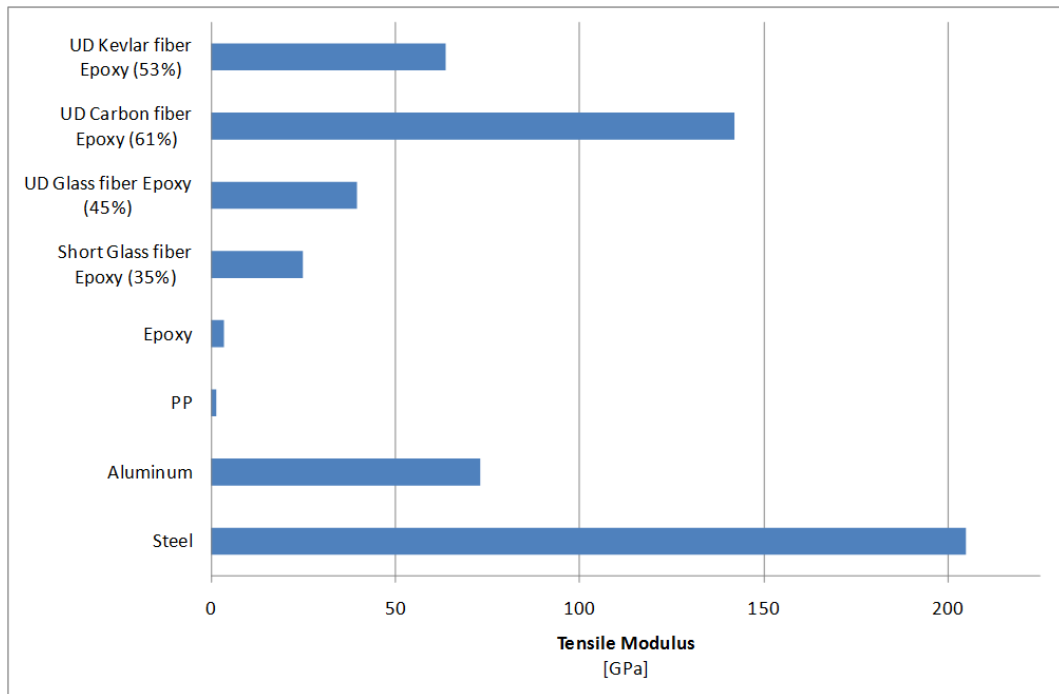
Figure 1:4 Density
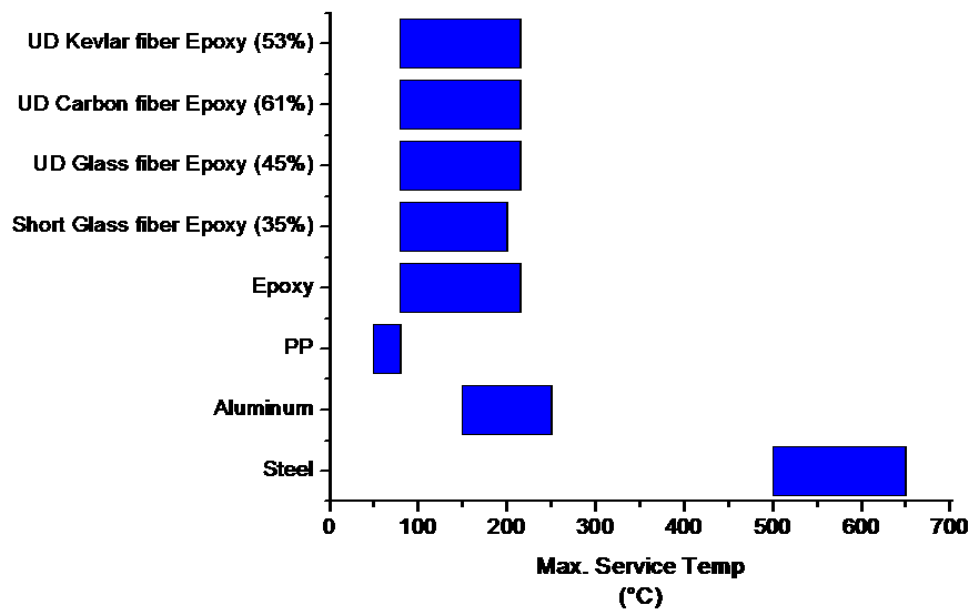
Figure 1:5 Maximum service temperature

Figure 1:6 reports the specific mechanical properties for different materials. This comparison highlights that composite materials outperform traditional materials when weight saving is the driving design factor.
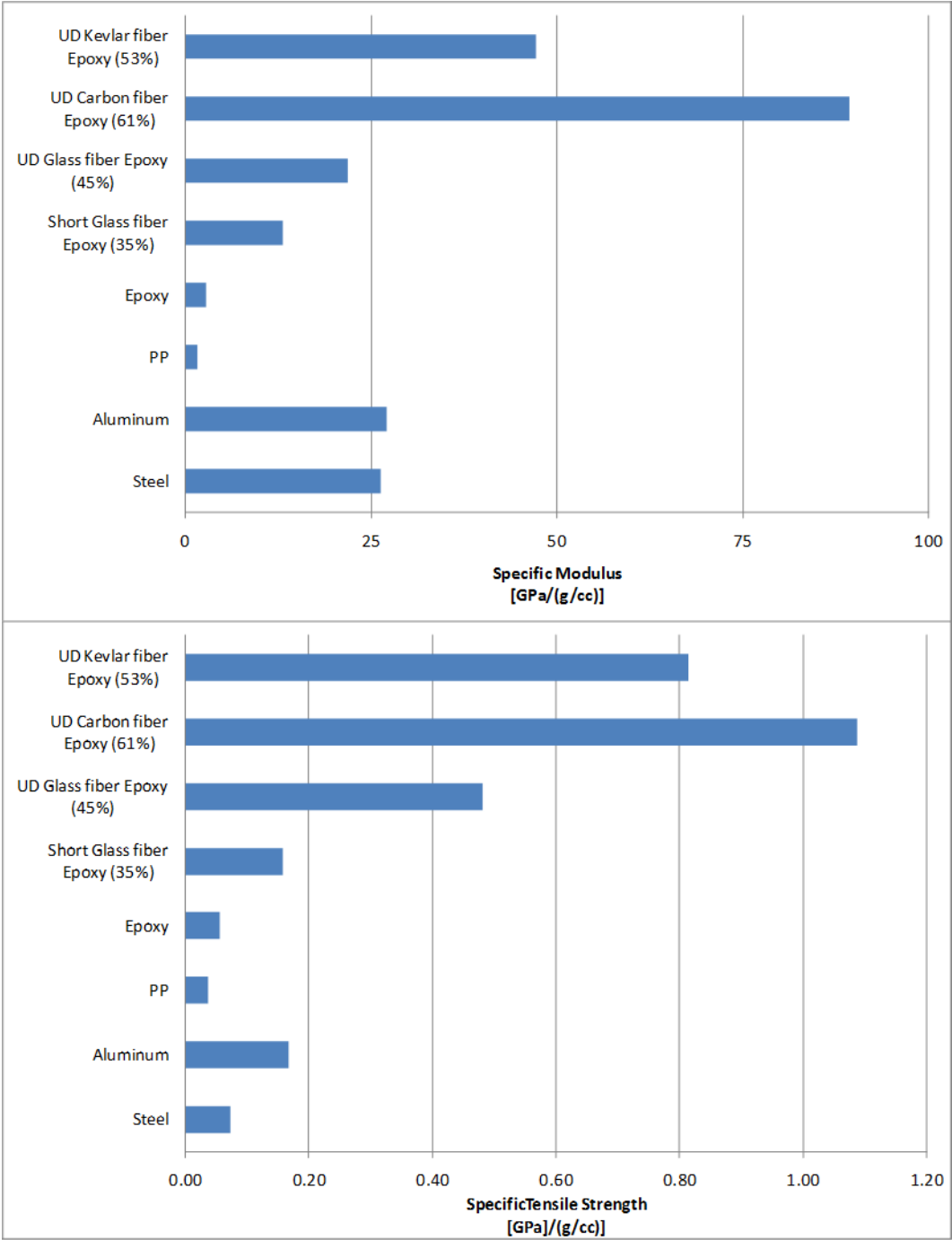
Figure 1:6 Specific mechanical properties

Two types of polymeric matrixes are commonly used: thermoplastics and thermosets. Thermoplastics can be melted by heating and solidified by cooling, which render them capable of repeated reshaping and reforming. Thermoplastics can be either amorphous or semicrystalline. Thermoset materials, once polymerized, cannot be melted or formed again. The polymerization process is commonly called *curing*. While curing, resin molecules form three-dimensional networks in which they are connected by covalent bonds (cross-links). Owing to these cross-links, thermosets present good thermal stability and chemical resistance but cannot be reshaped after curing. Thermoplastic and thermoset composites are commercialized in different forms and are processed using a range of techniques. The choice of the manufacturing technique is driven by many factors including production volume, capital equipment cost, component shape and size, reinforcement form and tooling cost. Table 1:1 compares different manufacturing techniques.

Table 1:1 Comparison of typical manufacturing techniques for polymeric composites

	Hand Lay Up	**Filament Winding**	**Pultrusion**	**Spray Up**	**Compression Moulding**	**Roll Wrapping**
Polymeric Matrix	Thermoset	Thermoset, Thermoplastic	Thermoset, Thermoplastic	Thermoset	Thermoset, Thermoplastic	Thermoset, Thermoplastic
Production Speed	Low	Slow to fast	Fast	Medium to fast	Fast	Medium to fast
Production Volumes	Low to medium	Low tomedium	High	Medium to high	Medium to high	Medium to High
Component Shape	Simple to Complex	Cylindrical and axisymmetric	Constant Cross Section	Simple to complex	Simple to complex	
Fiber Volume Fraction	Low	Medium to High	Medium tohigh	Low	Medium to high	Medium to high
Tool Cost	Low	Low	Low	Low	High	Medium
Capital Investement Cost	Low	Low	Low	Low	High	Medium

1.1 Thermoplastics

Thermoplastic resins are increasingly used as matrices for composites despite the fact that thermosets can be advantageous in terms of processability. Thermoplastics present some advantages over thermosets including:

- High delamination resistance and damage tolerance

- Low moisture absorption and excellent chemical resistance if semicrystalline thermoplastics are used

- Low toxicity and infinite storage life due to absence of reactive chemicals

- Recyclability by re-melting of used matrices

- Faster processing because no curing reaction is needed

The lack of tack of thermoplastics at room temperature is a key disadvantage over thermosets as it requires more sophisticated manufacturing processes for material deposition.

Over the last decade, interest in thermoplastic composites have increased as OEMs and part fabricators seek new ways to more efficiently produce structural components that have good damage tolerance and environmental performance.

Many thermoplastic types can be used as matrices. A common graph showing classification of thermoplastics consumption versus price and performance is shown in figure 1:7. Polyether-ether-ketones (PEEK), polyether-imides (PEI), polyphenyl-sulfides (PPS) and polysulfones belong to a special class of thermoplastics that can be used as matrices for niche applications. Commercial prepreg tapes such as carbon fibre/polyether-ether-ketone (CF/PEEK) and later carbon fibre/polyphenyl-sulfide (CF/PPS) were introduced in the early 1980s in the aerospace sector [1].
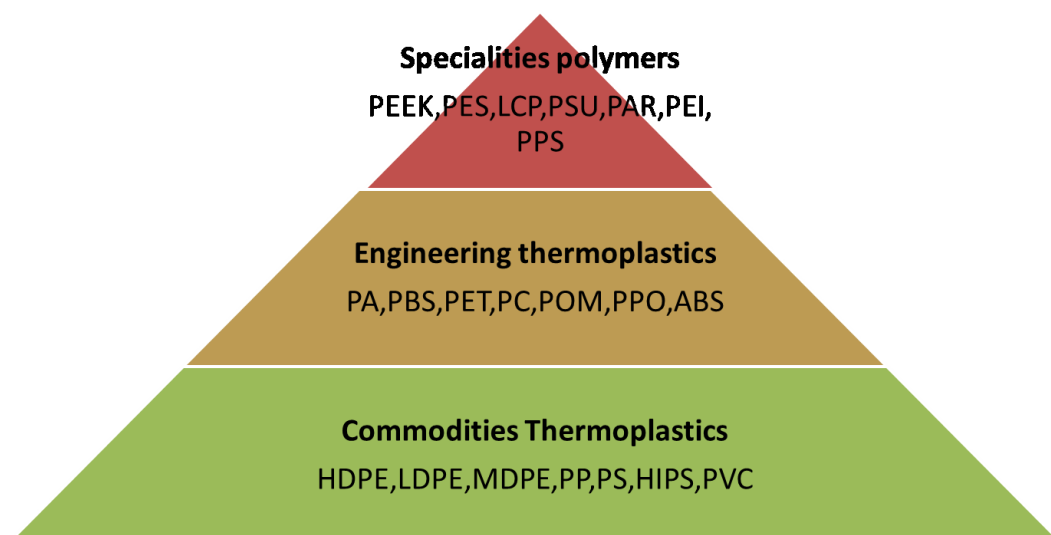
Figure 1:7 Price/performance profile for commercial thermoplastics

Traditionally, thermoplastics have not been suitable for processing at low pressures and in resin infusion processes such as RTM, VARTM or VAP. However, in the last decade novel thermoplastics with macro-ring structures, or cyclics, have been developed. These cyclic polymers can be processed at low pressures because their peculiar structure eliminates or reduces entanglements thus leading to very low viscosities. A typical structure for a cyclic-polybutylene-terephthalate (PBT) is shown in figure 1:8 where it is clearly shown that stannoxane molecules close the ring.
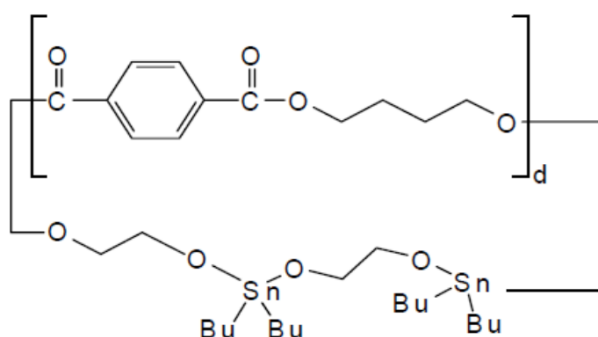
Figure 1:8 Cyclics-PBT structure

1.2   Thermosets

Thermosets are polymeric materials that form cross-linked networks after curing. These networks render the materials infusible and resistant to chemical agents. Thermosets have good heat retention and maintain their performance over time. They are less susceptible to ageing than thermoplastics. Thermosets present low viscosities in the unreacted state and thus they can be processed manually or at lower pressures compared to thermoplastics. The major limitation of thermosets is their inherent brittleness. Other shortcomings are their limited shelf life due to reactivity, the difficulty of reclaiming scrap material and, for some thermosets, the production of by-products during cross-linking reactions. Typical thermosets used as matrices for composites are reported in table 1:2.

Table 1:2 Thermoset composites: properties and applications

	Properties	Use Temp. [°C]	Cost	Application	Manufacturing Technique	Examples of Commercial Producers
Polyester	Simplest, room temperature curing, low mechanical properties, good chemical resistance (especially to acids)	60-150	Low	Piping, small boats, automotive, off-shore, civil industry	Hand lay-up, RTM, VARTM, filament winding, pultrusion, spray-up, compression molding	Dow, Ashland, Reichhold, Scott Bader, Cray Valley, DSM, Matrasur, Mapei
Vinyl ester	Better mechanical properties than polyesters, room to medium cure temperature, good chemical resistance (especially to acids)	60-150	Low	Piping, naval, automotive, off-shore, civil industry	Hand lay-up, RTM, VARTM, filament winding, pultrusion, spray-up, compression molding	Dow, Ashland, Reichhold, Scott Bader, Cray Valley.
Phenolic	Needs pressure over curing to avoid bubbling, medium mechanical properties, excellent fire resistance, excellent ablative properties	70-170	Low	Interiors, ablatives, laminates	Compression molding, RTM, filament winding	Dow, J D Lincoln, Gurit, Seal.
Epoxy	Excellent mechanical properties, needs toughening for primary structures, dimensional stability, room to high cure temperature, good chemical resistance (especially to alkalis), very good adhesion to metals	80-215	Medium to high	Piping, profile, automotive, naval, aerospace	Hand lay-up, pultrusion, filament winding, RTM, VARTM, autoclave, compression molding, out-of-autoclave	Gurit, Dow, Huntsman, Reichhold, Hexion, Cray Valley, Cytec, Hexcel, ACG, Toray, Seal, Sika, Mapei
Benzoxazine	Excellent mechanical properties, medium to high cure temperature, excellent fire resistance	80-250	Medium to high	Interiors, aerospace components	autoclave, RTM	Henkel, Huntsman

Epoxies are available in liquid, solid and semi-solid forms. Liquid epoxies are used in RTM, filament winding, pultrusion, wet hand lay-up and other processes with various reinforcing fibres including glass, carbon, aramid and boron. Semi-solid epoxies are used in prepregs for vacuum bagging and autoclave processes. Epoxies are more costly than polyesters and vinyl esters and are therefore not used in cost-sensitive markets (e.g., automotive and marine) unless specific performance is needed. Increasing concerns about costs have encouraged the research of curing methodologies alternative to thermal curing both for epoxy and polyester resins. Microwave, electron beam and ultraviolet light (UV) curing being the most exploited.

1.3   Polymer blends

In most cases of industrial interest, polymer matrices present some deficiencies that limit their use. For example thermosets have good thermal stability, high environmental resistance and high modulus, but they are usually brittle. The poor toughness is largely due to their cross-linked structure and is an intrinsic limit for thermosets. To overcome this limitation many approaches are proposed in the literature (figure 1:9).
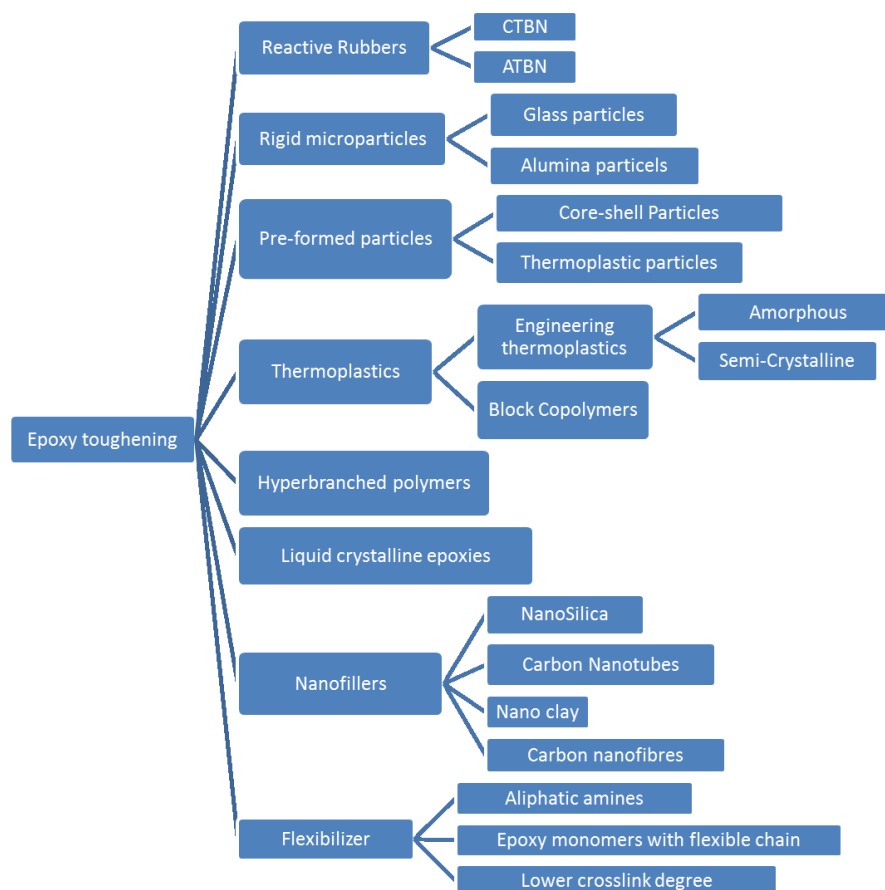
Figure 1:9 Toughening strategies for thermoset resins

The dominant approach has been to add a second phase which precipitates during cure and produces a multiphase morphology able to induce a variety of toughening mechanisms. Many different modifiers have been used: elastomers, polyurethanes, and ductile engineering thermoplastics among others. The use of elastomers typically causes a decrease in mechanical properties, particularly compression strength (due to the reduced resin modulus) and Tg.

Blending thermosets with thermoplastics is one of the most successful approaches because it does not have a significant effect on the balance of properties. Toughness enhancement is typically achieved by phase separation and is driven by many factors including the size and type of morphology, the polymer molecular weight, the backbone structure and end groups

and the ductility of the epoxy matrix. A co-continuous morphology is typically desired for the optimum balance of toughness and solvent sensitivity. A toughening technology used to obtain the highest damage tolerance is interlaminar or interleaf toughening. This exploits the concept of increasing the size of the interlaminar region in order to increase the size of the process zone and therefore the fracture toughness and compression after impact (CAI) of the composite. Methods to achieve interlaminar toughening include the additions of particles, films, fibres and veils.

Blending may improve resin or product performance by:

- producing materials having a full set of the desired properties at lowest cost,

- improving product performance, and

- improving processability.

1.4   Filled matrices

Filled matrices are matrices in which a sufficient quantity of a small size of a rigid material (filler) is well dispersed in order to improve certain key properties such as modulus, strength and viscosity or to reduce cost, shrinkage, etc. Conventional loading with traditional fillers typically ranges from 10 to 50wt%. The term filler is used for materials with characteristic dimensions in the range of 100-104 nm. This contrasts with nanofillers which range between 1 and 100nm. Fillers can be classified accordingly to their shape (figure 1:10), origin and size (figure 1:11).
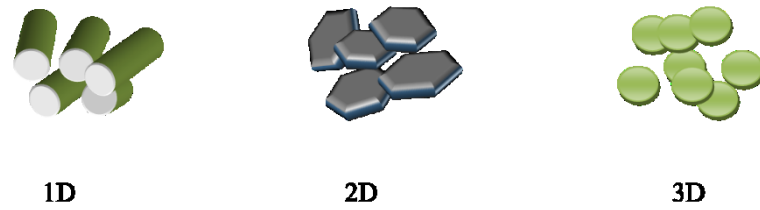
Figure 1:10 Filler classification according to shape
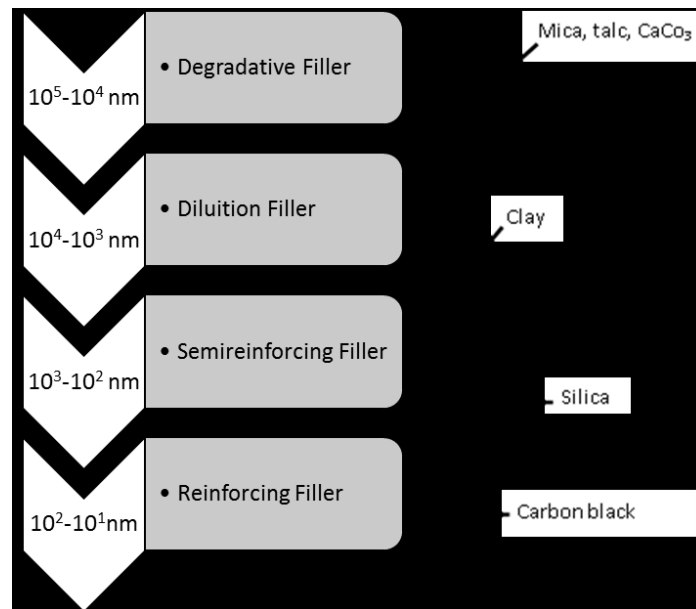
Figure 1:11 Filler classification according to their size

As reported in Fig. 24 some fillers exhibit reinforcing capabilities and others do not [2]. The reinforcing activity of a filler depends on four factors:

14
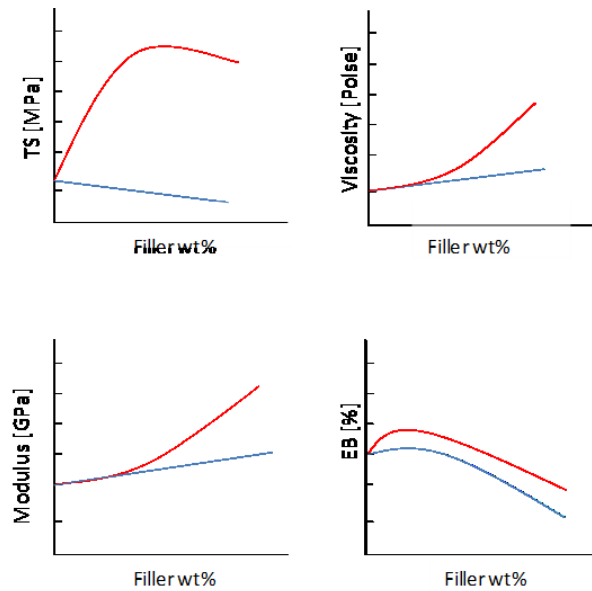
Figure 1:12 Effect of filler's activity on properties of filled matrices

The specific area of the filler is calculated with the BET method. The BET method is widely used for the calculation of surface areas of solids by physical adsorption of gas molecules. Nitrogen is widely used for powdery fillers. An important factor that controls filled matrix mechanical properties is the interfacial adhesion between the filler and the matrix. The adsorption of polymer molecules on the filler surface results in the development of a layer which has properties different from those of the matrix polymer. The character, thickness and properties of this interlayer or interphase are relevant factors to control filled polymer properties.

The term nanofilled matrices refers to polymeric matrices compounded with fillers with characteristic dimensions in the nanometer range. Polymer nanocomposite is the most common name used to refer to such matrices. The fillers used for nanocomposites are usually referred to as nanofillers. Several types of nanofillers can be found that present one or more dimension in the nanometer range (figure)

1D	**2D**	**3D**
Carbon Nanotubes (CNT)	NanoClay	Nanosilica
Carbon Nanofibers (CNF)	Graphene	Fullerene
Cellulose Whiskers		Nano Silver
		POSS.
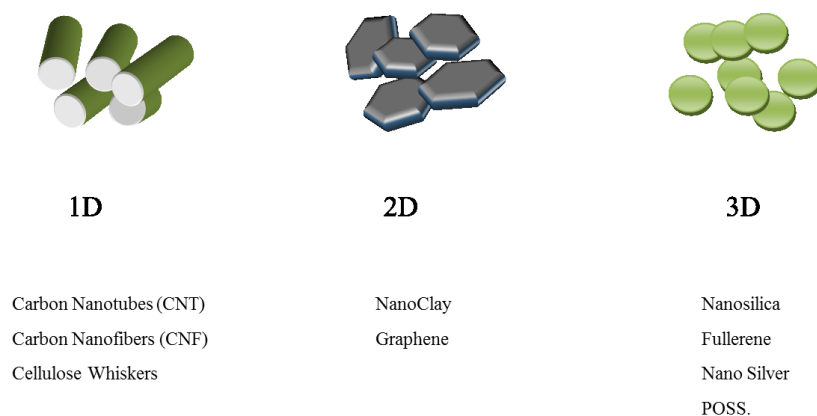
Figure 1:13 Common nanofillers of interest for nanofilled matrices

Traditional filled matrices contain reinforcements with length in micrometers, and the interface of fillers is close to the bulk polymer matrix. In the case of nanocomposites, where the length of the reinforcement is on the nanometer scale, they have ultra-large interfacial area per volume, and the distances between the polymer and filler components are extremely short. Polymer coils are 40 nm in diameter, and the nanofillers are on the same order of magnitude; as a result, molecular interaction between the polymer and the nanofillers are thought to give nanofilled matrices unusual material properties that conventional matrices do not possess [3]. These unpredicted effects are also referred to as "nano-effects". More recent results have, however, indicated that while the property profile is interesting, the nanoclay-based nanocomposites often obey continuum mechanics predictions and, in most cases, reinforcement effects obey composite theories where no "nano-effect" is considered [4]. Nanocomposites offer several advantages over the simple reinforcement effect that makes them of interest for composite materials. One big advantage is the possibility to realize matrices with sensing and actuation capabilities that can be used for the development of multifunctional composites [5]. Other non-structural functions achieved by nanocomposites include thermal and electrical conductivity, flame resistance and abrasion resistance. Thermal

and electrical conductivity are two of the most interesting functions that can be improved by the addition of nanofillers.

When developing nanofilled matrices key factors to achieve optimal reinforcing efficiency are: high dispersion degree to ensure the absence of nanofiller agglomerates in the micrometer range; good adhesion between matrix and nanofiller to ensure adequate stress transfer; and, in some cases (e.g., nanotubes and nanofibers), nanofiller orientation for optimal performance. The most complex and challenging task is to achieve fine and uniform dispersion because of the great interactions between nanofillers and the high matrix viscosity increase due to nanofiller addition.

1.5   Chapter 1 References

[1] L. A. Berglund in S.T. Peters, ed., Handbook of composites, Chapman & Hall, London, 1998, pp.115-130

[2] J.L. Leblanc, Filled Polymers: Science and Industrial Applications, CRC Press, Boca Raton, 2010.

[3] J.H. Koo Polymer Nanocomposites, McGraw Hill, 2006, DOI: 10.1036/0071458212

[4] D.R. Paul, L.M. Robeson, Polymer 49 (2008) 3187–3204

[5] C.Li, E.T. Thostenson, Tsu-Wei Chou, Composites Science and Technology 68 (2008) 1227–1249

2. Applications and drawbacks of epoxy/thermoplastic blends*

Epoxy resins are the most used chemicals among thermoset materials [1]. This is due to their versatility which comes from their low viscosity as monomers and, at the same time, the good mechanical and thermal properties once curing reaction is completed. The main drawback of epoxies is the brittleness in the cured state. Other limitations are the shrinkage upon curing, the poor recyclability and, for some formulations, the low thermal resistance.

Most applications requires for improvements of the brittleness. In order to satisfy this requirement, epoxy resins can be toughened by adding a dispersed second phase material, which can be either a rubber or a thermoplastic. This dispersed material "slows down" the crack propagation leading to much higher energy to fracture values. The main areas of interest for toughened epoxy resins are matrix for composites, adhesive bonding and coatings and corrosion protection. The addition of thermoplastic leads to improvements in toughness that were exploited in several commercial systems. Blending thermoplastics with epoxy can also serve as a mean to develop smart functions like self-healing and shape memory effects.
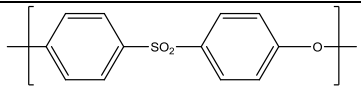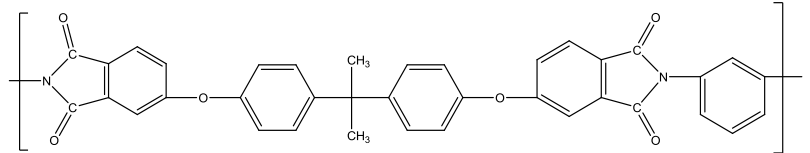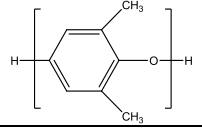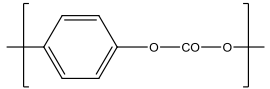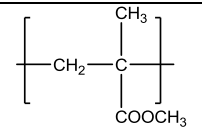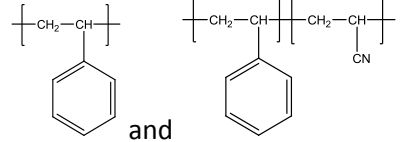
In the present chapter the fundamentals of thermoplastic/epoxy blends will be recalled first and the main applications will be treated thereafter.

2.1 Fundamentals of thermoplastic/epoxy blends

A lot of research has been carried out for the development of polymeric systems to increase the fracture toughness of epoxides without decreasing their thermal and mechanical properties. Back in 1983 Bucknall and Partridge proposed the use of polyaromatics like polyether sulfones (PES) as modifiers for

epoxy resins as a solution to overcome the limitation of rubber toughening. The choice of this class of polymers is due to their high modulus and glass transition temperature, which are comparable to those of the epoxide resins. Tables 2:1 and 2:2 summarize some common amorphous and semi-crystalline thermoplastic polymers used for thermoset/thermoplastic blends.

Table 2:1 Examples of amorphous thermoplastic polymers

Acronym	Name	Formula	Tg (°C)	Some commercial Refernces
PES	Polyether sulfone		220	Solvey Virantage VW-10200, Mn_{GPC}: 46,500 Virntage VW-10300, Mn_{GPC}: 55,000 Virntage VW-10700, Mn_{GPC}: 21,000 Virntage VW-30500, Mn_{GPC}: 14,000
PEI	Polyether imide		210	Sabic Ultem 1000, Mn=26,000 1040, Mn=9,900
PPE	Poly(2,6 dimethyl-1,4-phenilene ether)		210	Sabic 820, Mn=12,000
PC	Polycarbonate		140	Saic Lexan
PMMA	Polymethylmetacrylate		110	Numerous
PS and SAN	Polystyrene and Poly(styrene-co-acrylonitrile)		11	Numerous
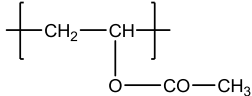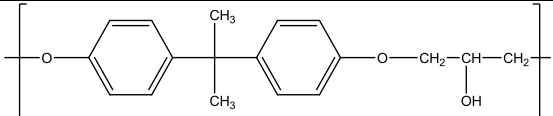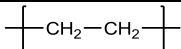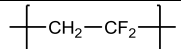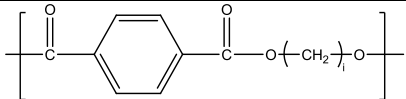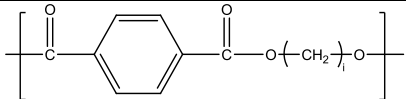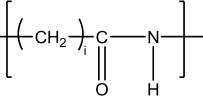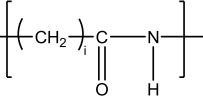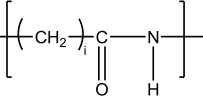
Acronym	Name	Formula		Value	Supplier
PVAc	Polyvinylacetate	[CH₂—CH with O—CO—CH₃] structure		40	Union Carbide LP40A, Mn=40,000
Phenoxy	Poly(hydroxyl ether of bisphenol A)	bisphenol A ether structure		90	Union Carbide Mn=20,000

Table 2:2 Example of semicrystalline thermoplastic polymers

Acronym	Name	Formula		Tg (°C)	Tm (°C)
PE	Polyethylene	$[CH_2—CH_2]$			110-140
PVDF	Polyvinyliedene fluoride	$[CH_2—CF_2]$		-50	170
PET	Polyethylene terephtalate	terephtalate ester structure	i=2	60	270
PBT	Polybutylene terephtalate		i=4	60	220
PA6	Polyamide	$[(CH_2)_i—C—N]$ amide structure	i=5	40	216
PA11			i=10	43	185
PA12			i=11	42	177

When thermoplastic is added to epoxy, homogenous or not homogenous unreacted blends can be obtained. Upon curing three different scenarios can happen that result in different phase morphology. All the scenarios have been exploited in commercial systems as described in figure 2:1.
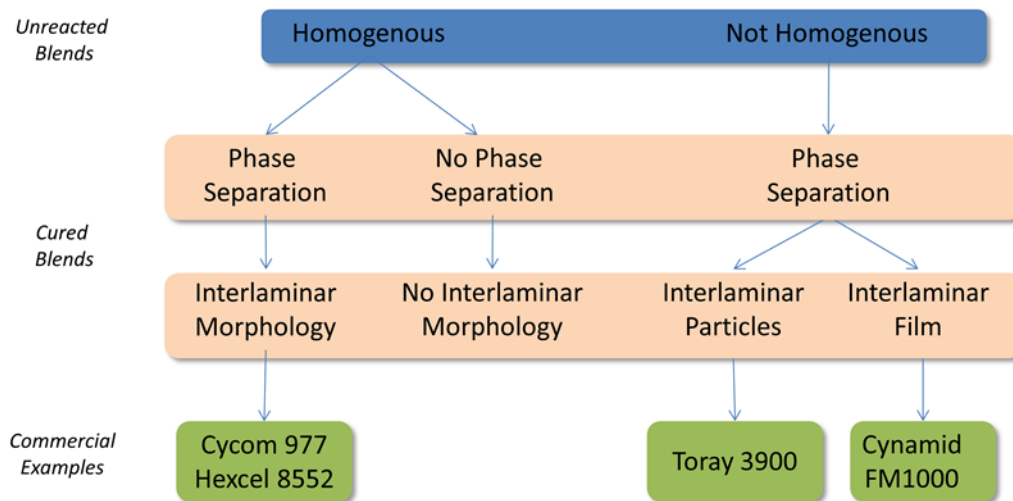
Figure 2:1 Toughening technologies of epoxy/thermoplastic blends

In the first case, if the thermoplastic is soluble in the resin, a homogeneous mixture is obtained. When curing starts, the mixture can either remain homogenous or phase-separate. This is the case for some commercial toughened epoxy prepreg systems like CYCOM® 977-series and HexPly® 8552. When phase-separation happens, it can lead to several types of morphologies, i.e. particulate, co-continuous and inverted. In the particulate morphology a thermoplastic-rich phase is dispersed in the epoxy-rich matrix; on the contrary, in the phase-inverted morphology an epoxy-rich phase is dispersed in the thermoplastic-rich phase. In the co-continuous morphology the two phases are segregated and interpenetrated altogether [2]. As described in figure 2:2 the initial thermoplastic concentration controls, among other parameters, the resulting morphology. Under particular circumstances, other special morphologies can be obtained (figure 2:3). bimodal Particulate morphology is one of the cases, in which the thermoplastic-rich particle present two average diameter values. Another case is he Secondary phase inversion, which

is the result of demixing of the epoxy phase inside the thermoplastic-rich domains occurring in post-curing conditions.
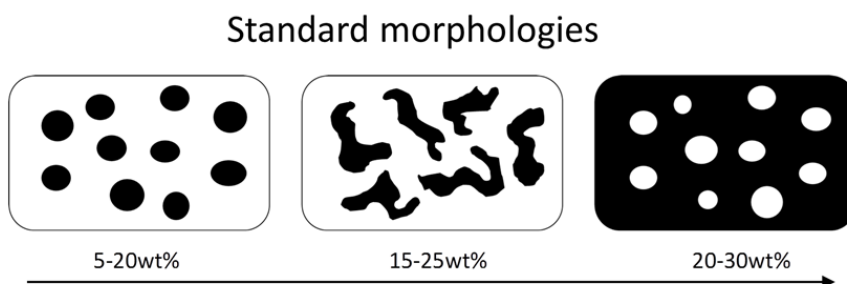
Figure 2:2 Effect of the thermoplastic concentration on the interlaminar morphologies of thermoset/thermoplastic blends
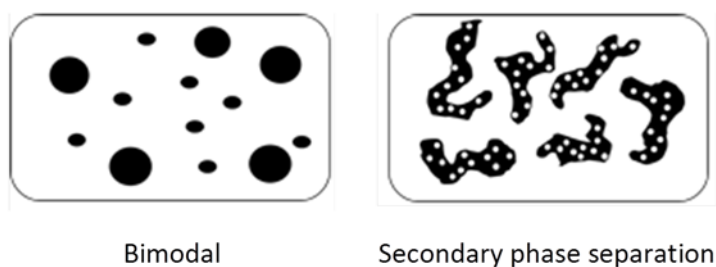
Figure 2:3 Special interlaminar morphologies for epoxy/thermoplastic blends

When the initial mixture is homogeneous but no phase separation occurs during the cure of the resin, the final composite is a homogeneous transparent material. This can be due to the low concentration of the thermoplastic or due to the chemical affinity between the thermoplastic and the epoxy-hardener. Polycarbonate-epoxy and Polycaprolactone (PCL)/epoxy are an example of blend which do not phase separate upon curing.

If the thermoplastic polymer is not soluble in the epoxy resin, the initial mixture is not homogeneous and the thermoplastic particles remains dispersed in the epoxy before and after the cure. An example of these are polyamides (PA), polybutylene terephtalate (PBT) and

polyvinylidene fluoride (PVDF) (Yee 2000). Commercially speaking, this is the principle used by Toray Industries for toughening their Toray 3900 epoxy system.

In general, to achieve toughening effects the thermoplastic phase should act as an obstacle for crack propagation resulting in crack deviation or crack bridging. However, to a certain extent, homogenous blends can also be toughened by the presence of the thermoplastic chains within the epoxy network. The limitation of this approach can be that less energy is dissipated and that the thermal properties of the blend depends linearly on the relative amounts of the two components. This can be a limitation when the wrong thermoplastic is chosen. Thermoplastic-epoxy blends were developed to obtain materials with improved properties, like thermo-mechanical and solvent resistance. The thermoplastics reported in Table 2:1 have high glass transition temperatures, high modulus and good solvent resistance. The choice to use this type of thermoplastic was largely due to their superior properties compared to traditional reactive rubbers. The latter are performing much better in terms of toughening improvements but they also results in reduction of glass transition, modulus and solvent resistance for the epoxy blends. Other properties are influenced by the blending of thermoplastic with epoxy.

For example, thermoplastic polymers can be used as low-profile additives to improve the dimensional stability of thermoset resins. Often, they are used in polyester blends to have a better surface quality and to compensate the resin shrinkage. One of the most common polymer for this specific use is the polyvinyl acetate (PVAc). The mechanism works with a continuous thermoplastic rich phase that promotes cavitation in response to tensile stresses coming from internal deformation in the presence of mechanical constraints [3]. In epoxy prepregs, thermoplastics are used both as tougheners and as modifiers in order to keep a high elastic modulus of the composite during the cure of the thermoset at low temperatures, lower than the Tg of the thermoplastic polymer. This property of thermoplastic is particularly useful

to counteract the warpage in composite manufacturing due to resin shrinkage. Exact values of the amount of thermoplastic added is not released by companies as it is covered by trade secret. In most cases, it ranges from 15 to 30% by weight with respect to the resin matrix, depending on the specific application of the material.

Another application of epoxy-thermoplastic blends is the case of epoxy-phenolic coatings for magnetic disks. Porosity (macro or micro) is needed in the coating to enhance the retention of a lubricant used to increase the durability of the head-disk interface [4]. A well-known thermoplastic polymer used for this purpose is polyvinylmethyl ether (PVME) which, once is blended with the thermoset resins, phase-separates. Then, PVME is degraded by annealing at 220°C in oxidative atmosphere (air). The emission of volatile products leads to the formation of macro- or micro-porosity as shown in figure 2:4.

Phase separated system   **PVME phase partially degradated**

Porous system after PVME degradation
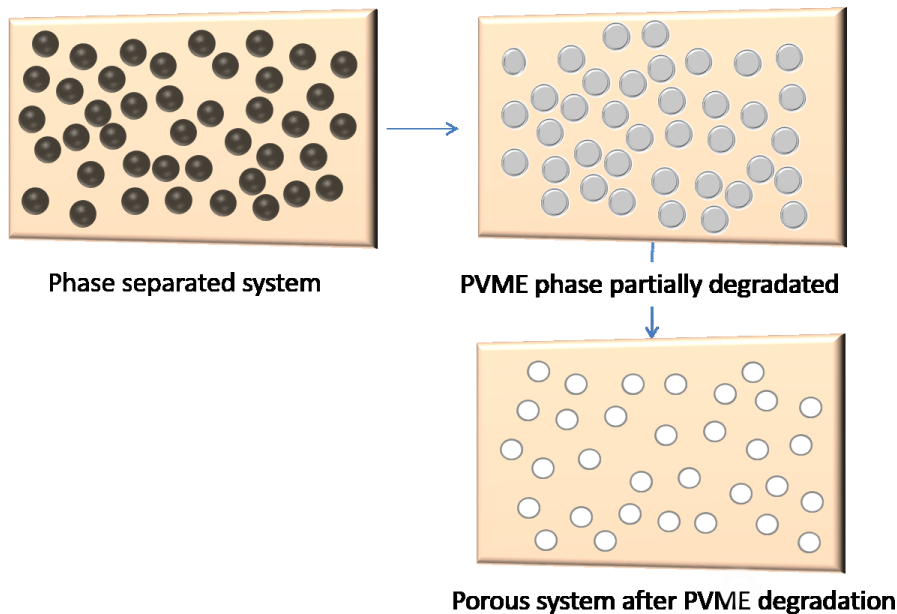
Figure 2:4 Steps to obtain a porous system from a PVME/Epoxy blend

Finally, in some cases, the epoxy is not the matrix of interest but thermoplastic/epoxy blending is used to enhance thermoplastic processing. Thermoplastic polymers can be

unprocessable. A common example is poly(2,6-dimenthyl-1,4-phenylene ether) (PPE), an amorphous thermoplastic with a glass transition temperature of 220°C. It softens at around 300-350°C, but at this temperatures it starts degrading as well. In order to overcome this issue, PPE is processed by blending with a small amount of an epoxy resin acting as a reactive solvent. Upon curing of the epoxy, when phase separation occurs, PPE matrix is obtained reinforced by a dispersed thermoset-rich phase [5].

In the following paragraphs the main applications down to earth are presented and some insight on future application under development or recent exploitation are also given. For commercial applications in relevant fields, like as matrices for composites, an extensive database of properties from producer is offered.

2.2   Matrices for composites

The business of epoxy/thermoplastic bends is well consolidated in the field of composite matrices for aerospace applications. Aircraft manufacturers are increasingly using composites because these materials offer great performances at a lower weight compared with metals, resulting in increased fuel efficiency, reduced maintenance and longer service life. Two examples of aircrafts with massive use of composites for primary structures are the Boeing 787 (figure 2:5) and the Airbus A380. The use of composites for primary structures requires tough systems therefore, thermoset/thermoplastic blends are the choice. The leading prepreg manufacturing companies (i.e. Cytec Engineered Materials, Hexcel and Toray Industries) are selling different systems based on thermoset/thermoplastic blends which are qualified for primary structures.

One of the largest supplier, in terms of volume, for the Boeing 787 is Toray Industries. The material used is Torayca 3900-series which is a highly toughened carbon fiber-reinforced

epoxy prepreg for the primary structures. The advantages of the use of composites are not limited to weight/economy benefits but extends to improved cabin pressure, bigger windows, less corrosion and extended maintenance schedules. The 787 incorporates also key components made with out-of-autoclave molding processes. Cytec Engineered Materials, now part of Solvay, offers a whole range of prepreg systems for out of clave curing ranging from the Cycom 5320 to the MTM series.

Figure 2:5 Boeing 787 "Dreamliner"

Hexcel has several new materials on the 787 as well. One is the HexMC. This product was selected for the 787's larger window frames, which are considered a primary structure. For other window frames Hexcel proposed the use of the aerospace-qualified 177°C-cure 8552 epoxy prepreg resin. This system is also used for the engine nacelles made by GE and Rolls Royce. The 8552 epoxy resin is an example of toughened epoxy blend containing aromatic engineering thermoplastic.

The use of toughened thermoset/thermoplastic blends is not limited to aircraft structures. Several applications exist in the field of racing and exotic cars. The crashworthiness is the main benefit offered by these blends in these applications [6]. The use of high toughness prepregs results in better specific energy absorption as required by FIA (Federation Internationale de l'Automobile) rules. The study by Lo Faro et al was focused on the effect of

28

prepreg parameters like resin matrix and carbon fiber type on the crush behavior of composite tubes used as crush absorber in F1 cars. The data (table 2:3) shows a clear correlation between SEA and resin toughness values. Similar requirements are needed for structures like the nose cone (figure 2:6) and the rear crash structure (figure 2:7).

The use of impact resistant resin is transferred into exotic cars as demonstrated by several application like Ferrari LaFerrari, Lamborghini Aventador etc. For the Ferrari "LaFerrari", Dr. Lo Faro, VP of Cytec, revealed the use of four different types of carbon fibre, all labour-intensively hand-laminated, before being cured in the autoclave [7].

Table 2:3 Impact resistance and failure modes of some CYCOM systems used in racing cars

Resin System	Resin Toughness (kJ/m^2)	SEA (J/g)	Predominant Micro Failure Mode	Predominant Macro Failure Mode
977-6	064	63	Fibre Breakage	Splaying/Fragmentation
977-2	0.62	61	Fibre Breakage	Splaying/Fragmentation
949	0.51	54	Mixed	Splaying
759	0.39	49	Delamination	Splaying
950-1	0.36	48	Delamination	Splaying
5250-4	0.24	44	Delamination	Splaying
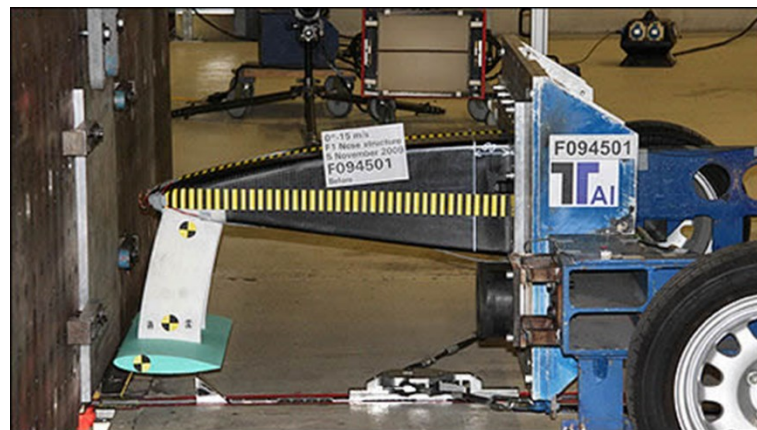
Figure 2:6 Impact test for a nose cone made by composite materials (from http://www.formula1-dictionary.net/crash_test.html)
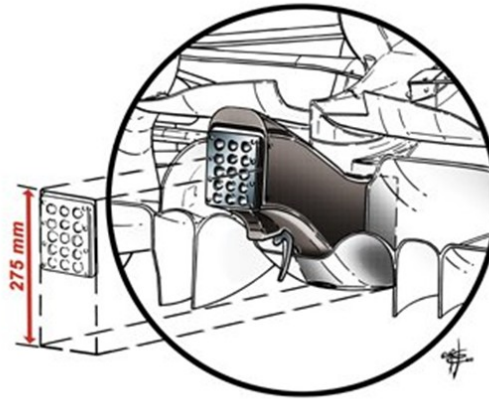
Figure 2:7 Rear crash structure made in composites for F1 cars (from http://leonardasf1.narod.ru/F1_Challenge/2011/2011_DEVELOPMENTS.html)

Cytec Engineered Materials, now part of Solvay, is one of the leading suppliers of composite materials for the aerospace applications. Its product portfolio (Table 2:4) includes prepregs and resin systems, adhesives and surfacing, carbon fibers, ancillary materials, tooling portfolio, process materials.

The CYCOM® 977 series, for example, include a number of epoxy prepregs toughened with aromatic thermoplastic. The formulation and structure of this thermoplastic is proprietary but the principle is based on the homogenous uncured blend turning into a phase separated cured blend. The toughening mechanism works with a co-continous morphology and shows excellent impact resistance. CYCOM® 977 prepregs are certified both for civil and military aircraft and used for several primary and secondary structures. CYCOM® 977-2 is a 177°C toughened epoxy resin (Table 2:5). Commercially speaking, it is the most important 977 system, being used for primary structures of commercial and military aircrafts and helicopters.

Table 2:4 Overview of commercial polymer matrixes for automotive and aircraft structures

°C	Features and Applications	Processing conditions	Toughness	Service temperature dry [°C]	Out-Life at 25°C
CYCOM 2020	Modified epoxy-based prepreg system which displays excellent retention of mechanical performance at elevated temperatures	10 h at 80°C + optional 1 h at 150°C post cure	High	-	8 wk
CYCOM 759	Modified epoxy prepreg. Provides superb surface finish with good hot/wet performance	14h at 70°C	Medium	91	4 wk
CYCOM 761	Modified epoxy prepreg. Designed for use as thermal barriers (non load bearing) in motor sport applications	14h at 79°C or 45 min at 121°C	Low	212	2 wk
CYCOM 919	Modified epoxy prepreg. 919 is widely recognized as the industry standard in race car construction. High toughness with mechanical performance and flame retardant. Self-adhesive with 4 wk tack life, suitable for sandwich panel construction. Also available in high flow version	1.5 h at 121°C	Medium	143	4 wk
CYCOM 950-1	Modified epoxy prepreg. A 121°C curing system with the performance of a 177°C curing epoxy. A toughened system exhibiting excellent mechanical properties	2 h at 127°C	Medium	177	4 wk
CYCOM 985	Modified epoxy prepreg. Suitable for the manufacture of carbon composite block for use in machining of solid carbon inserts	2 h at 127°C	Low	193	10 d
CYCOM 977-2	Modified epoxy prepreg. Excellent hot/wet properties. Controlled flow, good surface characteristics	3h at 177°C	High	200	10 d
CYCOM 977-6	Modified epoxy prepreg. Excellent hot/wet properties. Also used for primary aircraft structures	2 h at 154°C	High	180	10 d
CYCOM 5215	Modified epoxy prepreg. Curable at 66°C with only vacuum bag pressure. The cured part will yield <1% void content. Mechanical property and service temperature range equivalent to first generation epoxy prepreg after post-cure at 177°C. Prototyping, repair, tooling and structural application here controlled cost processing is desired.	14 h at 66°C + 2 h at 177°C post cure	Low	191	10 d

Table 2:5 Typical Neat Resin Properties of the CYCOM 977-2 at Room Temperature

Tensile Strength, ksi (MPa)	11.8 ± 1.6 (81.4 ± 11)
Tensile Modulus, msi (GPa)	0.51 ± 0.02 (3.52 ± 0.14)
Flexural Strength, ksi (MPa)	28.6 ± 1.0 (197 ± 7)
Flexural Modulus, msi (GPa)	0.50 ± 0.01 (3.45 ± 0.07)
G_{1C}, in-lb/in2 (J/m2)	2.73 ± 0.48 (478 ± 84)
K_{1C}, ksi·in1/2 (MPa·m 1/2)	1.34 ± 0.15 (1.22 ± 0.14)
T_g, °C (RDS, 10°C/minute)	212
Density, g/cc	1.31

Most commercial prepregs are formulated to be cured in autoclaves. The autoclave manufacturing has led in the past to very efficient composite and it is a well consolidated process. However, it has some main drawbacks. The first limitation is the high investment costs required for acquisition of the plant. Then the operation costs and the complexity of tooling have pushed the interest toward out-of-autoclave (OoA) manufacturing. OoA has been developed and suitable prepregs have been introduced leading to parts with autoclave-quality properties, by using vacuum bag-only (VBO) consolidation. In the VBO prepreg, the fabric is just partially impregnated in order to leave vacuum channels that let air escape during the consolidation in the vacuum bag. In this way, the amount of vacuums is reduced to very low values. Unlike the autoclave process, where the external applied pressure ($\approx$ 7 atms) prevents the formation of volatile gasses leaving them dissolved in the resin, the VBO process works with only 1 atm. This means that all the volatile gasses must be taken out before the resin starts curing. The laminate composites produced from VBO prepregs have shown fiber volume content of about 65% for UD tapes and of about 55% for fabrics [8]. This is the main way to reduced operation costs since only conventional ovens and heating toolings are needed.

Among the resins for OoA Cytec's CYCOM® 5320-1 OoA prepreg is a toughened epoxy prepreg system. It can be processed by vacuum-bag-only but its performances are equivalent

to primary-structure-capable autoclaved prepregs (Table 2:6). The systems is characterized by a very low porosity. With a wet glass transition temperature of 163°C, an average water uptake of 0,55 wt% and because of its low temperature curing capability, it is also suitable for prototyping where low cost tooling or vacuum-bag-only curing is desired.

Table 2:6 Resin Characteristics of the CYCOM 5320-1

Shelf Life	1 year at < 10°F (- 12°C)
Tack Life	20 days at room temperature
Shop Life	30 days minimum at room temperature
Cured Resin Density, g/cc	1.31
Wet Glass Transition Temperature, °F (°C) [1] [*]	324 (163)
Average Moisture Uptake, wt % [2]	0.55

However, one main drawback of adding a toughening agent to epoxies is the very high increases of the resin's viscosity. This makes most of the toughened commercial prepregs unsuitable for infusion techniques. To overcome such limitation, Cytec has developed the PRIFORM® technology. Manufacturing primary structure composite parts through liquid resin infusion requires the addition of the toughening agents to resin to assure performance standards are met. In Cytec's PRIFORM, the toughening agent is not blended with the resin but is woven into the textile preform. Figure 2:8 puts on evidence the scheme of the Priform fabric principle, showing the warp and the weft of the thermoplastic woven together among the carbon fibers. This solution allows resin infusion. The thermoplastic filaments are designed to be soluble in the resin at certain temperatures giving raise to homogenus dispersion in the epoxy first and, secondly, to phase separation. This unconventional approach leads to excellent structural performance coupled with infusion processability. The use of Priform in some airbus center fittings led to the international JEC awards for Cytec. The Priform technology has also some relevant side applications due to the self-binding aspect of

PRIFORM reinforcements. This means that the soluble fibers dispersed in the Priform fabrics can replace the use of binders helping to stabilize and process high quality preforms.
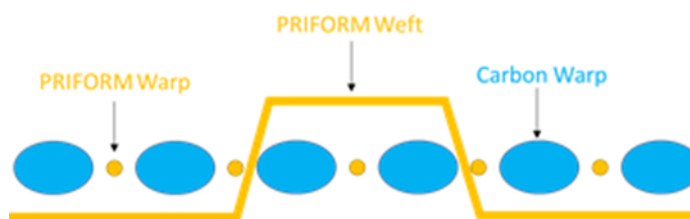
Figure 2:8 Scheme of the PRIFORM's weaving

Cytec's PRISM® resin infusion systems represent a new step in to the resin infusion capability, delivering primary structure level performance without limitation in reinforcement or processing type. PRISM™ EP2400 is a single part, 180°C curing, toughened liquid epoxy resin system offering simple and flexible processing with the damage tolerance required for composite primary and secondary structure. PRISM EP2400 offers a dry Tg of 179°C and an exceptional wet Tg of 163°C following a two-hour cure at 180°C. It shows also very good mechanical properties, like a flexural strength of 164 MPa, flexural modulus of 3,6 GPa and a fracture toughness of 279 Jm-2. More characteristics of the neat resin are reported in table 2:7.

Table 2:7 PRISM EP2400 Neat Resin Characteristics

Property	Specimen Conditioning	Value
Cured resin density, g/cm3 (lb/ft3)	Room Temperature, Dry	1.24 (77.4)
Tensile strength, MPa (ksi)	Room Temperature, Dry	95 (13.8)
Tensile modulus GPa, (msi)	Room Temperature, Dry	3.4 (0.49)
Tensile strain, %	Room Temperature, Dry	7.2
Flexural strength, MPa (ksi)	Room Temperature, Dry	164 (23.8)
Flexural modulus, GPa (msi)	Room Temperature, Dry	3.6 (0.52)
Strain energy release, GIC, J m-2	Room Temperature, Dry	279
Fracture toughness, KIC, MPa m½	Room Temperature, Dry	0.96
CTE, x10-6 C -1	Room Temperature, Dry	60.5
Tg, °C (°F)*	Room Temperature, Dry	179 (354)
Tg, °C (°F)*	Wet, 48 Hour Water Boil	163 (325)

As already said, aerospace is not the only application field for toughened epoxy. The serial automotive market needs light-weight, low-temperature, press-curable materials to meet legislative requirements for lower emissions, high safety and end-of-life recycling [9].

MTM®45-1 is a flexible curing temperature, high performance toughened epoxy matrix system optimized for low pressure, vacuum bag processing. This system offers a combination of properties (table 2:8) that make it an ideal candidate for the OoA production. A whole range of the products available for OoA is presented in table 2:9.

Table 2:8 Physical properties of MTM45-1

Test	Sample/test conditions	Results
Cured resin density	2 hours at 180°C	1.18 g/cm^3
DMA E' onset Tg, SACMA	2 hours at 180°C, dry	180°C
	2 hours at 180°C, wet*	160°C
Resin gel time	At 80°C	16.5 hours
	At 130°C	90 minutes
	At 180°C	10 minutes

*Wet - 14 days immersion in water at 70°C

Table 2:9 Current-generation aerospace grade OoA/VBO prepreg resin systems

Manufacturer	Resin family	Resin type	Description
ACG (now Cytec)	MTM44-1	Epoxy	Medium temperature molding (MTM) toughened epoxy. Qualified by Airbus for secondary and tertiary structure
	MTM45-1	Epoxy	
	MTM45-1FR MTM47-1	Epoxy	Lower temperature cure system optimized for compression performance
		Epoxy	Variant of MTM45-1 optimized for flame retardation
			Variant of MTM45-1 optimized for hot/wet notched performance up to 130°C
Cytec	Cycom 5320 Cycom 5320-1	Epoxy	Toughened epoxy designed for primary structure application
		Epoxy	Variation on 5320 system, formulated for increased out-life
Gurit	Sprint ST94	Epoxy	Single-sided moulding prepreg for parts requiring resistance to impact damage and microcracking
Hexcel	Hexply M56	Epoxy	High performance VBO epoxy system
Toray	2510	Epoxy	Formulated to meet the requirements of general aviation primary structure
Tencate	BT250E	Epoxy	Standard VBO system used in Cirrus aircraft and unmanned vehicles.
	TC250	Epoxy	Variations for fatigue and fracture resistance for helicopter rotor blades
	TC275	Epoxy	Second generation VBO system with increased toughness and higher

	TC350-1	Epoxy	service temperatures
	TC420	Cyanate ester	Third generation system with greater inspectability, resistance to hot/wet conditioning and curable at 135°C
	TC800 BMI	Bismaleimide	Third generation system with increased out-life (45+ days), high toughness, and ability to cure at 135°C with 177°C required post cure
			High temperature system (service temperatures up to 315°C)
			High-temperature, toughened BMI prepreg formulated for cure out-of-autoclave
Henkel	Loctite BZ	Benzoxazine	VBO prepreg based on a blended epoxy-benzoxazine resin formulation

The other big player for epoxy/thermoplastic for composites is the French company Hexcel. This company provides a wide range of prepregs for civil aircraft, military jets, helicopters, aero-engines or space satellite and launchers. Its range of resin formulations for aerospace prepregs includes a wide range of epoxies for highly loaded parts and toughness (table 2:10).

Table 2:10 Main commercially available Hexcel's toughened systems

Hexply Resin System	Attributes	Typical Application	Commercial aircraft	Interiors	Helicopters	Military jets	Nacelles engines	Space	Uav's
M26T	Self adhesives, self extinguishing	Fairings / sandwich structures	✓		✓				
M76	High toughness, self adhesive, flexible cure	Space appliclations	✓					✓	
913	Versatile system with high environmental resistance	Structural components / fairings / helicopter blades	✓		✓				✓
M92	Self adhesive, self extinguishing versatile system with high environmental resistance	Fairings / sandwich structures / structural components	✓		✓				
M20	High temperature performance from low temperature cure	Composite repair	✓			✓			
8551-7	Extreme damage resistance, very high toughness	Structural components / engine parts / fan blades	✓				✓		
M91	Latest product for aerospace structure and aeroengine, excellent toughness with very high residual compression strength after impact	Aircraft and aeroengine primary structure	✓				✓		
M21	Preferred product for aerospace structures, high toughness and excellent translation of IM fibre	primary structure	✓				✓		
8552	Preferred product for aerospace structures	Structural parts	✓		✓	✓	✓	✓	
M56	High temperature performance from out of the autoclave cure, low density	Primary and secondary structures out of autoclave	✓				✓		✓
M18	Low moisture uptake, low density	Space applications						✓	

Grade	Features	Applications							
M18/1	Self extinguishing, very high temperature wet performance	Helicopter structural parts			✓				
922-1	High service temperature	Engine / nacelle structures	✓				✓		
HT93	Low FST	Aircraft interior panels / partitions		✓					
200	Low FST, excellent ablative properties	Fire proof panels & components		✓					
M65	High temperature, resistant BMI system	Parts subjected to very high temperatures	✓		✓	✓	✓		
F655	High temperature	Primary / secondary structures, engine components toughnened	✓				✓		
996	Low water pick up	Space and satellite applications						✓	
954-3	Low water pick up	Space and satellite applications						✓	
954-6	Low water pick up	Space and satellite applications						✓	

HexPly M91 is the very latest aerospace primary structure prepreg from Hexcel. With excellent toughness including very high residual compression after impact (see table 2:11), HexPly M91 can meet the growing needs of aerospace industry to manufacture lighter, faster and more efficient aircraft. This system is also suitable to be processed with both automated tape laying (ATL) and advanced fiber placement (AFP). These processing technologies are the choice to manufacture big composites parts like the three sectors of the 787 fuselage.

Table 2:11 Mechanical properties of Hexcel's M91

Mechanical properties	Units	Temp °C	M91/34%/UD194/IM10-12K
T_g	°C		185 - 190
Tensile strenght	MPa	23	3520
Tensile modulus	GPa	23	176
Compression strenght	MPa	23	1880
Compression modulus	GPa	23	156
ILSS	MPa	23	105
CAI @ 30.5J	MPa	23	350

Another widely commercialised system is the HexPly® 8552. HexPly® 8552 is a high performance tough epoxy matrix for use in primary aerospace structures. It exhibits good impact resistance and damage tolerance for a wide range of applications. It is an amine cured, toughened epoxy resin system supplied with unidirectional or woven carbon or glass fibers. The typical neat resin data are reported in table 2:12.

Table 2:12 Hexcel's 8552 neat resin properties

Colour	Yellow
Density	1.301 g/cc
Glass Transition Temperature, Tg dry	200°C
Glass Transistion Temperature, Tg wet	154°C
Tensile Strength	121 MPa
Tensile Modulus	4670 MPa

Toray Group is the Japanese company that developed one of the most used thermoplastic/epoxy blend based on preformed particles. The full commercial product,

T800H/3900-2, has heterogeneous interlayer including fine thermoplastic particles (figure 2:9), and it is used in the primary structures of Boeing 777.
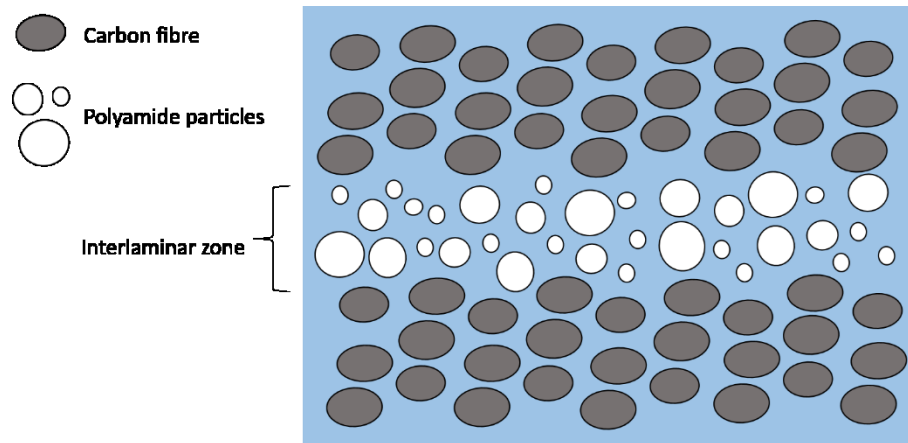

Figure 2:9 Interlaminar toughening particles at interlayer region for T800H3900-2 laminates (schematic drawing)

2.3   Adhesive Bonding

One drawback about composites is their cost of manufacturing and assembly. This is basically a problem for high volume production. In particular, the joining cost of composite components is one of the major cost drivers. One way to reduce cost of production is to apply specific joining technologies. Using epoxies as adhesive bonding is the main way to assemble composites components. Mechanical fastening, adhesive bonding and fusion bonding (welding) are the other developed joining technologies.

The disadvantages of epoxies as adhesive bonding are the need for surface preparation and, sometimes, long curing time. Composite welding is carried out by melting a thermoplastic polymer using it as adhesive. Usually a pre-treatment of surfaces is needed. By doing this, it is possible to achieve a very performant joint for composites, even better than adhesively bonded or mechanically fastened joints. Unfortunately, because of cross-linked nature, it is not possible to apply welding directly onto the thermoset surface of the composite. The use of a thermoplastic-thermoset blend as adhesive is a solution to indirectly overcome this issue,

otherwise it is also possible to use a thermoplastic film incorporated onto the cured thermoset surface. The thermoplastic and thermoset polymers partially blend before totally curing the thermoset resin. This leads to a thermoset surface with a thermoplastic attached on it. Therefore, it is possible to achieve fusion bonding of thermoset composites by means of various methods. The simultaneous application of heating and pressure, for example, causes the thermoplastic layers to soften, leading to a better contact between the adherent surfaces. Temperature also allows the thermoplastic chains to interdiffuse across the contact area. The welding of the surface layers is achieved with the disapperence of the interface due to the chains' interdiffusion, thus obtaining a strong joint with less sensitivity to aggressive environments than adhesive bonded joints.

Cytec is among the world-leading suppliers of top quality adhesives specifically designed for bonding composites. Its products are qualified for use on aircrafts, having a portfolio ranging from high-performance adhesives to surfacing films and primers in a variety of product forms to enable manufacturing flexibility. Cytec's aerospace adhesives and surfacing portfolio includes:

•   Aerospace Adhesives

•   Composite Surfacing

•   Core Splice Foams and Potting Compounds

•   Firewall Sealants

•   Bonding Primers

HT[®] 424 is an aluminum-filled, modified epoxy-phenolic resin coated on a glass carrier which meets the federal and Military requirements. It was developed for bonding metal-to-metal and sandwich composite structures requiring long-term exposure to 149°C and short-term exposure to 260°C. HT 424 has adaptability to many bonding procedures. FM[®] 300 is a

modified epoxy film adhesive available with three different moisture-resistant polyester carriers. It is designed for bonding metal-to-metal and sandwich composite structures. Extensively used as a surface finished ply on composites material outside layers, FM$^{®}$ 300 film adhesive has unique properties that drastically reduce time-consuming sanding and filling operations. FM$^{®}$ 300 film adhesive has high elongation and toughness with high ultimate shear strength. This makes it particularly suitable for redistributing the high shear stress concentrations of graphite epoxy- to-metal bonds, and allows it to accommodate the low interlaminar shear strength of the composite. It is particularly good in fatigue resistance in these joints.

Hexcel formulates and manufactures a comprehensive range of structural film adhesives as well. The Redux$^{®}$ film adhesives range includes epoxy, phenolic and bismaleimide adhesives, supplied in film form or roll. Once cured, the adhesives form a permanent structural bond which is able to withstand harsh environments, including elevated temperatures. The range includes adhesives for metal-to-metal and composite bonding which find wide application in transportation, recreation and construction industries.

Redux$^{®}$ 319 is a high performance modified epoxy film adhesive curing at 175°C. It is available in both supported and unsupported versions at areal weights between 180 and 400 g/m2. The supported versions contain a woven nylon carrier for glueline thickness control and improved handle ability. Redux$^{®}$ 319 is a hot melt film which is free from solvents and consequently it has a very low volatile content.

2.4   Future applications

Self-healing materials are defined as those that have properties of repairing themselves after a damage has occurred, without losing their main functionalities. The growing interest in the

development of polymer nanocomposites with enhanced tribological performance is parallel to the increasing number of applications of polymers and polymer matrix composites. In fact, damage and failure are unavoidable in materials lives. Among thermoset materials, epoxy resins present a number of well-known advantages including toughness, high electrical resistance and thermal stability, and ease of fabrication. Epoxy resins are widely used in applications that range from electric and electronic systems to automotive parts, aircraft components, biocompatible implants, protective coatings, and adhesives. However, the tribological performance of epoxy resins are extremely poor due to their high brittleness and lack of self-lubricating behaviour, with severe wear due to crack propagation and fracture under sliding conditions.

Self-healing materials exhibit the ability to repair themselves and to recover functionality using the resources inherently available to them. Whether the repair process is autonomic or externally assisted (e.g., by heating), the recovery process is triggered by damage to the material. Self-healing materials offer a new route toward safer, longer-lasting products and components.

Brostow et al. [10] described the increase in scratch recovery of epoxy resin by the addition of a fluoropolymer. There exist numerous precedents [11, 12] of self-repairing or self-healing epoxy resin systems, usually by the addition of encapsulated curing agents which are released in the presence of fracture cracks, following the mechanism described in figure 2:10.
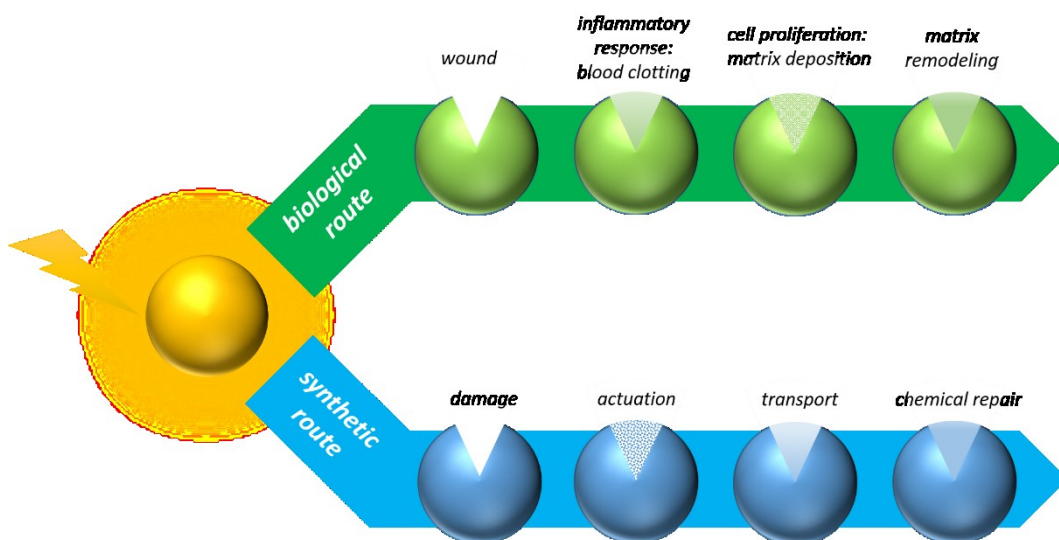
Figure 2:10 Autonomic healing (i.e. syntetich route) mimics the biological route of wound healing. Damages in the matrix can break the microcapsules, releasing the healing agent into the crack plane through capillary action (transport). The healing agent bonds the crack repairing the material

Liu et al. [13] demonstrated that it is possible to achieve self-healing properties by introducing epoxy microcapsules containing a healing agent into an epoxy resin. The microcapsules were introduced by simply dispersion into the resin at ambient temperature. These microcapsules, made by interfacial polymerization of epoxy resin droplets with ethylenediamine, can be broken by the propagation of a crack. This is very useful for coatings, so that when surfaces are scratched, the microcapsules break and release the healing agent repairing the composite material. The experimental results showed that the artificial scratches were successfully healed in about 4-h after made. The self-healing coatings loaded with epoxy microcapsules undoubtedly have promise applications in the coatings and the self-healing films.

The Cornerstone Research Group (http://www.crgrp.com) developed a self-healing version of shape memory polymer (SMP) called Veriflex® EH (figure 2:11). This healable SMP resin will enable increased survivability for manned and unmanned air vehicles, spacecraft, habitats for space exploration missions, automobiles, and more.
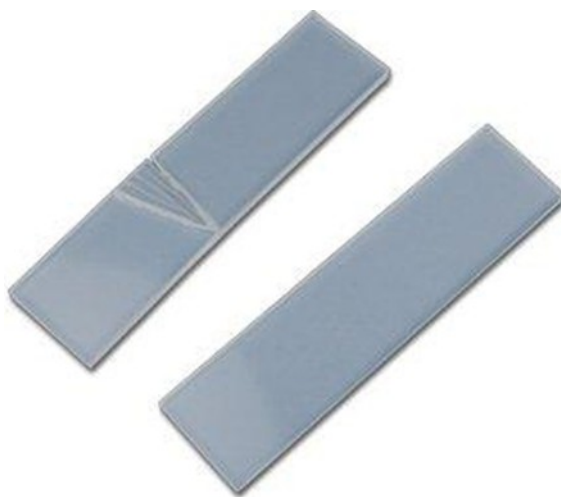
Figure 2:11 Damaged (top) and self-healed Veriflex EH epoxy

Veriflex® EH is an epoxy-based resin that will be a direct replacement for current aerospace-grade epoxy resins. Veriflex® EH can be processed using vacuum-assisted resin transfer molding (VARTM), RTM, or wet lay-up techniques. CRG is also developing a prepreg formulation. Veriflex® EH uses two healing mechanisms to restore up to 85% of original mechanical performance. The first healing mechanism, shape recovery, brings the cracked or damaged area back into intimate physical contact. The second healing mechanism, polymer diffusion, allows long polymer chains to diffuse across the failure line and restore mechanical integrity. Both healing mechanisms are thermally activated and are achieved in less than three minutes. The system is claimed to reach 85% recovery of flexural strength.

This chapter is under submission as contribution to the Handbook of Epoxy Blends, edited by Dr. Jyotishkumar Parameswaranpillai, Springer

2.5   Chapter 2 References

[1] Cicala G., Lo Faro C. (2012) Polymeric matrixes: materials type and modification strategies in Wiley Encyclopedia of Composites, John Wiley & Sons, New Jersey

[2] Williams R.J.J., Rozenberg B.A. and Pascault J.P. (1997), Adv. Poly,. Sci., 128: 95

[3] Lucas J. C., Borrajo J. and Williams R .J. J. (1993) Polymer, 34: 1886

[4] Prime R.B. (1997), "Thermoset", in Thermal Characterization of Polymeric Materials, E. A. Turi (ed.), 2nd Ed., Academic Press, San Diego

[5] Vendersbosch R. W., Meijer H. E. H (1997) "Processing of Polymers Using Reactive Solvents", in Material Science and Technology, R. W. Cahn, P Haase and E. J. Kramer (eds.), Vol. 18, Processing of Polymers, H. E. H. Meijer (ed.), Wiley-VCH-Weinheim.

[6] Lo Faro C, Cicala G., Recca A., Sanders D. (2003) "Crash behaviour of composite materials : a DOE and fracture mechanics approach" Sampe International Confererence 2003, Paris

[7] http://www.topgear.com/uk/car-news/new-ferrari-laferrari-f150-revealed-geneva-2013-03-05

[8] Cytec Engineered Materials, unpublished data

[9] Centea T., Grunenfelder L.K., Nutt S.R. (2015) A review of out-of-autoclave prepregs – Material properties, process phenomena, and manufacturing considerations, Composites: Part A 70:132–154

[10]   Brostow W., Bujard B., Cassidiy P.E., Hagg H.E., Montemartini P.E. (2002) Mater. Res. Mater. Res. Innov. 6: 7–12

[11]   Yuan Y. C., Yin T., Rong M. Z., Zhang M. Q (2008) eXPRESS Polymer Letters Vol.2: 238-258

[12]   Ratna D., Karger-Kocsis J. (2008) Journal of Materials Science, 43: 254–269.

[13]   Liu X.X., Zhang, H.R., Wang J.X., Wang Z., Wang S.C. (2012) Surf. Coat. Technol. 206: 4976–4980

3.Electrospinning: Process and Applications

When the diameters of polymer fiber materials are shrunk from micrometers to submicrons or nanometers, there appears several amazing characteristics such as very large surface area to volume ratio (this ratio for a nanofiber can be as large as 103 times of that of a microfiber), flexibility in surface functionalities, and superior mechanical performance (e.g. stiffness and tensile strength) compared with any other known form of the material. These outstanding properties make the polymer nanofibers to be optimal candidates for many important applications. A number of processing techniques such as drawing, template synthesis, phase separation, self-assembly, electrospinning, etc. have been used to prepare polymer nanofibers in recent years.

The drawing is a process similar to dry spinning in fiber industry, which can make one-by-one very long single nanofibers. However, only a viscoelastic material that can undergo strong deformations while being cohesive enough to support the stresses developed during pulling can be made into nanofibers through drawing. The template synthesis, as the name suggests, uses a nanoporous membrane as a template to make nanofibers of solid (a fibril) or hollow (a tubule) shape. The most important feature of this method may lie in that nanometer tubules and fibrils of various raw materials such as electronically conducting polymers, metals, semiconductors, and carbons can be fabricated. On the other hand, the method cannot make one-by-one continuous nanofibers. The phase separation consists of dissolution, gelation, extraction using a different solvent, freezing, and drying resulting in a nanoscale porous foam. The process takes relatively long period of time to transfer the solid polymer into the nano-porous foam.

The self-assembly is a process in which individual, pre-existing components organize themselves into desired patterns and functions. However, similarly to the phase separation the self-assembly is time-consuming in processing continuous polymer nanofibers.

The electrospinning process seems to be the only method which can be further developed for mass production of one-by-one continuous nanofibers from various polymers. Electrospinning has emerged as a powerful technique for producing high strength fibers due to its versatility, ease of use, ability to align structures and control fiber diameters. Some of these unique features cannot be otherwise achieved by conventional fiber processing techniques mentioned above. Another merit is that under the influence of an electric field, electrospinning self-assembles dispersed fillers along the axial direction such that composites can be formed by imposing additional spatial confinement to the polymer chains. These reinforced fibers display superior properties and function as basic building blocks for the fabrication of high strength structures using a bottom-up approach. For example, carbon nanotubes (CNTs) and carbon black (CB) particles are among the commonly used fillers which are dispersed within the fibers to mimic the functionality of silk fibers for high strength and toughness applications.

3.1   History of electrospinning

The origin of electrospinning as a viable fiber spinning technique can be traced back to the early 1930s. In 1934, Formhals patented his first invention relating to the process and the apparatus for producing artificial filaments using electric charges [1]. Though the method of producing artificial threads using an electric field had been experimented for a long time, it had not gained importance until Formhals's invention due to some technical difficulties in earlier spinning methods, such as fiber drying and collection. Formhals's spinning process

consists of a movable thread collecting device to collect the threads in a stretched condition, like that of a spinning drum in the conventional spinning. Formhals's process was capable of producing threads aligned parallel on to the receiving device in such a way that it can be unwound continuously. The first spinning method adopted by Formhals had some technical disadvantages. It was difficult to completely dry the fibers after spinning due to the short distance between the spinning and collection zones, which resulted in a less aggregated web structure. Formhals refined his earlier approach to overcome the aforementioned drawbacks.

Subsequently in 1940, Formhals patented another method [2] for producing composite fiber webs from multiple polymer and fiber substrates by electrostatically spinning polymer fibers on a moving base substrate. In the 1960s, fundamental studies on the jet forming process were initiated by Taylor [3]. In 1969, Taylor studied the shape of the polymer droplet produced at the tip of the needle when an electric field is applied and showed that it is a cone and the jets are ejected from the vertices of the cone. This conical shape of the jet was later referred to by other researchers as the "Taylor Cone" in subsequent literature. By a detailed examination of different viscous fluids, Taylor determined that an angle of 49.3 degrees is required to balance the surface tension of the polymer with the electrostatic forces. The conical shape of the jet is important because it defines the onset of the extensional velocity gradients in the fiber forming process. In subsequent years, focus shifted to studying the structural morphology of nanofibers. Researchers were occupied with the structural characterization of fibers and the understanding of the relationships between the structural features and process parameters. Wide-angle X-ray diffraction (WAXD), scanning electron microscopy (SEM), transmission electron microscopy (TEM), and differential scanning calorimetry (DSC) have been used by researchers to characterize electrospun nanofibers.

In 1987, Hayati et al. [4] studied the effects of electric field, experimental conditions, and the factors affecting the fiber stability and atomization. They concluded that liquid conductivity

plays a major role in the electrostatic disruption of liquid surfaces. Results showed that highly conducting fluids with increasing applied voltage produced highly unstable streams that whipped around in different directions. Relatively stable jets were produced with semi conducting and insulating liquids, such as paraffinic oil. Results also showed that unstable jets produce fibers with broader diameter distribution.

After a hiatus of a decade or so, a major upsurge in research on electrospinning took place due to increased knowledge on the application potential of nanofibers in different areas, such as high efficiency filter media, protective clothing, catalyst substrates, and adsorbent materials.

Research on nanofibers gained momentum due to the work of Doshi and Reneker [5]. They studied the characteristics of polyethylene oxide (PEO) nanofibers by varying the solution concentration and applied electric potential. Jet diameters were measured as a function of distance from the apex of the cone, and they observed that the jet diameter decreases with the increase in distance.

Deitzel et al.[6] showed that an increase in the applied voltage changes the shape of the surface from which the jet originates and the shape change has been correlated to the increase in the bead defects. They tried to control the deposition of fibers by using a multiple field electrospinning apparatus that provided an additional field of similar polarity on the jets.

3.2   The process

Electrospinning, uses high voltage to electrically charge the polymer solution for producing ultra-fine fibers. The basic electrospinning setup, consists of a pipette or a syringe filled with polymer solution, a high voltage source and a grounded conductive collector screen. In addition, a metering syringe pump can be used to control the flow rate of the polymer solution. The needle of the syringe typically serves as an electrode to electrically charge the

polymer solution and the counter-electrode is connected to the conductive collector screen. Under the influence of a strong electrostatic field, charges are induced in the solution and the charged polymer is accelerated towards the grounded metal collector. At low electrostatic field strength, the pendant drop emerging from the tip of the pipette is prevented from dripping due to the surface tension of the solution. As the intensity of the electric field is increased, the induced charges on the liquid surface repel each other and create shear stresses. These repulsive forces act in a direction opposite to the surface tension, which results in the extension of the pendant drop into a conical shape and serves as an initiating surface.

A schematic of the process is shown in figure 3:1. When the critical voltage is reached, the equilibrium of the forces is disturbed and a charged jet emanates from the tip of the conical drop. The discharged jet diameter decreases in size with concomitant increase in length before being deposited on the collector. This process can be explained by the three types of physical instabilities experienced by the jet. These instabilities influence the size and geometry of the deposited fibers. The first instability, also known as the Rayleigh instability is axisymmetric and occurs when the strength of electric field is low or when the viscosity of the solution is below the optimum value. Use of very low viscosity solutions causes jet break-up and leads to the bead-on-fiber morphology. It is attributed to the poor chain entanglement density in the solution and insufficient resistance to the electrostatic field. Rayleigh instability is suppressed at high electric fields (high charge densities) or when using higher concentration of polymer in the solution.
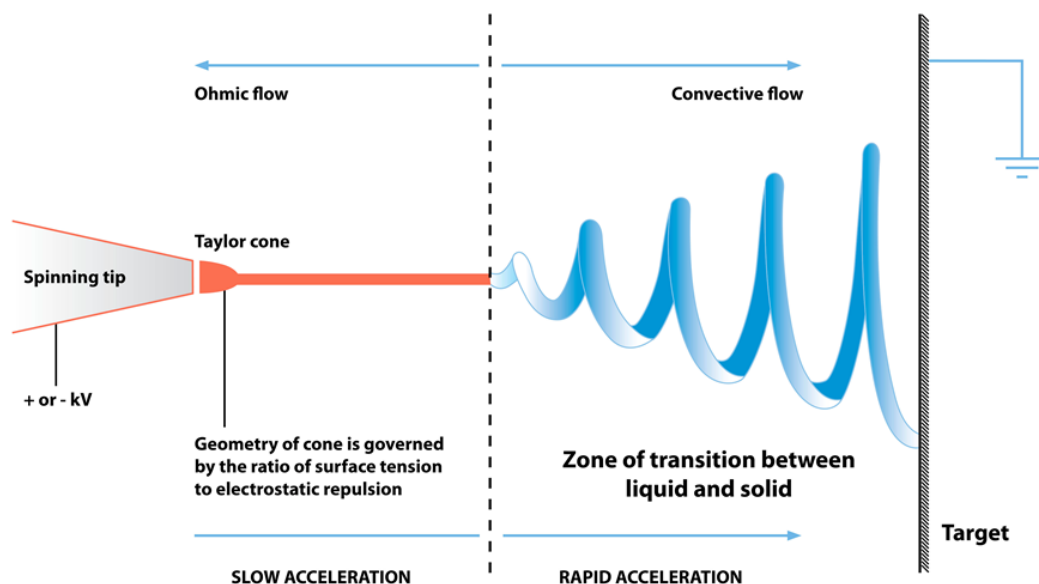
Figure 3:1 Schematic of the electrospinning process

Following the initial straight path of the jet, which is controlled by the Rayleigh instability, the polymer jet is influenced by two other instabilities: the bending and whipping instabilities. These instabilities arise owing to the charge-charge repulsion between the excess charges present in the jet which encourages the thinning and elongation of the jet. At high electric forces, the jet is dominated by bending (axisymmetric) and whipping instability (non-axisymmetric), causing the jet to travel in an ''inverse cone" manner. It produces wave or dumb-bell shaped patterns in the jet . At higher electric fields and at sufficient charge density in the jet, the axisymmetric (i.e., Rayleigh and bending) instabilities are suppressed and the non-axisymmetric instability is enhanced. The whipping instability produces a bending force on the jet, resulting in a high degree of elongation of the jet. During these processes, the solvent evaporates and finally leads to the deposition of ultra-fine fibers on the conductive ground electrode.

3.3   Spinning of Polymeric Nanofibres

Research activity on the electrospinning of nanofibers has been successful in spinning submicron range fibers from different polymeric solutions and melts.

Polymers with attractive chemical, mechanical, and electrical properties like high conductivity, high chemical resistance, and high tensile strength have been spun into ultrafine fibers by the electrospinning process, and their application potential in areas like filtration, optical fibers, drug delivery system, tissue scaffolds, and protective textiles have been examined [6-9].

As theoretical studies on the electrospinning process have been conducted by various groups [8-10] for a while to understand the electrospinning process, there have been some simultaneous efforts to characterize the structure and morphology of nanofibers as a function of process parameters and material characteristics. process is influenced both by the electrostatic forces and the viscoelastic behavior of the polymer. Process parameters, like solution feed rate, applied voltage, nozzle-collector distance, and spinning environment, and material properties, like solution concentration, viscosity, surface tension, conductivity, and solvent vapor pressure, influence the structure and properties of electrospun nanofibers.

3.3.1 Process parameters and fiber morphology

Applied Voltage

Various instability modes that occur during the fiber forming process are expected to occur by the combined effect of both the electrostatic field and the material properties of the polymer. It has been suggested that the onset of different modes of instabilities in the electrospinning process depends on the shape of the jet initiating surface and the degree of instability, which

effectively produces changes in the fiber morphology [6]. In electrospinning, the charge transport due to the applied voltage is mainly due to the flow of the polymer jet towards the collector, and the increase or decrease in the current is attributed to the mass flow of the polymer from the nozzle tip.

Deitzel et al. [6] have inferred that the change in the spinning current is related to the change in the instability mode. They experimentally showed that an increase in applied voltage causes a change in the shape of the jet initiating point, and hence the structure and morphology of fibers. Earlier in 1971, Baumgarten while carrying out experiments with acrylic fibers observed an increase in fiber length of approximately twice with small changes in fiber diameter with an increase in applied voltage [11].

Generally, it has been accepted that an increase in the applied voltage increases the deposition rate due to higher mass flow from the needle tip.

Nozzle collector distance

The structure and morphology of electrospun fibers is easily affected by the nozzle to collector distance because of their dependence on the deposition time, evaporation rate, and whipping or instability interval.

Buchko et al. [12] examined the morphological changes in SLPF and nylon electrospun fibers with variations in the distance between the nozzle and the collector screen. They showed that regardless of the concentration of the solution, lesser nozzle-collector distance produces wet fibers and beaded structures. SLPF fiber morphology changed from round to flat shape with a decrease in the nozzle collector distance from 2cm to 0.5cm. This result shows the effect of the nozzle collector distance on fiber morphology. The work also showed that aqueous polymer solutions require more distance for dry fiber formation than systems that use highly volatile organic solvents.

Polymer flow rate

The flow rate of the polymer from the syringe is an important process parameter as it influences the jet velocity and the material transfer rate. In the case of PS fibers, Megelski et al. [14] observed that the fiber diameter and the pore diameter increased with an increase in the polymer flow rate. As the flow rate increased, fibers had pronounced beaded morphologies and the mean pore size increased from 90 to 150 nm.

Spinning environment

Environmental conditions around the spinneret, like the surrounding air, its relative humidity, vacuum conditions, surrounding gas, etc., influence the fiber structure and morphology of electrospun fibers. Baumgarten [14] observed that acrylic fibers spun in an atmosphere of relative humidity more than 60% do not dry properly and get entangled on the surface of the collector. The breakdown voltage of the atmospheric gases is said to influence the charge retaining capacity of the fibers.

3.3.2 Solution parameters and fiber morphology

Solution concentration

Solution concentration decides the limiting boundaries for the formation of electrospun fibers due to variations in the viscosity and surface tension. Low concentration solution forms droplets due to the influence of surface tension, while higher concentration prohibits fiber formation due to higher viscosity.

Solution conductivity

Polymers are mostly conductive, with a few exceptions of dielectric materials, and the charged ions in the polymer solution are highly influential in jet formation. The ions increase

the charge carrying capacity of the jet, thereby subjecting it to higher tension with the applied electric field. Baumgarten [14] showed that the jet radius varied inversely as the cube root of the electrical conductivity of the solution.

Volatility of solvent

As electrospinning involves rapid solvent evaporation and phase separations due to jet thinning, solvent vapor pressure critically determines the evaporation rate and the drying time. Solvent volatility plays a major role in the formation of nanostructures by influencing the phase separation process.

Lee et al. [15] evaluated the effect of volume ratio of the solvent on the fiber diameter and morphology of electrospun PVC fibers. Average fiber diameters decreased with an increase in the amount of DMF in the THF/DMF mixed solvent. Lee et al. found the electrolytic nature of the solvent to be an important parameter in electrospinning. Megelski et al. [13] studied the characteristics of electrospun fibers with respect to the physical properties of solvents. The influence of vapor pressure was evident when PS fibers spun with different THF/DMF combinations resulted in micro and nanostructure morphologies at higher solvent volatility and a much-diminished microstructure at lower solvent volatility.

3.3.3 Properties of nanofibers

As briefly discussed, a major upsurge in research on nanofibers has taken place most recently due to its high surface area and nanostructure surface morphologies that enable a myriad of advanced applications. Nanofibers have been reported to have marked differences in their thermal and mechanical properties compared to regular fibers and bulk polymers.

Thermal properties

There are a few published reports on the thermal properties of nanostructured materials. Thermal analysis has been carried out on a number of electrospun polymeric materials to understand the relationship between nanostructure and thermal properties. DSC studies have indicated that electrospun PLLA fibers have lower crystallinity, glass transition temperature (Tg), and melting temperature (Tm) than semicrystalline PLLA resins [16]. Zong et al. attributed the decrease in the Tg to the large surface to volume ratio of nanofibers with air as the plasticizer. The high evaporation rate followed by rapid solidification at the final stages of electrospinning is expected to be the reason for the low crystallinity. The Tg and the peak crystallization temperature (Tc) of the electrospun polyethylene terephthalate (PET) and polyethylene naphthalate (PEN) decreased significantly, while the heat of crystalline melting increased. The decrease in Tg and Tm, and the increase in the heat of melting were attributed to the increase in the segmental mobility. The melting temperature of the PET and PEN electrospun fibers remained almost constant, without any significant variations compared to that of regular fiber forms. PEO nanofibers have shown a lower melting temperature and heat of fusion than the PEO powder, which is attributed to the poor crystallinity of the electrospun fibers. The crystallinity of the PLLA fibers was observed to be completely retarded by electrospinning, and the WAXD patterns of the electrospun PLLA fibers confirmed highly oriented fibers. This decrease in crystallinity has been shown to be a general phenomenon and has been observed in poly (meta-phenylene isophthalamide), poly (glycolide), and polyacrylonitrile. Deitzel et al. [6] inferred that PEO nanofibers retained the same crystal structure as PEO powders, while there is a clear indication of reduced crystalline order in nanofibers. Bognitzki et al. concluded with the help of a DSC thermogram that the degree of crystallinity of electrospun PLLA fibers was in the order of 40%.

Thermal degradation of PET and PEN before and after electrospinning was analyzed by Kim and Lee [17] using the TGA thermogram, and they found that on electrospinning the intrinsic viscosities of both PET and PEN reduced significantly. The thermal degradation and hence the decrease in intrinsic viscosities (i.e., decrease of molecular weight) were postulated to be the reasons for the decrease in Tg and Tc caused by reduced entanglements.

Mechanical properties

Electrospun fibers have nanostructured surface morphologies with tiny pores that influence mechanical properties like tensile strength, Young's modulus, etc. Gibson et al. [18] have found that there is no significant change in the Young's modulus of electrospun Pellethane thermoplastic elastomers. When compared with cast films, electrospun elastomers have shown a 40% reduction in the peak tensile strength and 60% reduction in elongation at maximum applied stress. The decrease in the tensile strength has also been reported by Buchko et al. [12] with SLPF fibers. Nanofiber reinforced polymer composites have shown more highly enhanced mechanical properties than the unfilled or carbon/glass fiber filled composites. Young's modulus of a nanofiber composite has been found to be 10-fold greater than the pure Styrene-Butadiene rubber. As is evident, there is less information available on the mechanical properties of nanofibers and nanofiber composites. Research on the mechanical properties of nanofibers and their composites from a variety of polymers is essential for a greater understanding on the contributions of nanofibers to the mechanical and performance related characteristics of nanofiber composites.

3.4   Application of electrospun nanofibres

Nanomaterials have been attracting the attention of global materials research these days primarily due to their enhanced properties required for application in specific areas like

catalysis, filtration, NEMS, nanocomposites, nanofibrous structures, tissue scaffolds, drug delivery systems, protective textiles, storage cells for hydrogen fuel cells, etc. A brief discussion on some of the applications shown in figure 3:2 (excluding nanocomposites application that will be discussed later) is given in this section.
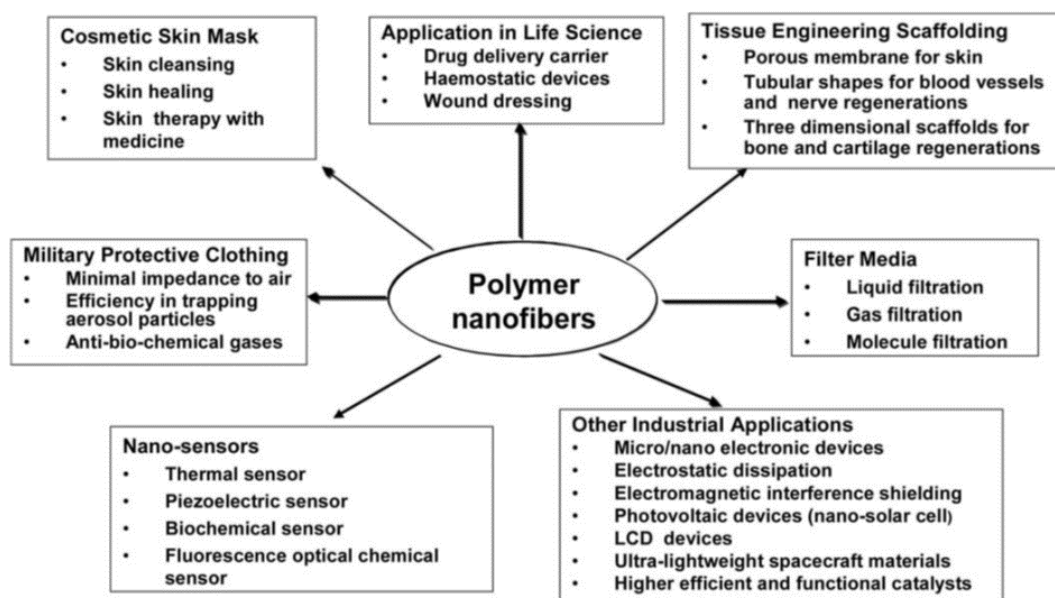

Figure 3:2 Potential applications of electrospun polymer nanofibers

3.4.1 Filtration application

Filtration is necessary in many engineering fields. Fibrous materials used for filter media provide advantages of high filtration efficiency and low air resistance Filtration efficiency, which is closely associated with the fiber fineness (figure 3:3), is one of the most important concerns for the filter performance. In the industry, coalescing filter media are studied to produce clean compressed air. These media are required to capture oil droplets as small as 0.3 micron. It is realized that electrospinning is rising to the challenge of providing solutions for the removal of unfriendly particles in such submicron range. Since the channels and structural elements of a filter must be matched to the scale of the particles or droplets that are to be captured in the filter, one direct way of developing high efficient and effective filter media is by using nanometer sized fibers in the filter structure. In general, due to the very high surface

area to volume ratio and resulting high surface cohesion, tiny particles of the order of <0.5 μm can be easily trapped in the electrospun nanofibrous structured filters and hence the filtration efficiency can be improved.

In addition to fulfilling the more traditional purpose in filtration, the nanofiber membranes fabricated from some specific polymers or coated with some selective agents can also be used as, for example, molecular filters. For instance, such filters can be applied to the detection and filtration of chemical and biological weapon agents.
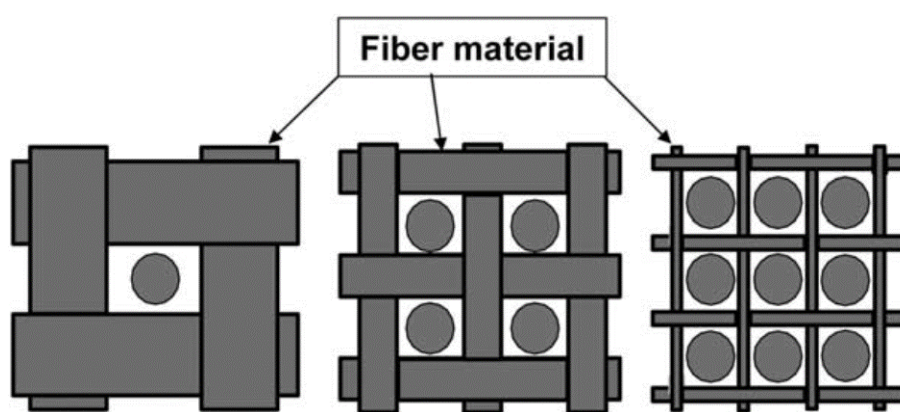
Figure 3:3 The efficiency of a filter increases with decrease in fiber diameter

3.4.2 Biomedical application

From a biological viewpoint, almost all of the human tissues and organs are deposited in nanofibrous forms or structures. Examples include: bone, dentin, collagen, cartilage, and skin. All of them are characterized by well organized hierarchical fibrous structures realigning in nanometer scale. As such, current research in electrospun polymer nanofibers has focused one of their major applications on bioengineering. We can easily find their promising potential in various biomedical areas. Some examples are listed later.

Medical prostheses

Polymer nanofibers fabricated via electrospinning have been proposed for a number of soft tissue prostheses applications such as blood vessel, vascular, breast, etc (figure 3:4). In addition, electrospun biocompatible polymer nanofibers can also be deposited as a thin porous film onto a hard tissue prosthetic device designed to be implanted into the human body. This coating film with gradient fibrous structure works as an interphase between the prosthetic device and the host tissues, and is expected to efficiently reduce the stiffness mismatch at the tissue/device interphase and hence prevent the device failure after the implantation.
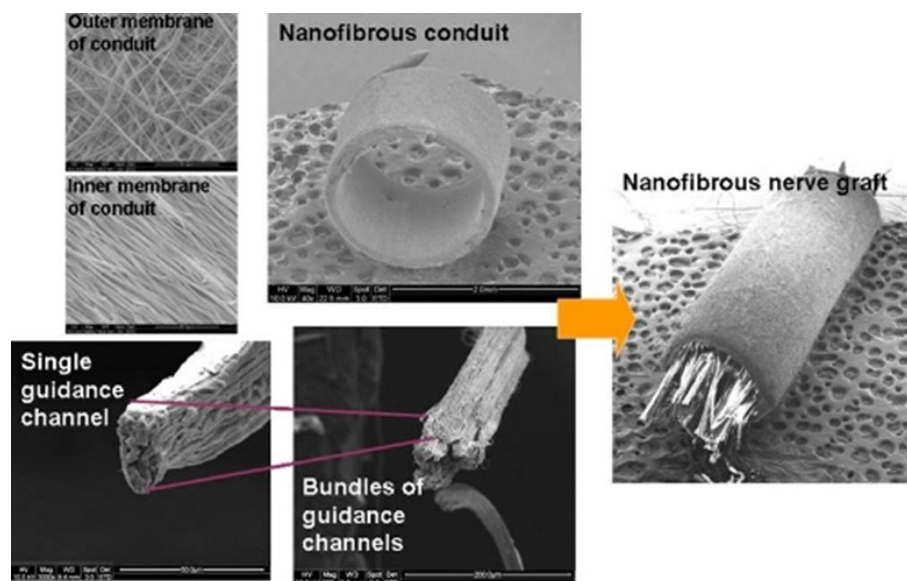
Figure 3:4 Structural organization of nerve guidance conduit [19]

Tissue template

For the treatment of tissues or organs in malfunction in a human body, one of the challenges to the field of tissue engineering/biomaterials is the design of ideal scaffolds/synthetic matrices that can mimic the structure and biological functions of the natural extracellurlar matrix (ECM). Human cells can attach and organize well around fibers with diameters smaller than those of the cells. In this regard, nanoscale fibrous scaffolds can provide an optimal template for cells to seed, migrate, and grow.

Of particular interest in tissue engineering is the creation of reproducible and biocompatible three-dimensional scaffolds for cell ingrowth resulting in bio-matrix composites for various tissue repair and replacement procedures. Recently, people have started to pay attention to making such scaffolds with synthetic biopolymers and/or biodegradable polymer nanofibers.

Wound dressing

Polymer nanofibers can also be used for the treatment of wounds or burns of a human skin (figure 3:5), as well as designed for haemostatic devices with some unique characteristics. With the aid of electric field, fine fibers of biodegradable polymers can be directly sprayed/spun onto the injured location of skin to form a fibrous mat dressing, which can let wounds heal by encouraging the formation of normal skin growth and eliminate the formation of scar tissue which would occur in a traditional treatment.
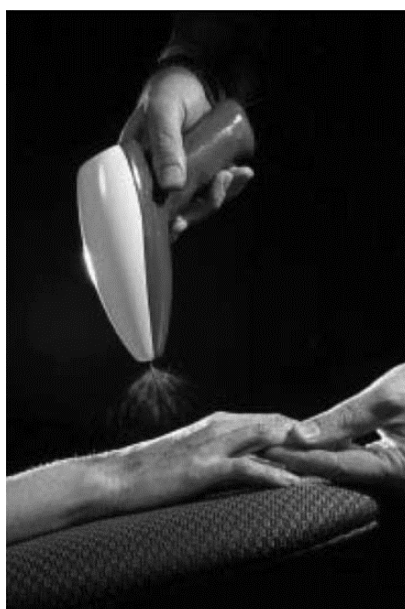
Figure 3:5 Nanofibers for wound dressing (www.electrosols.com)

Cosmetics

The current skin care masks applied as topical creams, lotions or ointments may include dusts or liquid sprays which may be more likely than fibrous materials to migrate into sensitive areas of the body such as the nose and eyes where the skin mask is being applied to the face.

Electrospun polymer nanofibers have been attempted as a cosmetic skin care mask for the treatment of skin healing, skin cleansing, or other therapeutical or medical properties with or without various additives. This nanofibrous skin mask with very small interstices and high surface area can facilitate far greater utilization and speed up the rate of transfer of the additives to the skin for the fullest potential of the additive. The cosmetic skin mask from the electrospun nanofibers can be applied gently and painlessly as well as directly to the three-dimensional topography of the skin to provide healing or care treatment to the skin.

Protective clothing application

The protective clothing in military is mostly expected to help maximize the survivability, sustainability, and combat effectiveness of the individual soldier system against extreme weather conditions, ballistics, and NBC (nuclear, biological, and chemical) warfare.

In peace ages, breathing apparatus and protective clothing with the particular function of against chemical warfare agents such as sarin, soman, tabun and mustard gas from inhalation and absorption through the skin become special concern for combatants in conflicts and civilian populations in terrorist attacks. Current protective clothing containing charcoal absorbents has its limitations in terms of water permeability, extra weight-imposed to the article of clothing. As such, a lightweight and breathable fabric, which is permeable to both air and water vapor, insoluble in all solvents and highly reactive with nerve gases and other deadly chemical agents, is desirable. Because of their great surface area, nanofiber fabrics are capable of the neutralization of chemical agents and without impedance of the air and water vapor permeability to the clothing. Electrospinning results in nanofibers laid down in a layer that has high porosity but very small pore size, providing good resistance to the penetration of chemical harm agents in aerosol form. Preliminary investigations have indicated that compared to conventional textiles the electrospun nanofibers present both minimal impedance

to moisture vapor diffusion and extremely efficiency in trapping aerosol particles, as well as show strong promises as ideal protective clothing.

Electrical and optical application

Conductive nanofibers are expected to be used in the fabrication of tiny electronic devices or machines such as Schottky junctions, sensors and actuators. Due to the well-known fact that the rate of electrochemical reactions is proportional to the surface area of the electrode, conductive nanofibrous membranes are also quite suitable for using as porous electrode in developing high performance battery (figure 3:6). Conductive (in terms of electrical, ionic and photoelectric) membranes also have potential for applications including electrostatic dissipation, corrosion protection, electromagnetic interference shielding, photovoltaic device, etc.
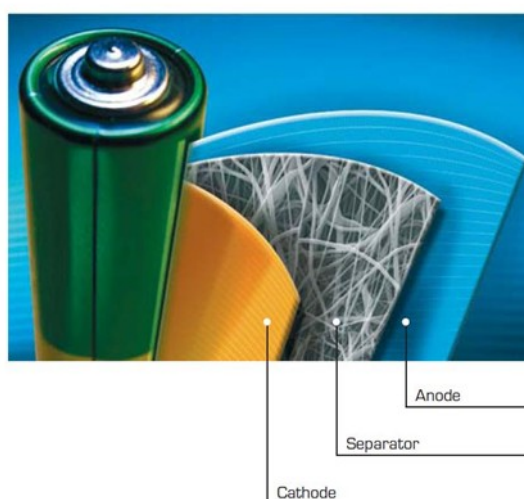
Figure 3:6 Battery with superior parameters by Elmarco's NanospiderTM technology

Waters et al. [20] reported to use electrospun nanofibers in the development of a liquid crystal device of optical shutter which is switchable under an electric field between a state in which it is substantially transparent to incident light and a state in which it is substantially opaque. The main part of this liquid crystal device consisted of a layer of nanofibers permeated with a

liquid crystal material, having a thickness of only few tens microns. The layer was located between two electrodes, by means of which an electric field could be applied across the layer to vary the transmissivity of the liquid crystal/nanofiber composite (figure 3:7). It is the fiber size used that determines the sensitivities of the refractive index differences between the liquid crystal material and the fibers, and consequently governs the transmissivity of the device. Obviously nanoscale polymer fibers are necessary in this kind of devices.

One dimensional (1D) nanostructures displaying luminescence i.e. photoluminescence, electroluminescence have attracted strong attention in recent years in particular in view of potential applications in light emitting diodes, full colour displays, lasers, data storage. The number of papers on electrospun light emitting nanofibers has correspondingly increased strongly with the last years. In principle three concepts were used to prepare such nanofibers based on (a) conjugated polymers frequently in combination with polymer blend components, (b) polymers into which functional components such as quantum dots or rare earth complexes were incorporated (here the argument is that such an approach allows to combine the favorable properties of the organic materials – flexibility, processibility, light weight – with the ones of the inorganic materials – hardness, thermal stability, chemical resistance, optical function), (c) inorganic materials doped among others also with rare earth complexes.
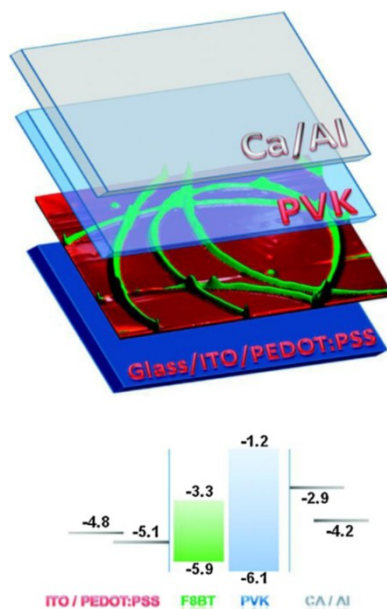
Figure 3:7 Planar organic light emission diode type architecture (OLED) with ribbonlike nanofibers of an electroluminescent polymer (F8BT) as active material, PEDOT/PSS: Poly(3,4-ethylenedioxythiophene) poly(styrenesulfonate), PVK: poly(N-vinyl carbazole).

3.5 Chapter 3 References

[1] Formhals Anton, Richard Schreiber Gastell, Process and apparatus for preparing artificial threads, US 1975504 A

[2] Formhals Anton, Richard Schreiber Gastell, Artificial thread and method of producing SME, US2187306 A

[3] Taylor, G.I., 1969. Electrically driven jets. Proceedings of the Royal Society of London A 313, 453–475

[4] Hayati, I.; Bailey, A. I.; Tadros, T. F. J Colloid Interface Sci 1987, 117, 205.

[5] Doshi, J.; Reneker, D. H. J Electrostatics 1995, 35, 151.

[6] Deitzel, J. M.; Kleinmeyer, J.; Harris, D.; BeckTan, N. C Polymer 2001, 42, 261.

[7] Warner, S. B.; Buer, A.; Grimler, M.; Ugbolue, S. C.; Rutledge, G. C.; Shin, M. Y. National Textile Center Annu Report November 1998, 83.

[8] Moses, M.; Hohman, M. M.; Shin, Y. M.; Rutledge, G. C.; Brenner, M. P. Phys Fluids 2001, 13, 2201

[9] Gibson, P. W.; Gibson, H. L.; Rivin, D. AIChe J 1999, 45, 190.

[10]   Yarin, A. L.; Koombhongse, S.; Reneker, D. H. J Appl Phys 2001, 89, 5

[11]   Baumgarten, P. K. JColloid Interface Sci 1971, 36, 71

[12]   CJ Buchko, LC Chen, Y Shen, DC Martin, Polymer, 1999 – Elsevier, Volume 40, Issue 26, 7397–7407

[13]   S Megelski, JS Stephens, DB Chase, JF Rabolt, Macromolecules, 2002 - ACS Publication, 35 (22), 8456–8466

[14]   PK Baumgarten, Journal of colloid and interface science, 1971 – Elsevier, 36 (19, 71-79

[15]   KH Lee, HY Kim, YM La, DR Lee, Journal of Polymer Science: Part B: Polymer Physics, Vol. 40, 2259–2268 (2002)

[16]   X Zong, K Kim, D Fang, S Ran, BS Hsiao, B Chu, Polymer, 2002, 43 (16) 4403–4412

[17]   J.-S. Kim, D.S. Lee, Polymer Journal, 2000 - nature.com

[18]   Gibson, P. W.; Gibson, H. L.; Rivin, D. AIChe J 1999, 45, 190

[19]   H S Koh et al. J. Neural Eng. 2010; 7: 046003

[20]   Waters CM, Noakes TJ, Pavery I, Hitomi C. US patent 5088807, 1992

4. Electrospun nanofibres reinforced composites

Composite products are used practically in every type of advanced structural applications including civil infrastructures, mechanical industry, land, sea and air transport vehicles, space exploration, military equipment and defense, healthcare and sporting items.

Fiber reinforced polymer (FRP) composites are commonly designed with the primary aim of obtaining superior mechanical properties (higher modulus and strength to weight ratio) with respect to existing materials for advanced structural applications, but they are also promising candidates as functional materials. The fiber component can also provide the possibility of modifying other functional properties of the plain polymer matrix, such as its optical and thermal properties, as well as its conductivity and dielectric constant.

With the aim of designing advanced and innovative FRP composites, the idea of further engineering the material through the incorporation of reinforcing nanofibers have attracted an increasing amount of interest. This research area has emerged starting from the consideration that either the use of nanofibers in place of the presently used micro-size fibers, or a suitable combination of micro- and nanofibers might further improve FRP composites mechanical properties.

4.1   Why nanofibers as composite reinforcement?

In traditional FRP composites, different configuration of the reinforcing fibers can be used, each leading to different mechanical performances. There are two principal fibres

configurations within the matrix: in the first one short fibres are randomly oriented while the other are represented by layers of long unidirectional fibers. Composites reinforced with short random fibers display isotropic mechanical properties while long unidirectional fibers are used when an orthotropic and strong reinforcing effect is desired.

In the field of FRP two main types of structural composites architectures can be distinguished:

- bulk composite structures,
- laminate composites.

In the first type of composites, the efficiency of the stress transfer from the polymer matrix to the filler governs the effectiveness of the reinforcement, thus the possibility to obtain improved mechanical properties with respect to those of the unfilled matrix. It has been widely demonstrated that fibers can carry out the reinforcing function, when they fulfill the following requirements: (a) suitable mechanical properties in terms of strength and stiffness with respect to the matrix; (b) large aspect ratio; (c) high surface area to volume ratio; (d) good fiber-matrix adhesion; (e) good dispersion and embedding in the polymer matrix; (f) proper orientation with respect to the applied external load. Since it is expected that nanofibers have the potentiality to greatly satisfy all the above listed characteristics, it can be easily understood why the engineering idea of using nanofibers to fabricate high-performance FRP composite structures, with further enhanced structural properties, is attracting growing interest nowadays.

Figure 4:1 sketches the potentialities of using nanofibers in place of microfibers for designing bulk composite structures.

FROM MICRO- TO NANO-SCALE FIBERS

Ultimate tensile strength (MPa)

Nanofibers

1.2E+04
1.0E+04
8.0E+03
6.0E+03
4.0E+03
2.0E+03
0.0E+00

Isotropic pitch based fibers

Carbon Microfibers

Aspect Ratio (L/d)

20.00
0.20
0.02

0.1   1.0   100.0

Surface to Volume Ratio (S/V)

Young Modulus (GPa)

Nanofibers

Carbon Microfibers

6.0E+02
5.0E+02
4.0E+02
3.0E+02
2.0E+02
1.0E+02
0.0E+00

Isotropic pitch based fibers

Aspect Ratio (L/d)

20.00
0.20
0.02

0.1   1.0   100.0

Surface to Volume Ratio (S/V)

Figure 4:1 From micro- to nano-scale fibers as reinforcement of bulk composites

In terms of fiber mechanical properties, going from micro- down to nano-dimensions, fibers are expected to show an improved elastic modulus and strength at break, thanks to their internal structure consisting of highly aligned macromolecular chains, especially in the case of fibers fabricated through spinning technologies.

Another advantage of using nanofibers in composites arises from the possibility to achieve high aspect ratios. Finally, since nanofibers possess very high surface area to volume ratio, that is a key factor in improving nanofiber-matrix interphase adhesion, an effective load-transfer from the matrix to the nanofibers is expected.

In the case of laminate composites the susceptibility to delamination along interlaminar planes is an intrinsic and severe problem, due to the ply-by-ply nature of such materials. Interlaminar stresses due to mismatch of anisotropic mechanical and thermal properties of plies occur at free edges, joints, and under out-of-plane loading. Delamination is often the dominating failure mode in laminates subjected to impact and fatigue loading. It is believed that nanofibers, being characterized by a diameter typically in the range of few hundreds nanometers, can be small enough to reinforce regions of the matrix located in between

70

adjacent plies of the laminate, as schematically illustrated in figure 4:2. The idea of using nanofibers to reinforce small-scale places, such as the regions at the interfaces of laminated composites, arises from the consideration that, in such composites, structural failures mainly occur in small critical areas, in particular in matrix-rich micro-volumes, where the matrix is not reinforced and it experiences high stress concentration.
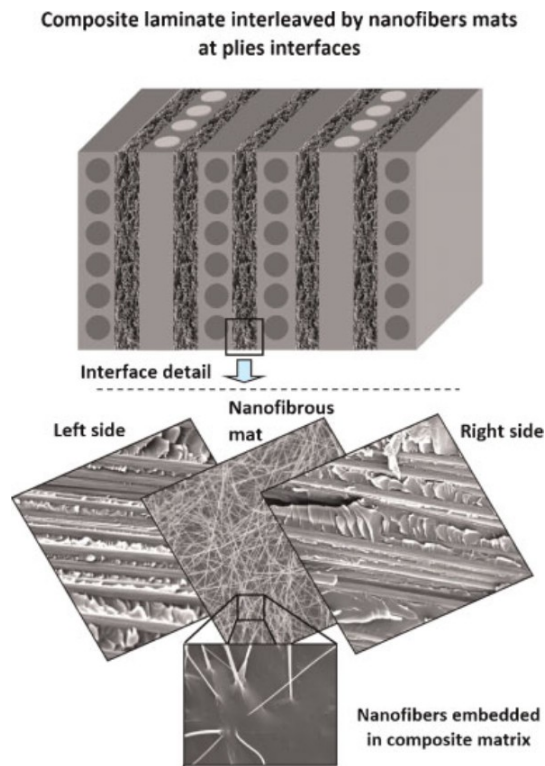

Figure 4:2 Composite laminate interleaved by nanofibrous mats at plies interfaces.This figure is available in colour online at wileyonlinelibrary.com

Nanofibers fabricated by electrospinning technology are considered as promising candidates for composite reinforcement. They are continuous, long fibers that, differently from nanofibers with finite length produced by other techniques, display an extremely high aspect ratio and do not present fiber edges that can act as stress concentration points. Moreover, the high stretching rate (estimated 10 s-1) and the high elongation (draw ratio up to 104) of the solidifying jet enables the spontaneous orientation of the macromolecular chains along fiber direction, thus contributing to increase the modulus and the strength of the single fiber. In

addition, electrospun fibers are usually obtained in the form of non-woven mats that can be easily dispersed in the polymer matrix and fiber alignment and highly ordered fiber architectures can be fabricated by means of proper collectors.

4.2 Polymer composites reinforced with electrospun nanofibres: Literature review

4.2.1 Electrospun nanofibers as bulk reinforcement of polymer matrix

Most of the works currently available in the literature on electrospun nanofibers as reinforcement of polymer composites aim at improving physical and chemical properties, as well as mechanical performances, of the polymer matrix.

One of the first papers about the fabrication and the structure property relationships of such composite materials was published by Kim and Reneke in 1999 [1]. They investigated the reinforcing effect of polybenzimidazole (PBI) electrospun nanofibers (fiber diameter around 500 nm) both in a diglycidyl ether of bisphenol-A (DGEBA) epoxy matrix and in a styrene-butadiene rubber (SBR) matrix. Composite specimens of PBI nanofibers reinforced epoxy matrix were prepared from several plies of the fabric sheets, cut and folded to fit a compression mold. The nanofiber sheets were then impregnated with the resin and thermally cured. Two kinds of specimens were prepared: in the first one the tensile axis was along the winding direction of the nanofiber sheets and in the second one the tensile axis was perpendicular to the winding direction. It was found that with increasing fiber content the bending Young modulus and fracture toughness of the epoxy non-woven fabric composites were increased marginally, whereas the fracture energy increased significantly. Moreover, the fracture toughness and the fracture energy of the composites were found to depend on the

direction of the crack: when the crack was transverse to the fabric winding direction both fracture toughness and fracture energy were higher with respect to the situation where the crack was along the winding direction. The rubber composites reinforced with PBI nanofiber were prepared by milling 0.5 cm squared nanofiber sheets in order to obtain a homogeneous dispersion of the filler into the matrix, followed by curing through compression molding. Also in this case, the reinforcing effect of PBI chopped nanofibers was proved by an increase of both Young modulus and tear strength respect to those of the pristine rubber.

Nylon nanofibers have been extensively employed as reinforcement of several polymeric matrices. Nylon 6 nanofibers (fiber diameter 250 nm) were used by Romo-Uribe et al. [2] as effective mechanical reinforcement of thin films of polyaniline (PANI). Composite membranes were prepared through a solvent-casting procedure: a PANI solution was poured onto either aluminium plates or previously prepared nylon 6 nanofiber coated aluminium plates and dried at 80°C under a stream of air. Subsequently, the as-cast PANI films and PANI-nylon 6 nanofiber composite films were detached from the plates by soaking in distilled water. The asymmetrical reinforced membrane obtained, composed of a dense PANI layer and a 6 mm thick PANI-nylon 6 nanofiber layer, showed good adhesion at the interface attributed to the presence of hydrogen bonding between the amine and the carbonyl moieties of PANI and nylon 6 respectively. Thermal and dynamic mechanical analyses revealed that the composite membrane had a significantly higher tensile modulus than the plain PANI film at room temperature, and that introduction of the nylon 6 nanofiber layer extended the composite working temperature from around 100 °C up to over 200 °C.

Nanocomposites made of a DGEBA epoxy resin reinforced with poly(ethylene oxide) (PEO) electrospun nanofibers were fabricated by Lee et al. [3]. The epoxy resin was mixed with 5wt% of PEO nanofibers and the mixture was subjected to high-energy ultrasonication at 60 °C followed by the addition of the curing agent. The obtained mixture was then degassed to

remove bubbles, casted into a mould and thermally cured at 120, 150 and 200 °C. The fracture toughness parameters, critical stress intensity factor and specific fracture energy, were evaluated by single edge-notched specimens tested under three-point flexural loading. All the parameters were found to increase in composites containing PEO nanofibers with respect to the unfilled epoxy resin, resulting in an improvement of the nanocomposites toughness.

The attention toward the chemical properties of electrospun nanofibers in order to improve fiber–matrix interface adhesion is the main focus of the paper by Ozden et al. [4], who prepared poly(styrene-co-glycidyl methacrylate), P(S-co-GMA), electrospun fibrous mats that were crosslinked and embedded into an Araldite epoxy resin matrix containing a polyamine hardener. Electrospun fiber cross-linking was achieved by spraying ethylenediammine (EDA) on the fibrous mat before embedding it into epoxy resin, layer-by-layer, and curing at 50 °C for 15 h. The epoxy matrix composites reinforced by 10 layers of fiber mats (2 wt%) were mechanical characterized by dynamic mechanical analysis (DMA) measurements (three-point bending mode) and by three-point flexural test. It was found that the storage modulus of P(S-co-GMA)/EDA fiber-reinforced epoxy was 10 and 2.5 times higher than that of neat and P(S-co-GMA) fiber-reinforced epoxy respectively. Three-point bending flexural tests performed on a composite containing a single layer of fibrous mat, indicated that incorporation of low-weight-fraction (0.2 wt%) of P(S-co-GMA)/ EDA fibers in the epoxy matrix increased the composite flexural modulus by 30% with respect to that of the neat epoxy. The improvement of mechanical performances was attributed to the combination of two main factors: (i) the fiber cross-linking, which leads to an increase in inherent stiffness of the fibrous mat and (ii) surface modification, i.e. chemistry, of the electrospun fibers, resulting in a better fiber-matrix interfacial bonding.

4.2.2 Electrospun nanofibers as interface reinforcement of composite laminates

With respect to the employment of electrospun nanofibers as nano-reinforcing agents of bulk polymer composite, the literature review concerning the nanofiber reinforcement of composite laminates is probably more structured. It takes inspiration from the pioneer idea proposed by Dzenis and Reneker [5] in their patent issued in 1999. Their invention regards a novel generation of microfiber reinforced composite laminated materials containing a secondary reinforcement made of nanofibers located at one or more ply interfaces. Here, the main role of nanofibers is to reduce the stress concentration due to mismatch of ply properties, typical of multidirectional laminates, as well as to bond the adjacent plies without increasing either the composite weight and the laminate thickness. Therefore such innovative composites are expected to display an improved interlaminar fracture toughness, strength, and delamination resistance with respect to static, fatigue, and impact loadings. As examples of their invention the authors manufactured laminate composites from a unidirectional graphite/epoxy prepreg with and without non-woven electrospun fabrics of polybenzimidazole (PBI, fiber diameter range 300–500 nm) by using a specialized press-clave. The use of PBI sheets increased the total laminate thickness and the laminate weight by less of 12% and of 2.5%, respectively. The Arcan test method and the mixed-mode interlaminar fracture testing were performed in order to investigate the effect of nanofiber interleaving membranes on both the peel mode (Mode I) and the sliding shear mode (Mode II). Results showed that the use of nanofibrous sheets increased the critical energy release rate by 130% and by 15% in the Mode II and in the Mode I, respectively. Specimens tested under Mode I were also investigated by optical microscopy and SEM observations. This analysis highlighted a variety of fracture modes including rather extensive intralaminar delamination. Indeed, due to the high toughening effect of the nano-interface, cracks were in some cases induced to propagate inside the ply.

Shivakumar et al. [6] prepared composite laminates of a commercial carbon fiber reinforced epoxy resin by using nylon 6,6 nanofibers (fiber diameter range 75–250 nm) and they investigated the effect of nanofiber interleaving on damping factor, interlaminar fracture toughness under static and fatigue loading and low velocity impact behavior. Results were compared with a commercial thermoplastic particulate interleaved composite. DMA tests performed both on plain and interleaved laminates revealed the presence of a single glass transition temperature (Tg). Moreover DMA tests showed that the addition of about 1.4% thick nanofabric interleave in composite laminates determined the increment of damping factors of about 13%. Differently, the Torayca composite showed two values of Tg, the lower one attributed to the thermoplastic particles and the higher one to the matrix. Mode I delamination was evaluated both under static and under fatigue loading conditions and results showed that the average critical strain energy release rate, G_{ic}, was about 150% greater than the pristine laminate. In plane laminate, the fracture resistance increased with the delamination propagation till reaching a constant value, on the contrary, in interleaved laminates the fracture resistance decreased with delamination growth and it reached a plateau after a certain value of the crack extension. The SEM analysis of the fractured surfaces showed the presence of stretching, separation, and breakage of nylon-6,6 nanofibers that could explain the toughness enhancement due to the presence of the nanofibrous membrane at the plies interface. Results of the fatigue delamination tests showed that the onset threshold values, $G_{ic,threshold}$, of nanofabric interleaved laminates is 67% greater than the plain one. It's possible to conclude that, in the case of impact, electrospun nylon-6,6 nanofiber interleaving increased the impact damage resistance three times with minimal increase in the thickness or weight.

A very recent paper by Zhang et al. [7] investigated the effect of fiber diameter and mat thickness in carbon/epoxy composite laminates interleaved with polyetherketone cardo (PEK-

C) nanofibres (average fiber diameters: 450, 750, and 950 nm). They evaluated the Mode I delamination fracture toughness and the flexural properties of the composites. The flexural strength of the interleaved laminates remarkably decreased when thick fibers (diameter 950 nm) were used with a concomitant reduction of the elastic modulus. The critical strain energy release rate, G_{ic}, was found to be rather independent from the fiber diameter. Mechanical tests performed on samples interleaved with electrospun mats of different thickness (40, 70, or 105μm) revealed a constant elastic modulus, a decrease of flexural strength and an increase of G_{ic} with the increase of membrane thickness. The authors concluded that composites interleaved with thinner nanofibers had better improvement in the interlaminar property without compromising the in-plane performance of the toughened composites.

Li et al.[8] manufactured laminates made of a carbon fiber/ epoxy prepreg by interleaving prepreg plies with polysulfone electrospun nanofibers (average fiber diameter 230 nm). Upon curing treatment at high temperature, the polysulfone melted and fiber morphology was lost. Since polysulfone was not miscible with the matrix a phase segregation phenomena occurred and well-dispersed microparticles of polysulfone were visualized by SEM analysis at the interfaces between the laminate plies. Therefore, in these papers electrospun fibers were not directly used as nanoreinforcing agents and the electrospinning technique was employed to obtain a more homogeneous distribution of polysulfone microparticles at the interfaces with respect to conventional approaches. Authors recognized a significant increase of composite strength in the case of polysulfone microparticles obtained by electrospun nanofibers with respect to the polysulfone microparticles obtained by interleaving polysulfone thin sheets at plies interfaces.

4.3 Chapter 4 References

[1] J-S. Kim, D. H. Reneker, Polym. Compos. 1999, 20, 124.

[2] A. Romo-Uribe, L. Arizmendi, M. E. Romero-Guzman, S. Sepulveda- Guzman, R. Cruz-Silva, ACS Appl. Mater. Interfaces (2009), 1, 2502

[3] J-R. Lee, S-J. Park, M-K. Seo, J-M. Park, Proc. Mater. Res. Soc. Symp. 2005, 851, 217.

[4] E. Ozden, Y-Z. Menceloglu,M. Papila, ACS Appl. Mater. Interfaces 2010, 2, 1788.

[5] Y. A. Dzenis, D. H. Reneker, PCT/US99/11755, 1999.

[6] K. Shivakumar, S. Lingaiah, H. Chen, P. Akangah, G. Swaminathan, L. Russel, AIAA J. 2009, 47, 1723

[7] J. Zhang, T. Lin, X. Wang, Compos. Sci. Technol. 2010, 70, 1660.

[8] G. Li, P. Li, C. Zhang, Y. Yu, H. Liu, S. Zhang, X. Jia, X. Yang, Z. Xue, S. Ryu, Compos. Sci. Technol. 2008, 68, 987

5.Aim of the project

The aim of this project was focused on the development of novel hybrid thermoplastic/carbon fabrics (figure 5:1) by means of electrospinning, in order to manufacture toughened and nanorinforced composite laminates by Resin Transfer Molding (RTM) and other infusion techniques.
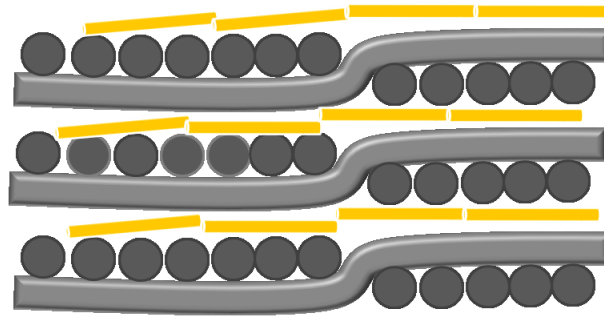
Figure 5:1 Scheme of the hybrid electrospun thermoplastic/carbon fabric

Figure 5:2 show the concept: using the hybrid fabrics in order to take the toughener out of the epoxy resin which can be injected into the mould without any viscosity issue. Furthermore, the electrospun thermoplastic veils can act as nanofiller carriers as well, if multifunctionality is desidered.
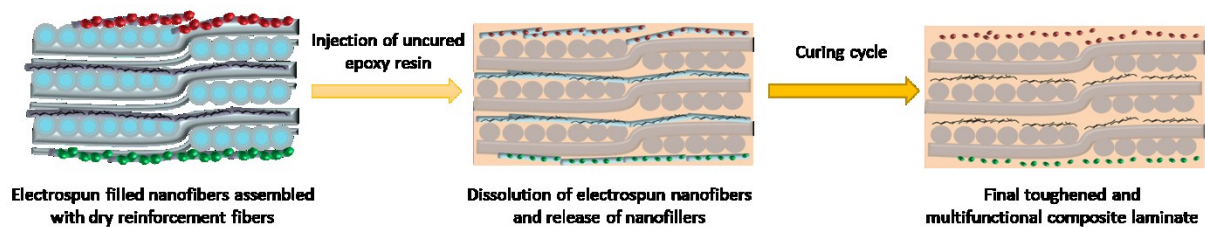
Figure 5:2 Concept of the manufacturing of multifunctional toughened composite laminates by the use of hybrid electrospun thermoplastic/carbon fabrics

The choice of RTM as processing technique has some pros and cons over the autoclave molding. The main pro is the easiness to obtain complex shape composites with fast

production rate. The main cons is the impossibility to use the toughened resins systems developed for the autoclave molding since they show too high viscosity values to be injected. The RTM process is summarized in its main steps in figure 5:3. The lay-up sequence (preform) is draped in a half mold, then the closure of the mold follows and the preform is compacted and stabilized. After that, the priform is transferred into the RTM mold and then the resin injected by using a positive gradient pressure through the gate points replacing the air entrapped within the preform. Usually, vacuum can be applied at dedicated vents in order to favorite the air escape from the mold. When the resin reaches the vents, the gates are clamped and the preform is impregnated. At this point, the cure phase is considered to start. Finally, the mold is opened and the part removed.
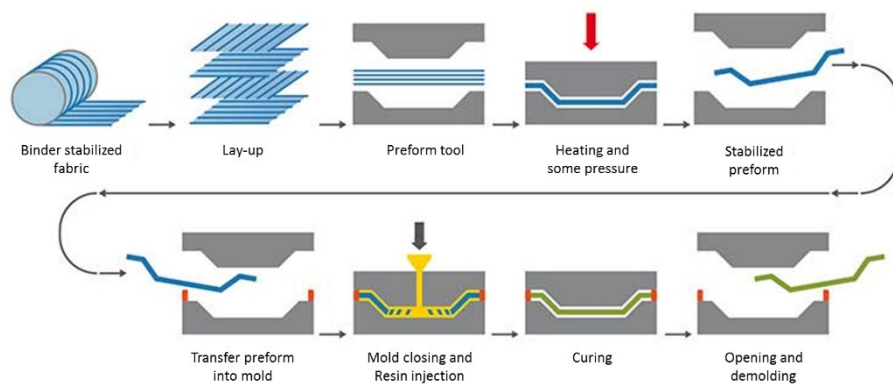
Figure 5:3 Sequence of the main steps of RTM process

Especially for aerospace structures, an additional free-mold post-curing phase can be necessary in order to guarantee the total polymerization of the matrix and the release of internal thermal stress. The closing mold step is characterized by the compaction of the fiber reinforcement, which permits to achieve the desired thickness and designed fiber volume fraction. The compaction changes the microstructure and the dimensions of the preform, producing large deformations and nonlinear viscoelastic effects. These effects are accompanied by a change in energy within the material, which causes the residual stresses due to the viscoelastic behavior of the fibers. However, during the impregnation phase, a release

of stress, probably due to the balance, occurs. The injection phase must guarantee the complete impregnation of the preform: a bad impregnation of the fibers results in dry spot areas with missing adhesion between the layers, which makes the surface rough and irregular. If partial impregnation occurs in the proximity of a connecting zone among elements, it can cause a bad integration with a consequent loss of mechanical properties.

In aerospace systems, RTM is considered the best choice in order to substitute the autoclave molding. In fact, it allows to save money and to eliminate the so called "operator effects" that affect the autoclave procedures. Another important reason that makes RTM such a successful technique is the high automation degree that this process allows to achieve. Although the RTM technique provides all these advantages, just a few systems for RTM have been developed due to the fact that this process requires, as work conditions, very low viscosity values (around 1 Pa*s). This condition is difficult to achieve with currently systems certified for the autoclave molding due to the fact that the resin modification, by adding the thermoplastic as toughener, leads to an exponential increase of viscosiy.

Although composite materials provide many advantages compared to traditional materials, there are also some disadvantages connected with their use. The main problem is represented by delamination along interlaminar planes due to the ply-by-ply nature of such materials. Delamination is often the dominating failure mode in laminates subjected to impact and fatigue loadings. For this reasons, in the last years studies have been directed to the resolution or the mitigation of this problem using nanofibers that can be small enough to reinforce regions of the matrix located in between adjacent plies of the laminate.

Another area of interest for the use of thermoset systems as matrices for advanced composites is represented by the epoxy resins with nanofillers. These systems show very high performance but they cannot used in the RTM process due to their increased viscosity caused by nanofillers. However, some of these nanofillers, like carbon nanotubes, have been shown

to be promising as functional fillers in order to either reinforce and give multifunctionalities to composites such as fire resistance, lightining-strike, self-sensing, etc.

The present project aims at overcoming the limitation of the already-available resin systems to be used in RTM process, combining the use of soluble thermoplastic nanofibres with the addition of nanofillers as well. In order to achieve this goal, the use of electrospun thermoplastic nanofibres that can be dissolved into the resin without any increase in thickness and weight, will be studied. Furthermore the dispersion of the nanofillers into the electrospun nanofibres will be analyze so that, after the fiber dissolution, they can be diffused where they are necessary. This approach seems to be more efficient than direct mixing of the nanofiller into the resin since the viscosity in the injection phase will not influenced from the presence of the nanofillers into the thermoplastic fibres. Using the thermoplastic toughener as electrospun veils placed inside the mold allows to inject the resin avoiding the wash-out effect that can occur if placing the modifier as powder. Moreover, the concept of the present project goes over the main issue of the Prifom technology developed by Cytec. In fact, Priform technology involves firstly the extrusion of the thermoplastic and then the weaving of the extruded fibers inside the carbon fabric. These two steps can be quite expensive and time-consuming for lage production amounts.

6.Experimental section

In this section, all the experimental phases will be following. Firstly, the production and the characterization of the electrospun veils will be viewed in details, including the upscale of the process at Elmarco facilities (Liberec, Czech Republic). Then, neat-resin systems will be introduced and characterized in order to compare the veils route to the conventional route using thethermoplastic premixed in the epoxide as powder (the latter will be called prepreg route). Finally, these systems will be transferred to the composite laminates' study, in order to evaluate the final complex systems with the addition of carbon fibers.

6.1 Materials

6.1.1 Epoxy resins

DGEBA

The epoxy resin DGEBA is a diglycidly ether of Bisphenol A. It is a difunctional epoxy resin provided by Hunstman (Araldite GY 240) and it has been used as received. In figure 6:1 the DGEBA structure is shown.
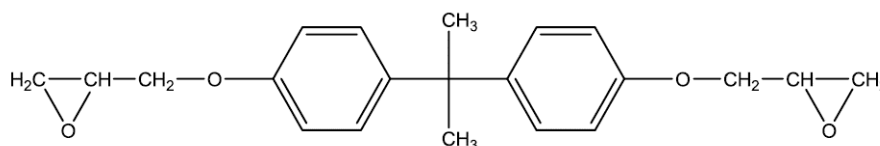
Figure 6:1 DGEBA structure formula

The molecular weight is 330 g/mol and the epoxy equivalent weight is 165 g/mol. It has a low viscosity and is liquid at ambient temperature but tends to crystallize after some time, becoming a white solid. If heated at 50°C it returns to its viscous state.

TGAP

The epoxy resin N,N-diglycidyl-p-aminephenol (TGAP) is commercially supplied by Shell Chemical Company. At room temperature is a viscous liquid with amber color. It is a trifunctional resin synthesized starting from p-aminephenol and its chemical structure is shown in figure 6:2.
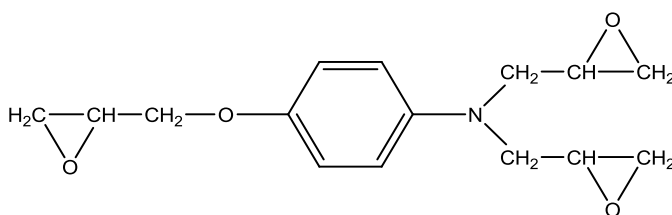
Figure 6:2 TGAP structure formula

TGAP has a molecular weight of 277 g/mol with an equivalent epoxy weight of 92.3 g/mol.

6.1.2 Tougheners

coPES9k and coPES20k

The thermoplastics used as tougheners are two copolyetherether sulfones that have been synthesized in laboratory [1]. They are random copolymers, which have been functionalised with amine end-groups so that can react and chemically link to the epoxy network. coPES9k average molecular weight is around 9000 Da, while coPES20k average molecular weight is around 20000 Da. They have been used after drying at 45°C. The structure is shown in figure 6:3.
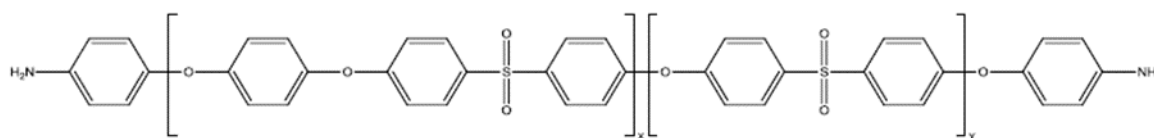
Figure 6:3 Structural formula of coPESs

Virantage 30500 RP and 10200 RP

Two polyethersulfones sold by Solvay were selected for the scale-up of the electrospinning process: Virantage[®] 30500 RP and Viratange[®] 10200 RP. Both of them are PESs but differ for the average molecular weight and for chemistry of the reactive end-groups. Main properties are reported in table 6:1.

Table 6:1 Main properties of Viratange[®] polymers

Virantage[®] Grade	M_{GPC} [g/mol *1000]	End Groups
30500 RP	45	-NH$_2$
10200 RP	14	-OH

OpteSTAT™ NC PES 6010

OpteSTAT™ master batches are Ovation Polymers' line of nano-compounds based on carbon nanotubes (figure 6:). The proprietary dispersion technology debundles and disentangles carbon nanotubes without compromising their integrity. OpteSTAT™ compounds exhibit good conductivity at minimal nanotube loadings, achieving exceptional cleanliness and physical property retention. OpteSTAT™ NC PES 6010 is Polyether Sulfone-based carbon nanotube compound. The material resistivity can be tailored to the application, while retaining the physical and thermal properties of the base polymer. Target applications include components of disk drives, business machines or other electronic assemblies where ESD control is required.
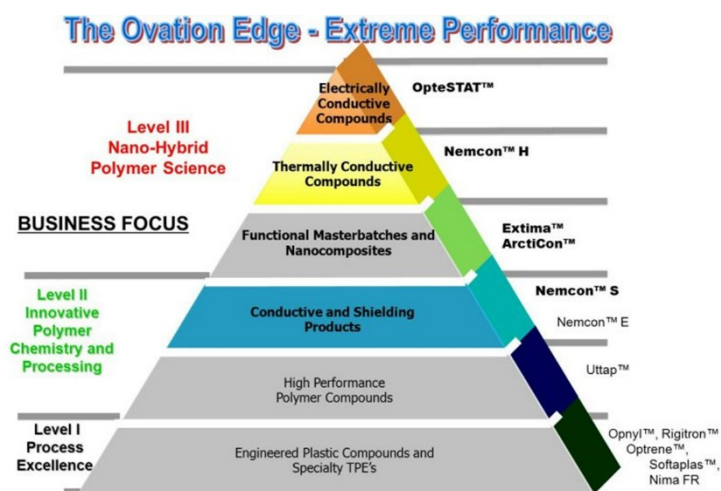
Figure 6:4 Ovation Polymers' compounds, OpteSTAT at the top of technology

6.1.3 Crosslinkers

MDEA

The crosslinker used in this work is the 4-4'-metilenebis(2,6-dietil)-aniline. It is an aromatic diamine available by Lonza Chemical. It is a white cristallin solid at ambient temperature. Its meltin point is about 88-90°C and its structure is reported in figure 6:5.
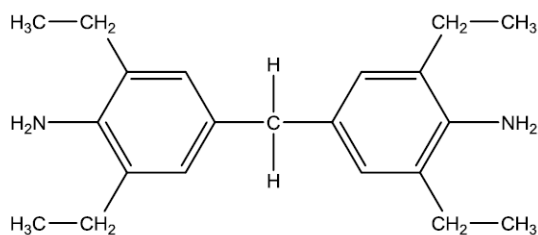
Figure 6:5 MDEA structure formula

MDEA molecular weight is 310.5 g/mol while its amine equivalent weight is 76.625 g/mol. At room temperature it is partially soluble in the epoxy resins, at 80°C it is totally soluble and allows to achieve homogenous solutions.

6.1.4 Nanofillers

Multi-Wall Carbon Nanotube

Multi-wall carbon nanotubes Graphistrenght TM C100 (provided by Arkema) have been used. Their properties are reported in table 6:2.

Table 6:2 Graphistrenght TM C100

Description		CCVD multi-wall carbon nanotubes
Appearance		Black powder
Powder characteristics	Apparent density	50-150 kg/m^3
	Mean agglomerate size	200-500 μm
	Weight loss at 105°C	<1%
MWCNT characteristics	C content	>90wt%
	Free amorphous carbon	Not detectable (SEM/TEM)
	Mean number of walls	5-15
	Outer mean diameter	10-15 nm
	Length	0.1-10 μm

As a consequence of their outstanding mechanical properties, and electrical and thermal conductivities, high-quality Graphistrengt TM C100 multi-wall carbon nanotubes can be used in a variety of applications, such as: high-performance electrostatic dissipative plastic parts and coatings, high-strength thermosetting composites, high-strength rubbery materials, and electrode materials for batteries, super-capacitors, and fuel cells. GraphistrengtTM C100 can also be used as catalyst support in different industrial chemical processes.

Nanosilica

CAB-O-SIL® M-5, an untreated fumed silica provided by Cabot, was used. It is a synthetic, amorphous, colloidal silicon dioxide that is generally regarded as unique in industry because of its unusual particle characteristics (table 6:3). CAB-O-SIL fumed silica's extremely small particle size, its enormous surface area, its high purity, and its chain-forming tendencies set it apart in a class of its own. CAB-O-SIL fumed silica is a light, fluffy powder that is white in appearance and is used in many applications and a variety of industries.

Table 6:3 Properties of CAB-O-SIL® M-5

BET Surface Area	$200 m^2/g$
pH (4% aqueous slurry)	3,7-4,3
Loss on heating	<1,5% max
Loss on ignition (@1000°C)	<2wt%
Specific gravity	$2,2 g/cm^3$
X-ray form	Amorphous
Average particle lenght	0,2-0,3 μm

POSS

Polyhedral oligomeric silsesquioxanes (POSSs) were laboratory synthetized [2]. POSSs are hybrid inorganic/organic compounds of general formula (RSiO1.5)n, where R = H or organic substituents directly linked to silicon cage and n = 6, 8, 10 or 12 (figure 6:6).
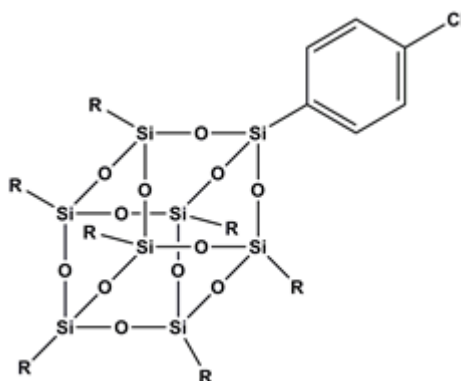
Figure 6:6 Molecular structure of ph,hib-POSS

POSSs can be well used as drug materials and imaging agents, since these materials have potential advantages such as their biodegradation, thermodynamic stability and biocompatibility [3]. The increasing importance of POSSs is also due to their employment as fillers or end-linking agents in the production of polymer and shape memory polymers nanocomposites, materials that have acquired application relevance in a variety of technological fields ranging from medical to aeronautics [4].

Zinc Oxide

The zinc oxide used in this work was purchased from Sigma Aldrich, with a specific density of 5.61 g/cm3. Nanostructured ZnO materials have received broad attention due to their distinguished performance in electronics, optics and photonics. From the 1960s, synthesis of ZnO thin films has been an active field because of their applications as sensors, transducers and catalysts. ZnO is a key technological material.

In addition, ZnO is a wide band-gap (3.37 eV) compound semiconductor that is suitable for short wavelength optoelectronic applications.

Carbon Black

Carbon black is a material that has been known and produced since olden days but only found its widespread manufacture and use in the last century when it was discovered that when mixed into rubber it improves its mechanical properties. Carbon black is virtually pure elemental carbon in the form of colloidal particles that are produced by incomplete combustion or thermal decomposition of gaseous or liquid hydrocarbons under controlled conditions. Its physical appearance is that of a black, finely divided powder. Its use in tires, rubber and plastic products, printing inks and coatings is related to properties of specific surface area, particle size and structure, conductivity and color.

6.2 Samples preparation

6.2.1 Electrospinning of thermoplastic nanofibers

The two thermoplastics used as tougheners were solubilized in a mix of N,N-dimethylformamide (DMF) and tholuen as electropinning solvent, with a 1:1 volume ratio. The choice of tholuen together with DMF relies on the necessity of having an enough volatile

solvent during the electrospinning process. coPES 20k was solubilized with a concentration of 0.25 g/ml; PES 9K with a concentration of 0.5 g/ml, in order to obtain as similar as possible viscosities. The solutions have been magnetically stirred while heating until polymers were completely solubilized. After obtaining homogenous solutions, nanofillers were added into the solution and dispersed by using an ultrasound probe (UP 200 Ht by Hielscher).

An electrospinning apparatus by IME Technologies (figures 6:7 and 6:8) was used. It consists of a syringe that is filled with the polymer solution, a high voltage source and a grounded conductive collector. In addition, a metering syringe pump is used to control the flow rate of the polymer solution.

Figure 6:7 Electrospinning apparatus by IME Technology
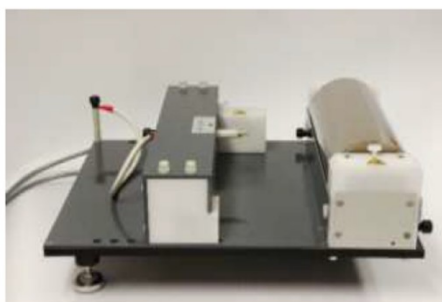
Figure 6:8 Rotating collector

6.2.2 Neat-resins preparation

Cured neat-resin samples, following two preparation procedures which replicates the prepreg and the soluble veil routes, were prepared. These samples were studied to understand the effect of the neat matrix without carbon fiber reinforcements. For prepreg matrices, the uncured blends, obtained by predissolving thermoplastic powder in the epoxy resin, were poured into aluminum dishes and degassed for 30 min at 130 °C. Next, the temperature was increased by 2 °C/min up to 180 °C and held at that value for 3 h. At the end of the curing cycle, the samples were left to cool down slowly at room temperature. For soluble veil matrices, a selected amount of electrospun veils were laid up in the aluminum dish, after which the unmodified epoxy resin (preheated at 130°C for 5 min) was poured on the veils to impregnate them. The dish was finally transferred to the oven, which was set at 130°C and kept at this temperature for 30 min. The oven temperature was increased by 2 °C/min up to 180 °C and held at that value for 3 h. At the end of the curing cycle, the samples were left to cool down slowly at room temperature.

The electrospun membranes of coPES9k and coPES20k were laid in a dish and impregnated with the resin. After that, the cure cycle began. It consisted of three phases: in the first one the membranes-resin system is put in a oven at 130°C for 10 minutes in order to operate the membrane dissolution into the resin. It is maintained at the same temperature for other 30 minutes and then the temperature is increased at 180°C for 180 minutes. The entire neat resin preparation procedure is shown in figure 6:9.
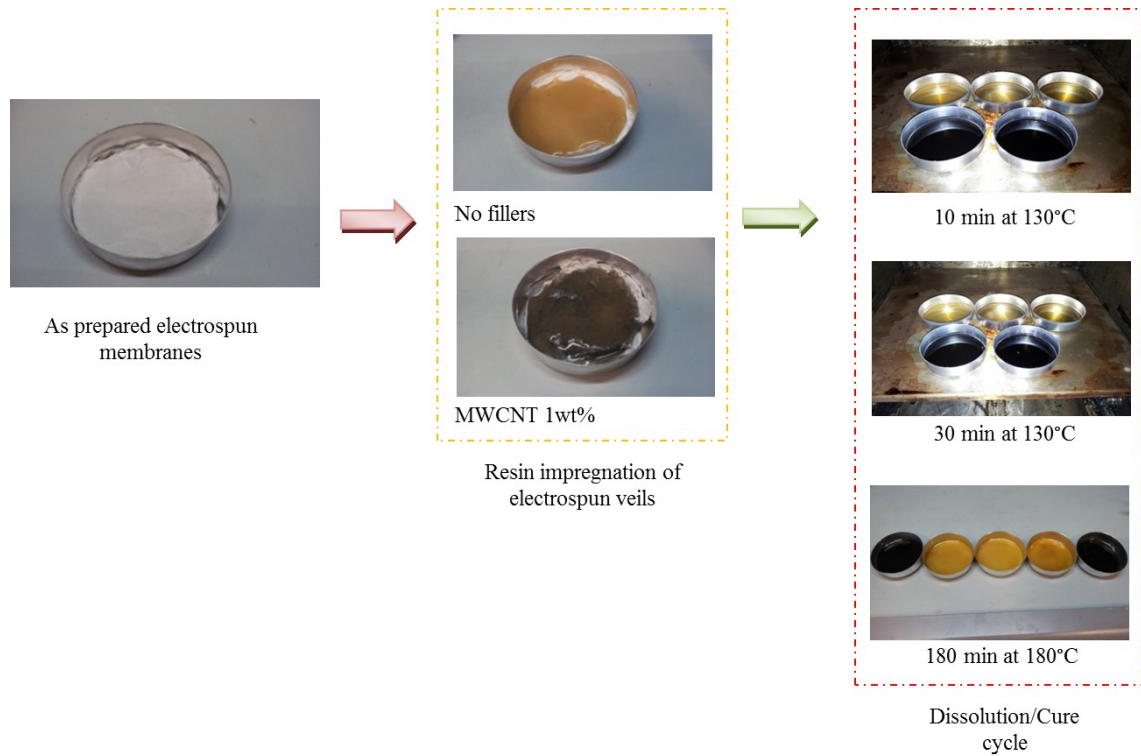
Figure 6:9 Main steps of neat resins preparation

6.2.3 Composite laminates preparation

Six layers of dry carbon fabrics with veils electrospun onto were stacked on a steel plate. An adhesive silicone tape was placed around the perimeter of the layered stack to provide a proper seal and a flexible vacuum bag was placed on top. An inlet tube and an outlet tube were placed inside the vacuum bag. The inlet tube was connected by a valve to a pot filled with unmodified epoxy resin while the outlet tube was connected to a vacuum pump. The vacuum was applied while the inlet valve was closed in order to compact the layers and to remove excess air. Based on the neat-reasin samples curing cycle, all the stacked layers were placed in an oven preheated to 130°C. The epoxy resin was vacuum infused into the stacked layers, which was maintained at 130 °C under a constant vacuum (75 cmHg). The temperature was kept at 130°C for 30 min and then increased by 2°C/min up to 180 °C and held at that value for 3 h.

A similar cure cycle was used for the prepreg composites. However, in this case the epoxy/coPES blends were used to impregnate the carbon fabrics which were then laid on the steel plate. The obtained stack was compacted using a vacuum bag at room temperature for 15min. The stack was placed in an oven preheated to 130°C for 30 min. The temperature was then increased to 180°C and held at that value for 3 h.

6.3   Characterization techniques

Mechanical, thermos-mechanical and morphological properties of the samples were carried out.

6.3.1 Dynamic Mechanical Analysis

Dynamic Mechanical Analysis, otherwise known as DMA, is a technique where a small deformation is applied to a sample in a cyclic manner. This allows the materials response to stress, temperature, frequency and other values to be studied.

At the beginning the DMA tests were developed for structural investigations on metals. Today it is one of the most efficient technique used in order to study polymeric materials since the value of a DMA test is very significant allowing a large number of information on the sample under consideration. The value of the modulus below the Tg depends from molecular orientation and crystallinity. The transition that occurs can be related to the polymer structure and can be very useful studying multicomponent mixtures.

In a dynamic mechanical test it is the sample stiffness and loss that are being measured. The sample stiffness will depend upon its Modulus of Elasticity and its geometry or shape. The modulus measured will depend upon the choice of geometry, Young's (E*) for tension, compression and bending, Shear (G*) for torsion. The modulus is defined as the stress per

unit area divided by the strain resulting from the applied force. Therefore it is a measure of the material's resistance to deformation, the higher the modulus the more rigid the material is.

The definition given above for modulus does not take time into account. For materials that exhibit time-invariant deformation, for example metals and ceramics at room temperature, any measurement of strain will lead to a constant value of modulus. However for materials that exhibit time-dependent deformation, such as polymers, the quoted modulus must include a time to be valid. This is where dynamic mechanical testing offers a powerful advantage. Dynamic mechanical testers apply a periodic stress or strain to a sample and measure the resulting strain or stress response. Due to the time-dependent properties of polymers the resultant response is out-of-phase with the applied stimulus. The Complex Modulus M* is defined as the instantaneous ratio of the stress/ strain. To understand the deformational mechanisms occurring in the material this is resolved into an in-phase and out-of-phase response. This is equivalent to a complex number (see below), where M' is the in-phase or elastic response this being the recoverable or stored energy.

DMA works by applying a sinusoidal deformation to a sample of known geometry. For an applied stress varying sinusoidally with time, a viscoelastic material will also respond with a sinusoidal strain for low amplitudes of stress. The strain of a viscoelastic body is out of phase with the stress applied, by the phase angle, δ. This phase lag is due to the excess time necessary for molecular motions and relaxations to occur. Dynamic stress, σ, and strain, ε, given as:

$$\sigma = \sigma_0 \sin{(\omega t + \delta)}$$

$$\varepsilon = \varepsilon_0 \sin{(\omega t)}$$

where ω is the angular frequency. Using this notation, stress can be divided into an "in-phase" component ($\sigma_0 \cos\delta$) and an "out-of-phase" component ($\sigma_0 \sin\delta$) and rewritten as,

$$\sigma = \sigma_0 \sin(\omega t)\, cos\delta + \sigma_0 \cos(\omega t)\, sin\delta$$

Dividing stress by strain to yield a modulus and using the symbols E´ and E´´ for the in-phase (real) and out-of-phase (imaginary) moduli yields:

$$\sigma = \varepsilon_0 E'\, \sin(\omega t) + \varepsilon_0 E''\, \cos(\omega t)$$

$$E' = \frac{\sigma_0}{\varepsilon_0} cos\delta$$

$$E'' = \frac{\sigma_0}{\varepsilon_0} sin\delta$$

$$\varepsilon = \varepsilon_0 e^{i\omega t}$$

$$\sigma = \sigma_0 e^{i\omega t}$$

$$E^* = \frac{\sigma}{\varepsilon} = \frac{\sigma_0}{\varepsilon_0} e^{i\delta} = \frac{\sigma_0}{\varepsilon_0}(cos\delta + isin\delta) = E' + iE''$$

The last equation shows that the complex modulus obtained from a dynamic mechanical test consists of "real" and "imaginary" parts.

The real (storage) part, E' describes the ability of the material to store potential energy and release it upon deformation (figure 6:10). So, for a perfect elastic material $E^* = E'$, while for a total viscous material $E^* = E''$
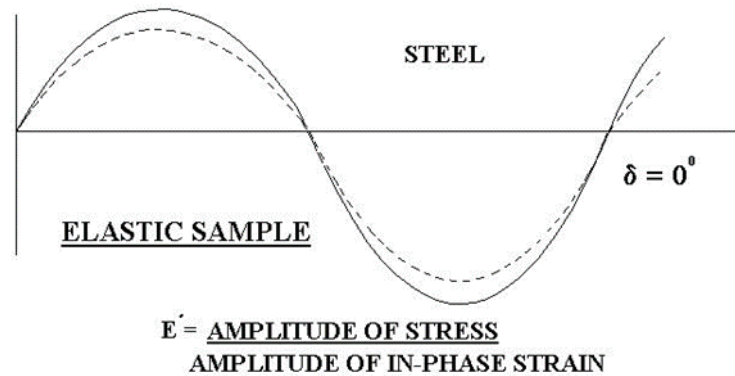
Figure 6:10 Out phase component of a viscous system

The imaginary (loss) portion, E'' is associated with energy dissipation in the form of heat upon deformation (figure 6:11).
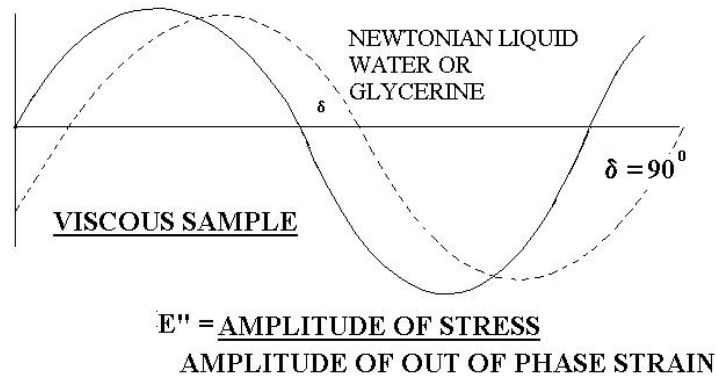
Figure 6:11 Complex component of a viscoelastic system

Figure 6:12 reports the typical behavior of visco-elastic materials like polymers.
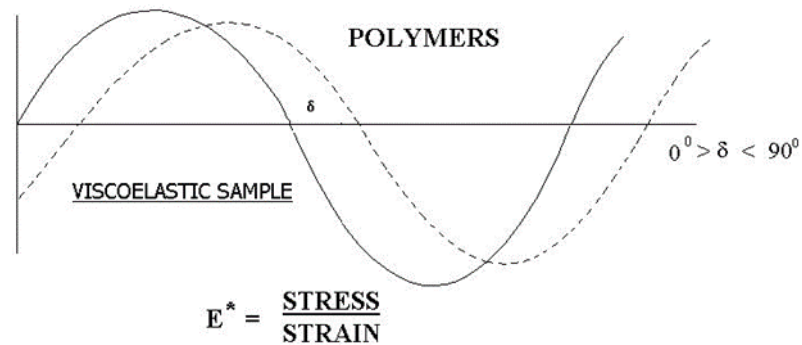
Figure 6:12 Representation of the visco-elastic behavior of polymers

The above equation is rewritten for shear modulus as:

$$G^* = G' + iG''$$

where G' is the storage modulus and G'' is the loss modulus. The phase angle δ (figure 6:13) is given by:

$$tan\delta = \frac{G''}{G'}$$
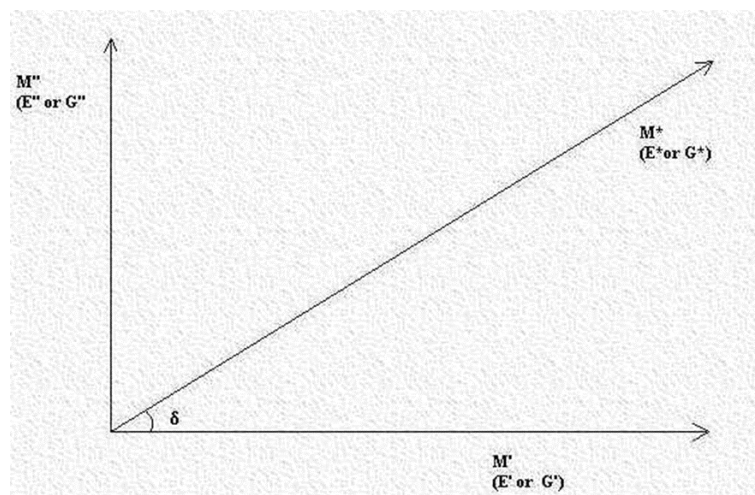
Figure 6:13 Geometric graphic description of phase angle δ

The storage modulus is often times associated with "stiffness" of a material and is related to the Young's modulus, E. The dynamic loss modulus is often associated with "internal friction" and is sensitive to different kinds of molecular motions, relaxation processes, transitions, morphology and other structural heterogeneities. Thus, the dynamic properties provide information at the molecular level to understanding the polymer mechanical behavior.

Table 6:4 lists the experimental methods used in dynamic mechanical testing. Of the experiments summarised below thermal scan mode (method 5) is the most commonly used technique, especially in analytical laboratories. Here the typical use is to look for differences in materials' batches, thermal history, different grades, etc. The stepped isotherm experiment of method 6 is mainly used in studies involving detailed mechanical property determination for either structural or vibrational analysis. Such tests are only normally carried out in R&D environments. Methods 1, 2 and 3 can be regarded as "quick" experiments, taking at the most 30 minutes and more typically a few minutes. Method 4 is application specific.

Table 6:4 Lists of the experimental methods used in dynamic mechanical analysis

No	Temperature mode	Frequency method	Typical use & comments
1	None	Single or sweep	Modulus and tan d at RT.
2	Constant isotherm	Single or sweep	Modulus and tan d at T
3	Conisothermstant	Single	Strain sweep at T
4	Rapid ramp, isotherm	Sweep	Cure studies, crystallisation kinetics
5	Thermal scan	Single or multiple	Typical polymer fingerprint, Tg
6	Stepped Isotherms	Sweep (full range)	Full data set, better T accuracy

The thermal scan method is the one used in this work as it provides more relevant DMA data.

The temperature range scanned changes depending to the sample under consideration with a speed of 2°C/min. The frequencies used are 1 Hz and 10 Hz. Measures were conducted using a TRITECH 2000 from TRITON Technology.

6.3.2 Double Cantilever Beam Testing

The following paragraph is taken from the book *"Mechanical testing of advanced fibre composites"*, chapter 9, edited by J.M. Hodgkinson.

Laminated fiber-reinforced composites made of high strength fibers in a relatively weak matrix material are susceptible to delamination (i.e. separation of the layers). A typical quasi-

isotropic carbon-fiber reinforced epoxy laminate has an in-plane tensile strength of 700-1200 MPa, dependent on precise layup, but through-thickness tensile strength can be as low as 50 MPa and the through-thickness shear strength is also relatively low. It is clear therefore that through-thickness stresses in a component may give rise to the initiation of delamination if they exceed the through-thickness strength. The subsequent propagation of a delamination will, however, be controlled not by the through-thickness strength but by the interlaminar fracture toughness of the composite material. Interlaminar fracture toughness of composites is normally expressed in terms of the critical energy release rate, which is usually represented by the symbol G_c. the critical energy release rate is the energy consumed by the material as the delamination front advances through a unit area. The units commonly used for G_c are Juoles per square meter or Newtons per meter. Interlaminar fracture toughness can be measured in several modes or in a combination of modes shown in figure 6:14 or in a combination of these modes.
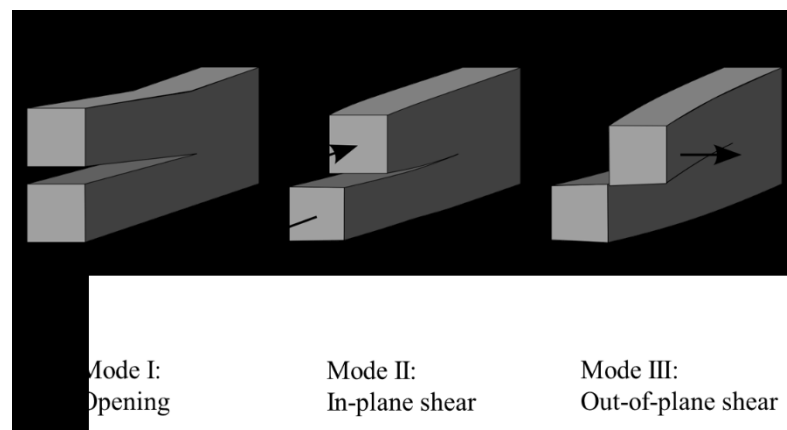
Figure 6:14 Schematics of the basic modes of crack loading: mode I (opening), mode II (shear), mode III (tearing)

In isotropic materials, toughness values are usually only quoted for the mode I case. For these materials the toughness is lowest in this mode, so that even if a crack is loaded to drive the growth in mode II, as shown in figure 6:15a , the crack will deviate and grow in a direction which will be pure mode I, as shown in figure 6:15b. In laminated composites, however, the

delamination can be constrained to lie between the strong fiber-reinforced layers, so that it is possible to have delamination growth in all of the three modes shown in figure 6:14.
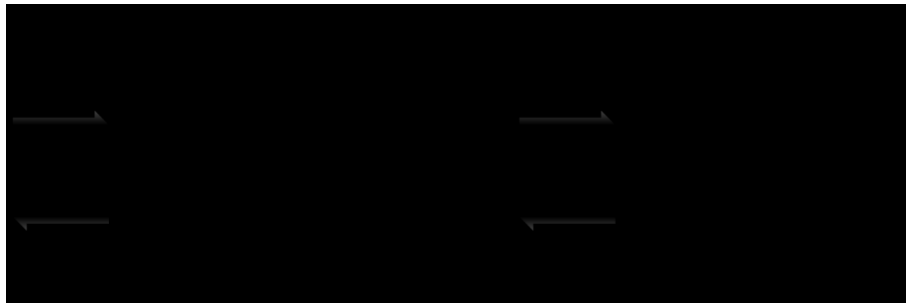
Figure 6:15 Crack propagation in isotropic materials

There has been considerable research into the development of suitable test methods for the measurements of interlaminar toughness. Standard organizations such as the American Society for Testing and Materials (ASTM), the European Structural Integrity Society (ESIS) and the Japanese Industry Standards (JIS) have been evaluating some of the proposed methods. The test methods for measuring interlaminar fracture toughness generally involve beam-type-specimens and have been developed almost exclusively for application to unidirectional laminates, with the delamination growth in the direction of the fibers. The strategy in all of these tests requires measurement of the load and applied displacement at which a delamination of known length grows. For some specimens the growth is stable, so that data can be collected at many points during the delamination growth. In other specimens, the delamination growth is unstable, and the critical load and applied length can only be measured for the initial delamination length. From the load-displacement.crack length data it is then possible to determine the interlaminar toughness.

For mode I the commonest test uses the double cantilever beam (DCB) specimen shown in figure 6:16 . test standards using this specimens have been produced by both JIS and ASTM and limited to the testing of uniderctional laminates. Similarly, ESIS has published a protocol for DCB testing.
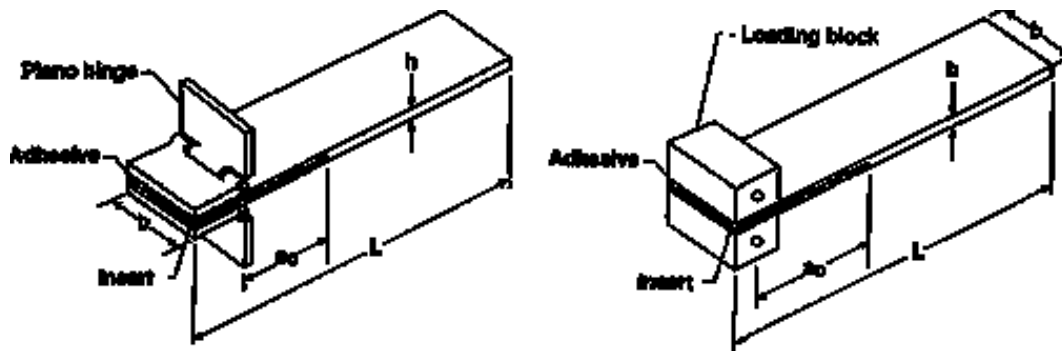
Figure 6:16 Double cantilever beam (DCB) specimen geometry with end-blocks (right) and piano hinges (left)

For mode II there are two methods which have received most attention; these are the three-point loaded end-notched flexure (ENF) test shown in figure 6:17, standardized by JIS, and the end-loaded split (ELS). Both of these test methods are currently being evaluated in "round-robin" trials by standard organization, with ESIS having published a protocol for the ELS test.
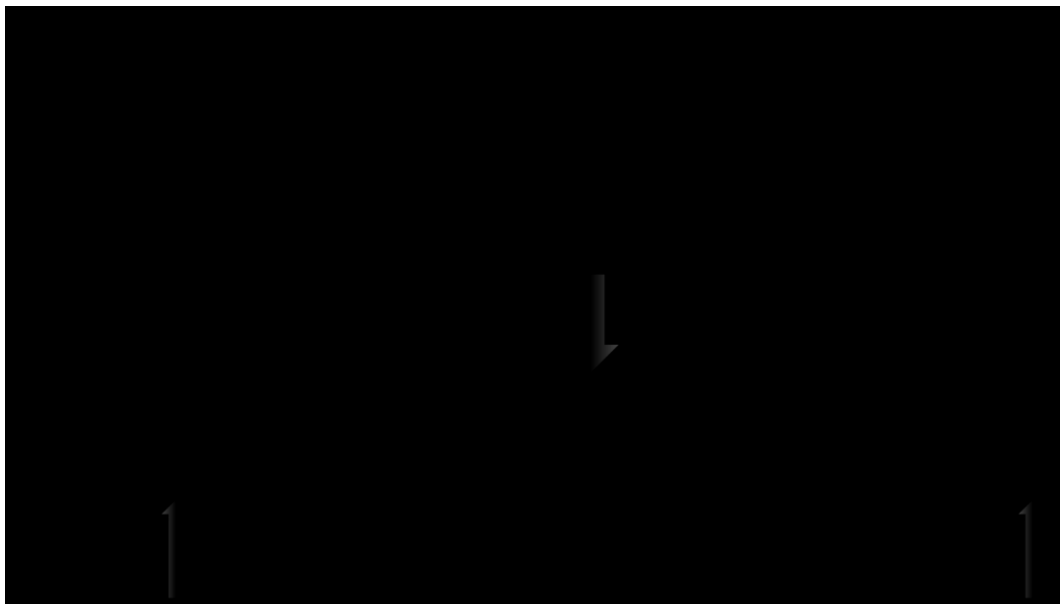
Figure 6:17 End-notched flexure)ENF) mode II test specimen in the unloaded (a) and loaded (b) conditions

Other methods have also been proposed. However, there remains some concern over the variability of measured mode II toughness data and the dependence on delamination insert thickness and the presence of any pre-cracking. In view of the difficulties surrounding the

101

measurement of G_{iic} and observations the many failures in composite structures involve mixed mode I/II fracture, with mode I component being dominant, it has been suggested that mode I and mixed mode I/II toughness data may prove to be the most useful for prediction of delamination failure of practical composite structures.

In the following lines, mode I interlaminar toughness is described; G_{ic} measurements were recorded according to the ASTM D5528 standard. Linear elastic behavior is assumed in the calculation of G_{ic} used in this test method. This assumption is valid when the zone of damage or nonlinear deformation at the delamination front, or both, is small relative to the smallest specimen dimension, which is typically the specimen thickness for the DCB test. In the DCB test, as the delamination grows from the insert, a resistance-type fracture behavior typically develops where the calculated G_{ic} first increases monotonically, and then stabilizes with further delamination growth. In this test method, a resistance curve (R curve) depicting G_{ic} as a function of delamination length will be generated to characterize the initiation and propagation of a delamination in a unidirectional specimen (figure 6:18).
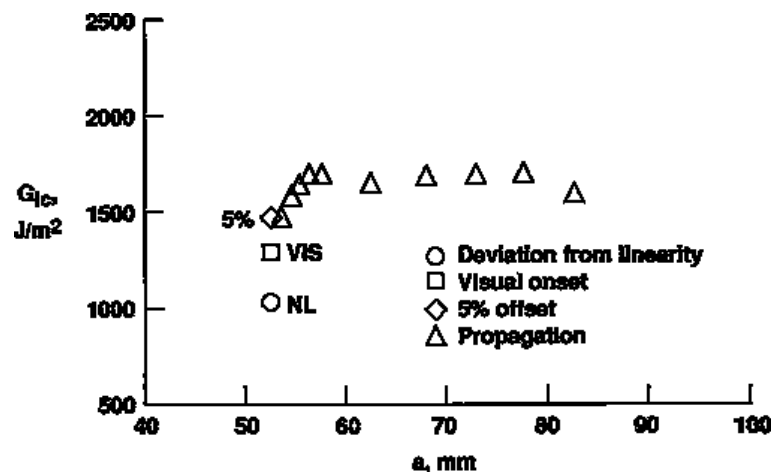
Figure 6:18 Delamination Resistance Curve (*R* Curve) from DCB Test

The principal reason for the observed resistance to delamination is the development of fiber bridging. This fiber bridging mechanism results from growing the delamination between two

0° unidirectional plies. Because most delaminations that form in multiply laminated composite structures occur between plies of dissimilar orientation, fiber bridging does not occur. Hence, fiber bridging is considered to be an artifact of the DCB test on unidirectional materials. Therefore, the generic significance of GIc propagation values calculated beyond the end of the implanted insert is questionable, and an initiation value of G_{ic} measured from the implanted insert is preferred. Because of the significance of the initiation point, the insert must be properly implanted and inspected. A nonadhesive insert (a PTFE film is recommended) shall be inserted at the midplane of the laminate during layup to form an initiation site for the delamination as shown in figure 6:16. The film thickness shall be no greater than 13 μm . Specimens should not be precracked before testing.

Three definitions for an initiation value of G_{ic} have been evaluated during round-robin testing [5] These include G_{ic} values determined using the load and deflection measured (1) at the point of deviation from linearity in the load-displacement curve (NL), (2) at the point at which delamination is visually observed on the edge (VIS) measured with a microscope and (3) at the point at which the compliance has increased by 5 % or the load has reached a maximum value (5 %/max) (see Section 11). The NL G_{ic} value, which is typically the lowest of the three G_{ic} initiation values, is recommended for generating delamination failure criteria in durability and damage tolerance analyses of laminated composite structures. All three initiation values can be used for the other purposes. However, physical evidence indicates that the initiation value corresponding to the onset of nonlinearity (NL) in the load versus opening displacement plot corresponds to the physical onset of delamination from the insert in the interior of the specimen width. In round-robin testing of AS4/PEEK thermoplastic matrix composites, NL GIc values were 20 % lower than VIS and 5 %/max values [5].

Delamination growth may proceed in one of two ways: (1) by a slow stable extension or (2) a run-arrest extension in which the delamination front jumps ahead abruptly. Only the first type

103

of growth is of interest in this test method. An unstable jump from the insert may be an indication of a problem with the insert. For example, the insert may not be completely disbonded from the laminate, or may be too thick, resulting in a large neat resin pocket, or may contain a tear or fold. Furthermore, rapid delamination growth may introduce dynamic effects in both the test specimen and in the fracture morphology. Treatment and interpretation of these effects is beyond the scope of this test method. However, because crack jumping has been observed in at least one material in which the guidelines for inserts were not violated, the specimens are unloaded after the first increment of delamination growth and reloaded to continue the test. This procedure induces a natural Mode I precrack in the DCB specimen. The first propagation G_{ic} value is referred to as the Mode I precrack G_{ic}.

Toughness values measured on unidirectional composites with multiple-phase matrices may vary depending upon the tendency for the delamination to wander between various matrix phases. Brittle matrix composites with tough adhesive interleaves between plies may be particularly sensitive to this phenomenon resulting in two apparent interlaminar fracture toughness values: one associated with a cohesive-type failure within the interleaf and one associated with an adhesive-type failure between the tough polymer film and the more brittle composite matrix.

Nonunidirectional DCB configurations may experience branching of the delamination away from the midplane through matrix cracks in off-axis plies. If the delamination branches away from the midplane, a pure Mode I fracture may not be achieved as a result of the structural coupling that may exist in the asymmetric sublaminates formed as the delamination grows. In addition, nonunidirectional specimens may experience significant anticlastic bending effects that result in nonuniform delamination growth along the specimen width, particularly affecting the observed initiation values.

Woven composites may yield significantly greater scatter and unique R curves associated with varying toughness within and away from interlaminar resin pockets as the delamination grows. Composites with significant strength or toughness through the laminate thickness, such as composites with metal matrices or 3D fiber reinforcement, may experience failures of the beam arms rather than the intended interlaminar failures.

The DCB measurements carried out in the present project were performed at the Advanced Composite Centre for Innovation and Science (ACCIS) of the University of Bristol, UK, under the supervision of Prof. Fabrizio Scarpa, Professor of Smart Materials & Structures at the Faculty of Engineering.

6.3.3 Scanning Electron Microscopy

The scanning electron microscopy (SEM) works with a focused beam of high-energy electrons to generate a variety of signals at the surface of solid specimens. The signals that derive from the electron-sample interactions reveal informations on the sample including external morphology (texture), chemical composition, and crystalline structure and orientation of materials making up the sample. In most applications, data are collected over a selected area of the surface of the sample, and a 2-dimensional image is generated that displays spatial variations in these properties. The resolution of a SEM is about 5 nm but some models exist with a 1nm resolution.

Accelerated electrons in an SEM carry significant amounts of kinetic energy, and this energy is dissipated as a variety of signals produced by electron-sample interactions when the incident electrons are decelerated in the solid sample. These signals include secondary electrons (that produce SEM images), backscattered electrons (BSE), diffracted backscattered electrons (EBSD that are used to determine crystal structures and orientations of minerals),

photons (characteristic X-rays that are used for elemental analysis and continuum X-rays), visible light (cathodoluminescence-CL), and heat. Secondary electrons and backscattered electrons are commonly used for imaging samples: secondary electrons are most valuable for showing morphology and topography on samples and backscattered electrons are most valuable for illustrating contrasts in composition in multiphase samples (i.e. for rapid phase discrimination). X-ray generation is produced by inelastic collisions of the incident electrons with electrons in discrete orbitals (shells) of atoms in the sample. As the excited electrons return to lower energy states, they yield X-rays that are of a fixed wavelength (that is related to the difference in energy levels of electrons in different shells for a given element). Thus, characteristic X-rays are produced for each element in a mineral that is "excited" by the electron beam. SEM analysis is considered to be "non-destructive"; that is, x-rays generated by electron interactions do not lead to volume loss of the sample, so it is possible to analyze the same materials repeatedly. inside the fibres.

It has been said that in a SEM different signal are produced due to the electron-sample interaction. In particular, when a high-energy electron beam hits a specimen, X-rays characteristic of the atoms in the specimen are generated within the region illuminated. This allows the possibility of microanalysis, that is, the chemical analysis of a small amount of material, or a small part of a larger specimen. If we can measure the energy of the X-rays (or equivalently their wavelength, since they are related by Planck's constant, $E = hc/\lambda$ or specifically $EkV = 12.4/\lambda Angstroms$), then we can immediately tell qualitatively which elements are present in the part of the specimen under investigation. If we measure X-ray intensities, we also get an immediate rough idea of how much of each element is present (EDX Analysis).

6.3.4 Hot-Stage Microscopy

The optical microscope, often referred to as the "light microscope", is a type of microscope which uses visible light and a system of lenses to magnify images of small samples. Basic optical microscopes can be very simple, although there are many complex designs which aim to improve resolution and sample contrast. Historically optical microscopes were easy to develop and are popular because they use visible light so that samples may be directly observed by eye.

There are two basic configurations of the conventional optical microscope: transmission or reflection. In the first case the microscope allows to see the details of the sample using light transmitted through the same, from a small built-in lamp or routed through a mirror from an external source. It is used widely in educational, scientific, technical and industrial applications. In the first historical models daylight or light from a candle or oil lamp was used. In current models the used source of light is a halogen lamp. Note that in compound microscopes the observed image is reversed. In the case of reflection microscope, instead, the illumination comes from the top, via different systems.

In this work a transmission optical microscope, Optika, was used in order to analyze the dissolution of the thermoplastic fibres in two different kinds of resin: DGEBA and TGAP.

6.3.5 ANOVA and DoE Analysis

The study of fibers production by electrospinning is important to optimize the process. In fact, as it has been said before, final results depend on lots of variables and factors. In order to optimize and characterize the process, two analysis were undertaken: the Analysis of Variance (ANOVA) and the Design of Experiment (DoE).

The principal aims of the design of experiments are the following:

- To characterize the problem defining the input parameters that principally influence the outputs;

- To optimize the problem by acting on such parameters, determined in the characterization phase, in order to determine the "optimum region" where the obtained outputs are the best ones possible.

ANOVA

Analysis of variance (ANOVA) is a statistical technique that is intended to analyze variability in data during an experiment. Two principal sources of variability exits:

- Sources of systematic variations that depend on the person that conducts the experiment;

- Sources of random variations (intrinsic stochastic variability, environmental conditions, measurement errors).

The differences eventually observed in the samples implies that it is to be analyzed from an inferential point of view. It is important to understand whether they are significant, this means if such differences exist among population or they are results of chance.

From a mathematics point of view, two opposite hypothesis are formulated: the null one, H_0, and the alternative one, H_1. The first one states that all population or treatment means are equal while the second one states that the members of at least one pair are not equal.

The null hypothesis can be verified using a statistic test, F, from which is possible to calculate the so called p-value. It indicates if the H_0 hypothesis can be accepted or not. Very low p-value states that, considering the H_0 hypothesis, the result observed is anomalous and so the H_0 hypothesis has to be rejected and the H_1 must be used.

Design of Experiment

The Design of experiment (DoE) is a method used in order to obtain the maximum level of information using the minimum number of sources.

The steps involved in a DoE method are:

- Problem identification and formulation;
- Factors choice, levels and intervals;
- Output variable selection;
- Experimental plan choice;
- Experiment execution;
- Statistic analysis of data;
- Conclusions.

In these steps ,, it is important to define:

- The output variable;
- Factor: controlled variable;
- Factor level: value assumed from each factor.

Possible experiment goals can be:

- Determine which variable has the most influence on the output;
- Determine which values can be assigned to the controlled variables in order to obtain the desired output;
- Determine which values can be assigned to the controlled variable in order to obtain minimum variation of the output variables.

6.4   Results and discussions

In this paragraph the study and characterization of the samples will follow by this order: nanofibers veils, neat-resin samples and composite laminate samples.

6.4.1 Electrostpun fibres characterization

ANOVA and DoE analysis

The goal of DoE analysis was to understand which parameters have the most influence on the fibre dimensions. The experiment plan is reported in table 6:5.

Table 6:5 DoE plan

Factor	Levels	Values	Output
Concentration [g/ml]	3	0.15; 0.25; 0.35	Average diameter, Areal density
d.d.p [kV]	3	22; 25; 28	Average diameter, Areal density
Gap [cm]	3	14; 17; 20	Average diameter, Areal density

Using the Minitab software, the Analysis of Variance for every factor was done. The observed output was the average fibre diameter and the areal density. A p-value < 0.05 (tolerance level sets) was obtained only for the concentration factor. This result indicates that the only factor that influences both outputs is the solution concentration. In fact, if it is increased the average fibre diameter also increases. As for the areal density, it also increases along with the solution concentration. All this considerations are shown in the figure 6:19 and 6:20.
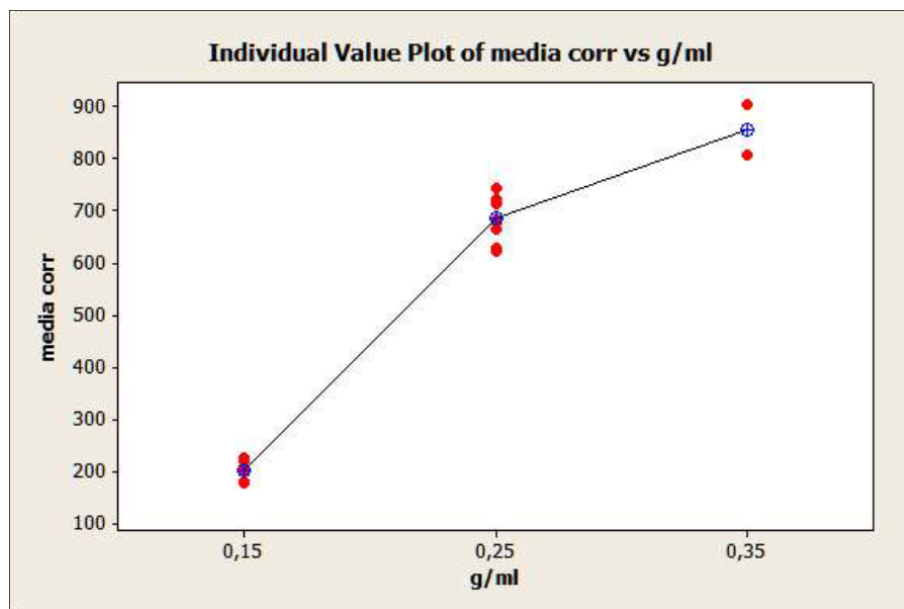
Figure 6:19 Average diameter output
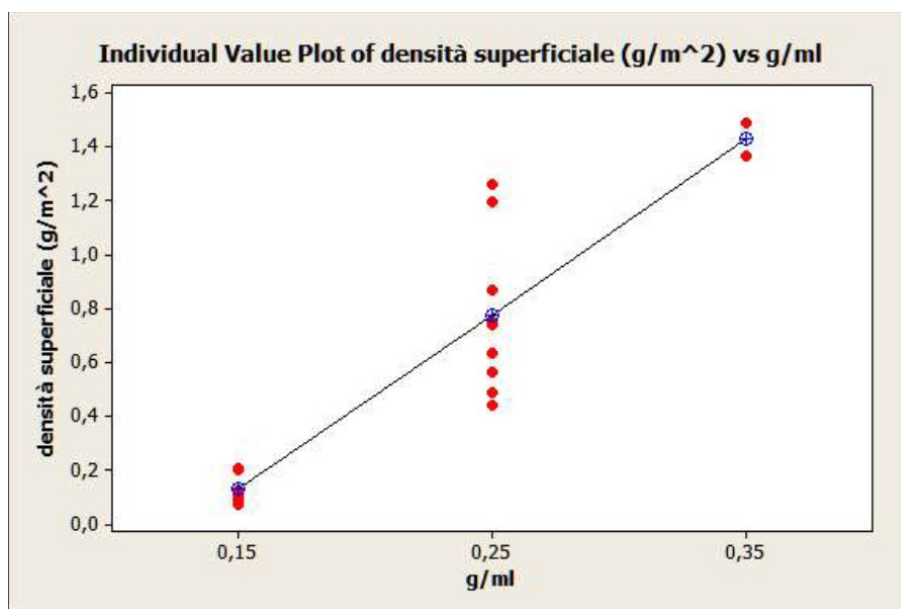
Figure 6:20 Areal density output

Since it has been assessed that the concentration is the key parameter, in order to understand how we can control the process other experiments were performed by defining the concentration as a fixed factor, and varying ddp, the flow rate and nozzle-collector distance. The areal density was the analyzed output.

In table 6:6 the factors used in these experiments are summarized:

Table 6:6 DoE plan

Factor	Type	Levels	Values	Output
Concentration[g/ml]	Fix	-	-	Surface density
d.d.p[kV]	Variable	3	17; 22.5; 28	Surface density
Gap[cm]	Variable	3	6.5; 12.5; 18.5	Surface density
Flow rate [μl/min]	Variable	3	30; 45; 60	Surface density

The analysis of variance shows that flow rate is the only factor that influence the areal density. In fact, as the flow rate increases also the areal density does (figure 6:21).
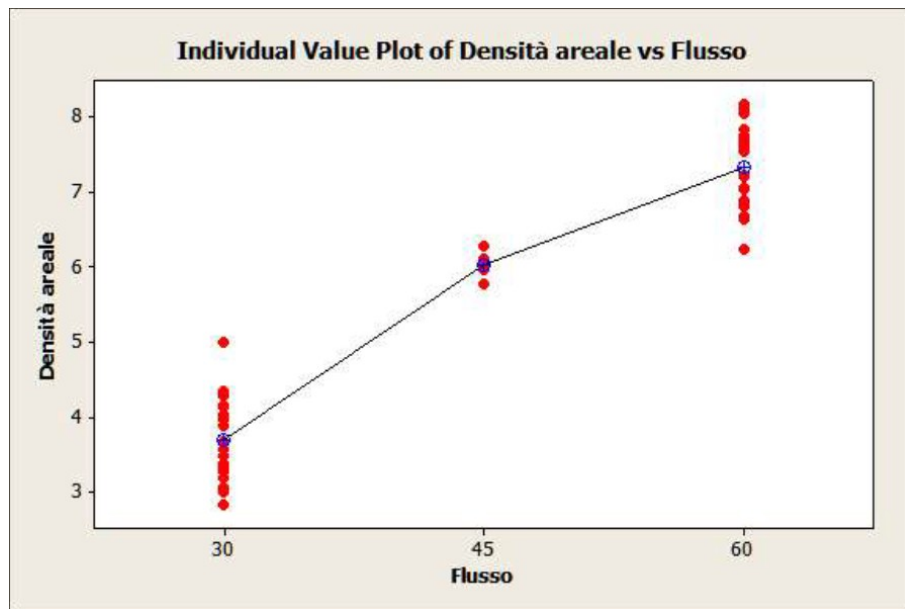
Figure 6:21 Areal density vs flow rate

SEM analysis

SEM images reported in figure 6:22 show the morphology of the electrospun nanofibers respectively for coPES9k (a) and coPES29k (b). The fibers show smooth surfaces and no sign of significant defects is observable.

112
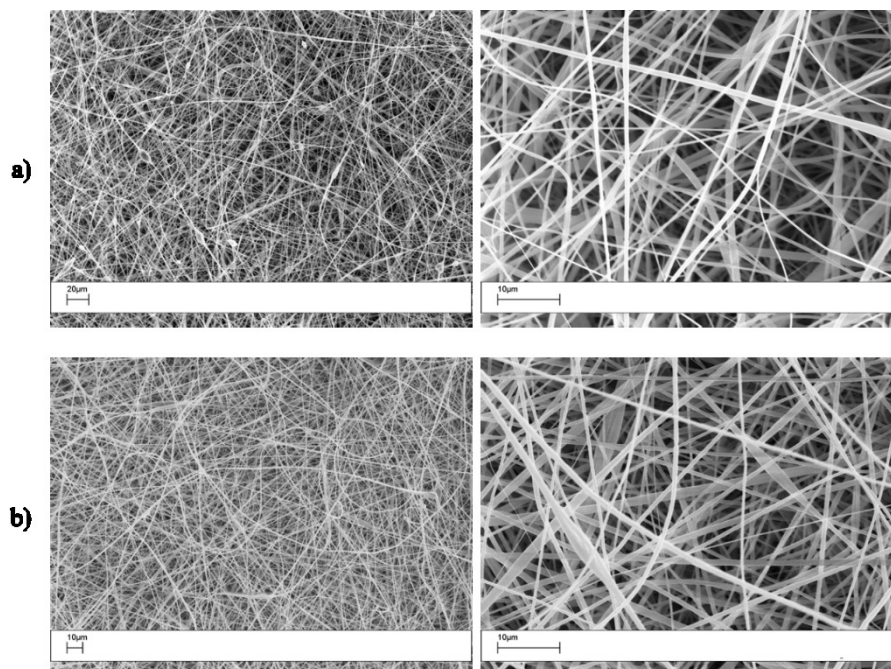
Figure 6:22 SEM images of coPES9k (a) and coPES20k (b) electrospun nanofibres

Figure 6:23 shows the SEM analysis of the electrospun coPES20k nanofibres with respectively 1wt% (a) and 10wt% (b) of MWCNTs. The coPES20k with MWCNTs shows bead-on string morphology, whereas fibers without MWCNTs are bead-free. This can be caused by an incomplete dispersion of MWCNTs in the solution during sonication or, by the agglomeration of carbon nanotubes during the electropinning process. Furthermore, it is clear that, by increasing the percentage of MWCNTs, the amount and dimension of beads increase.
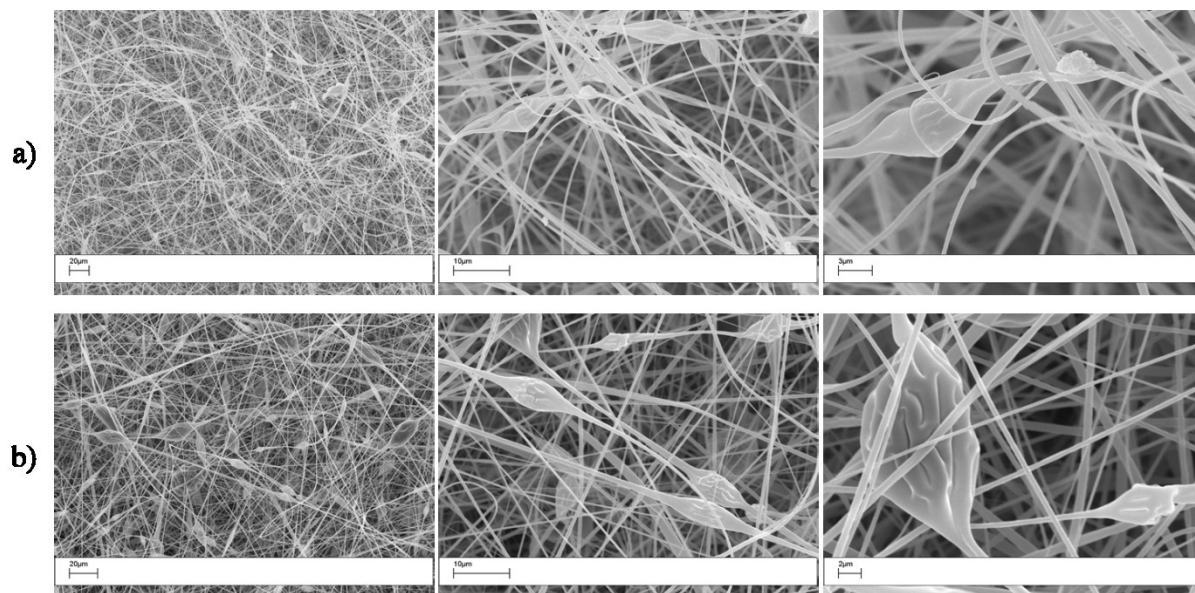
Figure 6:23 SEM images of coPES20k nanofibers filled with 1wt% (a) and 10wt% (b) of MWCNT

In figure 6:24 the comparison of the different MWCNTs content is shown with the final average diameters of the nanofibres.
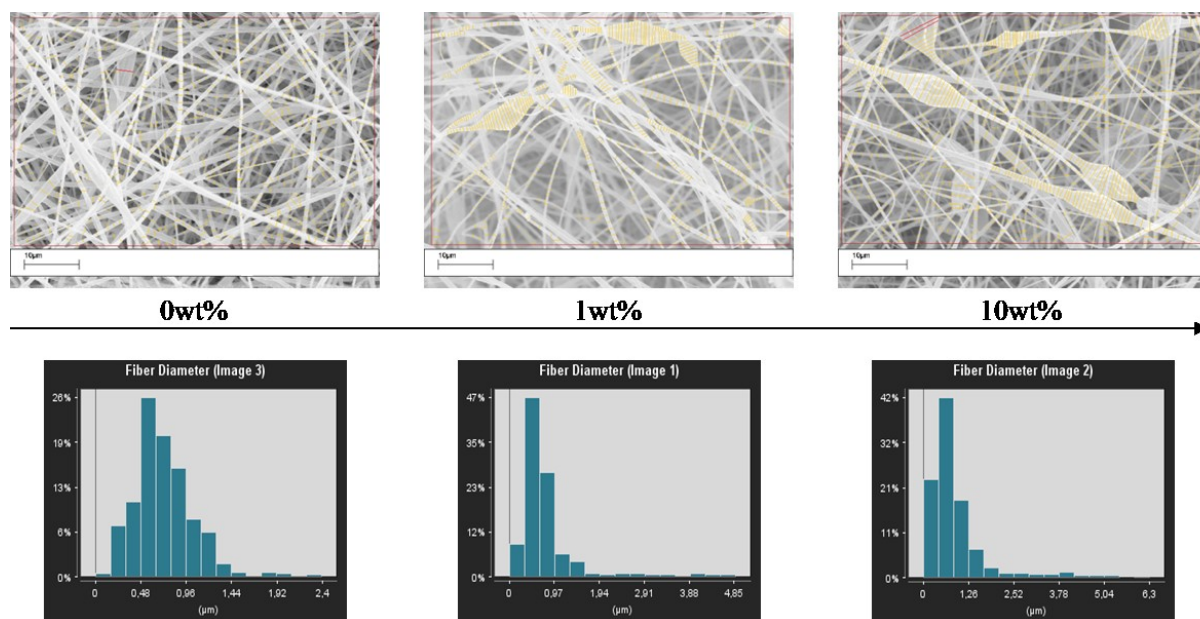
Figure 6:24 Comparison of electrospun coPE20k nanofibers with different amount of MWCNTs with average fiber diameters

In figure 6:25 sections of coPES20k nanofibres are shown. It is possible to note that fibres without nanofillers are more compact than the ones filled with MWCNT. Furthermore, as the percentage of MWCNTs increases the nanofibres become larger and it is possible to imagine MWCNTs wrapped by thermoplastic inside the nanofibres.

In order to better confirm the presence of MWCNTs inside the fibres, TEM analysis was carried out as well (figure 6:26). Nanofibers were electrospun directly onto the TEM grid. Both agglomerates (figure 6:26a) and dispersed nanotubes (figures 6:26 b, c, d) aligned in the fiber-direction were observed.
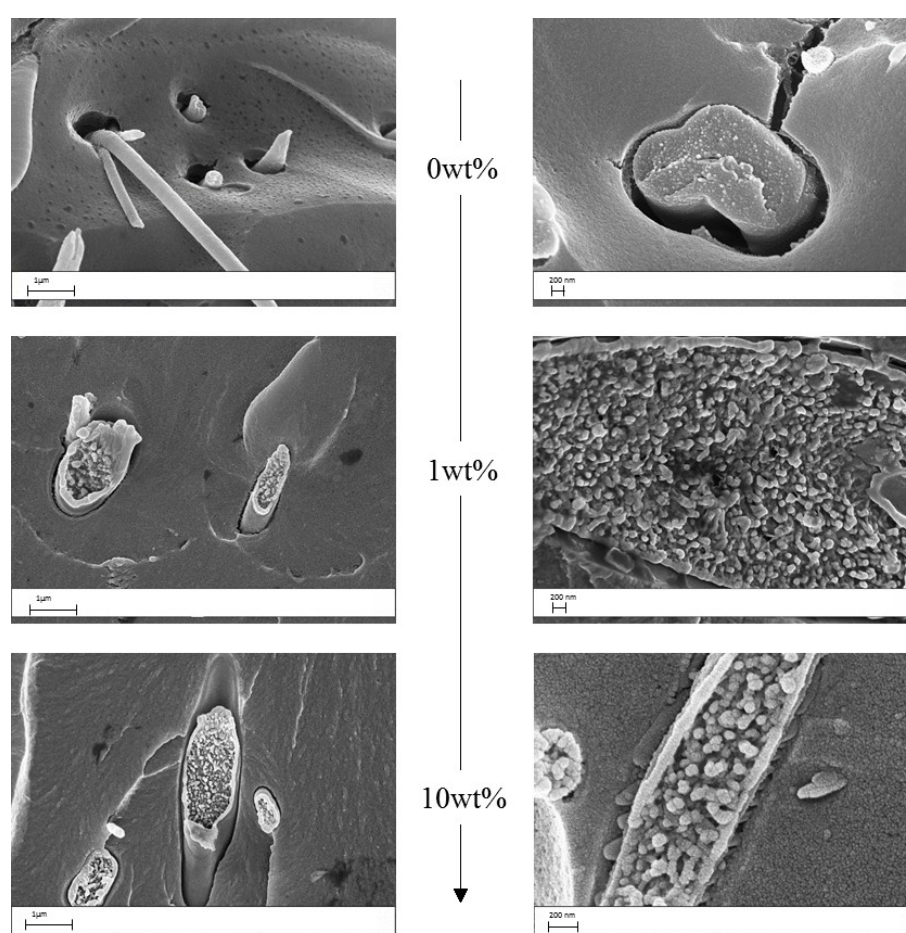
Figure 6:25 Sections of coPES20k nanofibres filled with MWCNTs
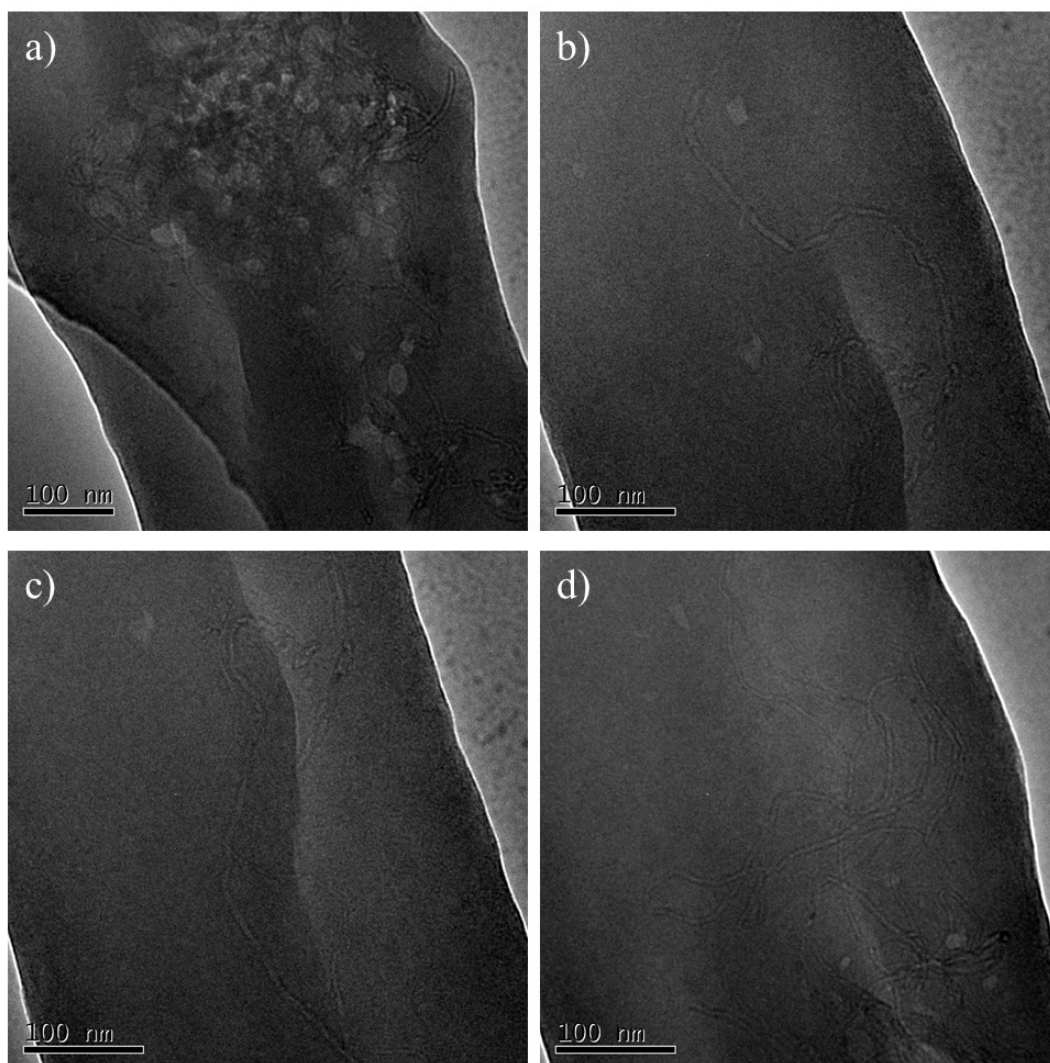
Figure 6:26 TEM images of coPES20k nanofibres filled with MWCNTs

It is also possible to see that MWCNTs are not well dispersed and kind of aligned along the fibres' direction. MWCNT distribution inside the nanofibres may be the one shown in figure 6:27.
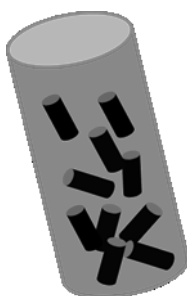
Figure 6:27 Scheme of MWCNTs inside the fibre

Figure 6:28 and 6:29 show the SEM analysis of the coPES20k nanofibres electrospun respectively with 1wt% of SiO2 and 1wt% of carbon black.
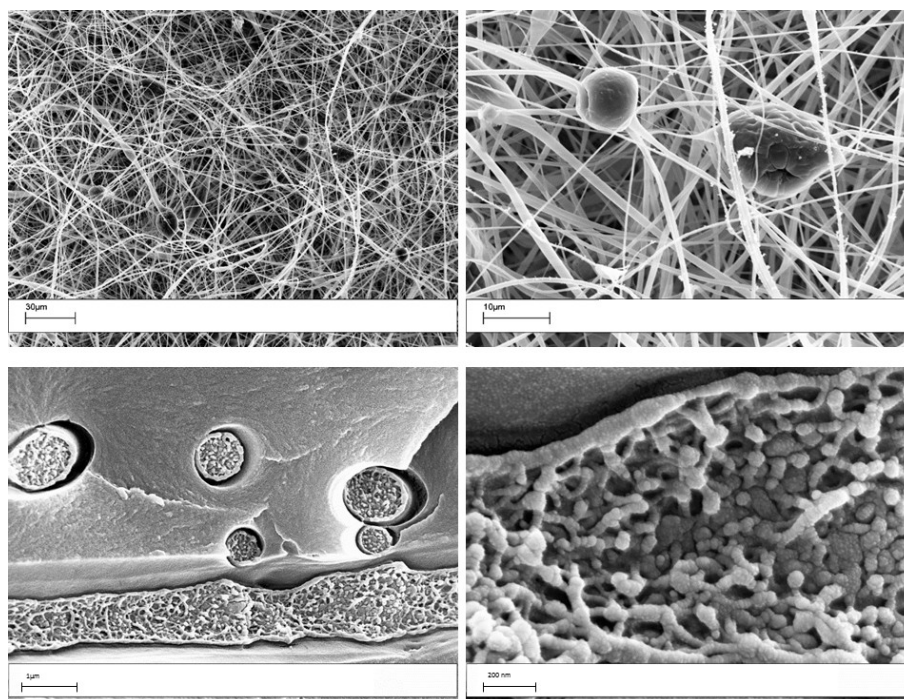
Figure 6:28 Sections of coPES20k nanofibres filled with 1wt%SiO$_2$
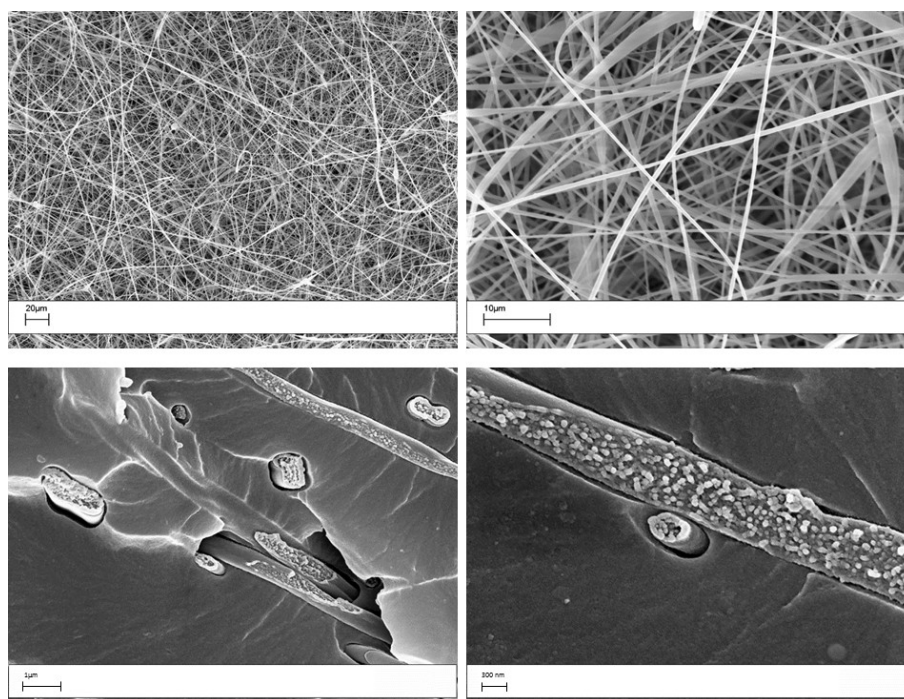
Figure 6:29 Sections of coPES20k nanofibres filled with 1wt%carbon black

It is possible to see that fibres with nanosilica show bead-on string morphology, as seen with MWCNTs, whereas fibres with CB are bead-free. This is an evidence of a better dispersion and stability of CB compared to MWCNTs and SiO_2. For both SiO_2 and carbon black nanofillers, an irregular inner morphology similar to that one of MWCNTs is observable.

It was seen that with SEM analysis it is not possible to effectively see the nanofillers inside the fibres. In oreder to overcome this issue, EDX analysis was performed proving the actual presence of such nanofillers inside the fibres.

EDX analysis was conducted on ZnO filled nanofibers. ZnO was used in order to have Zn as a distinctive element to follow. In fact, MWCNT and CB have not any specific peak that distinguish from coPES chains, while SiO_2 has the Si peak overlapped to that ones of the resin or of the polymer. On the contrary, in the case of ZnO is possible to distinguish the Zn peak (figure 6:30).
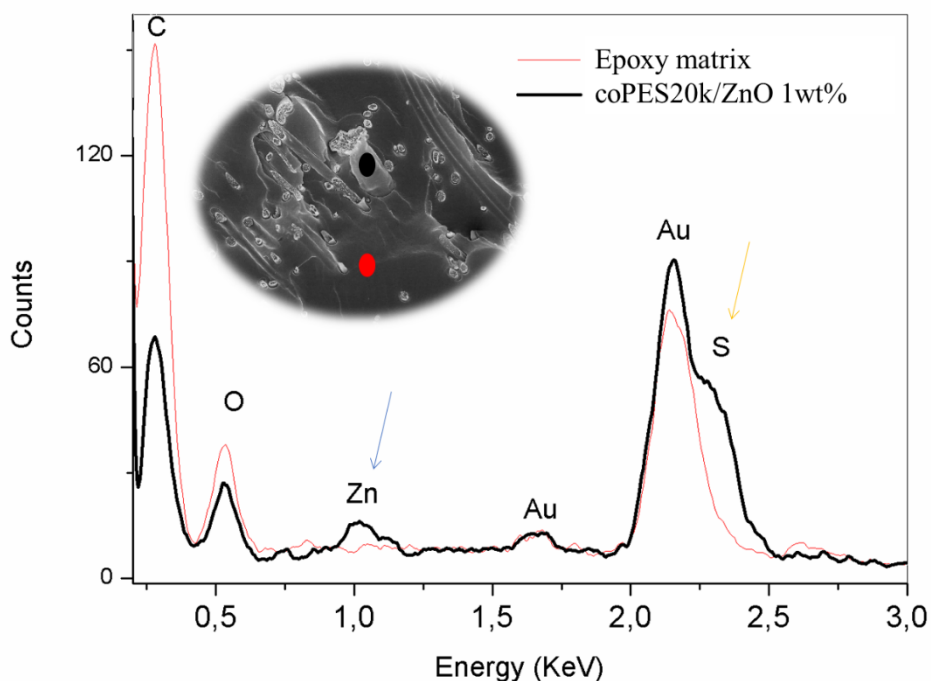
Figure 6:30 EDX Analysis of ZnO-filled nanofibers

SEM images of OpteSTAT electrospun fibers are reported in figure 6:31. It is very clear the larger amount of CNTs achievable with technology polymer, since a lot of defects due to CNT-agglomerates are present.
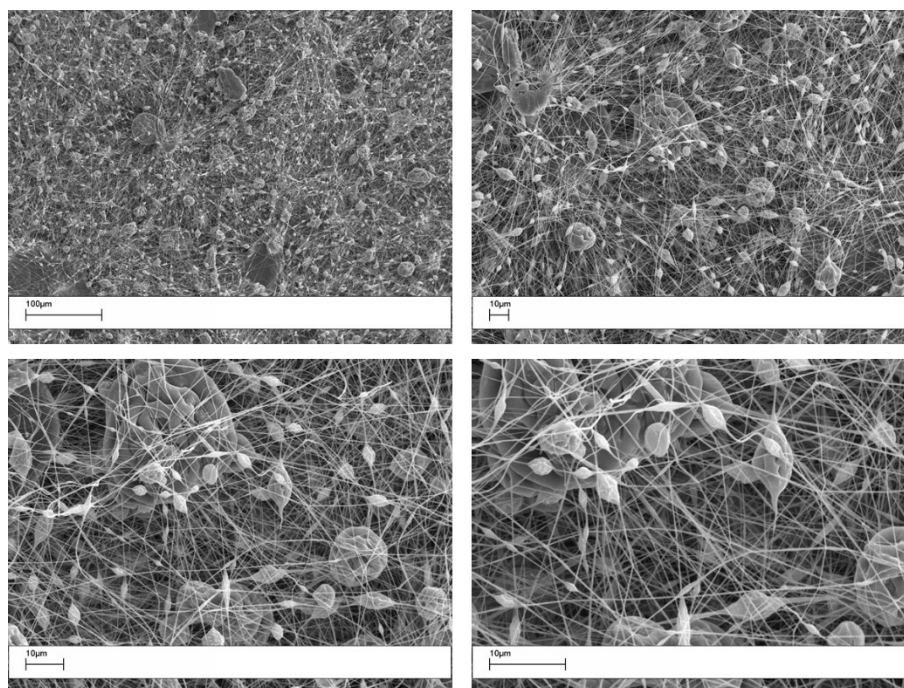
Figure 6:31 SEM images of OpteSTAT electrospun fibers

Hot-Stage Microscopy analysis

The kinetic of the dissolution behavior of the nanofibers was studied by means of optical microscopy. The dissolution trend in a DGEBA-MDEA resin was obtained at several temperatures. This study was performed for coPES9k, coPES20k and coPES20k/MWCNT 1wt%. In figure 6:32 the images of the fibre dissolution were recorded at 100°C at different times.

a) t=0   b) Half dissolution   c) Full dissolution
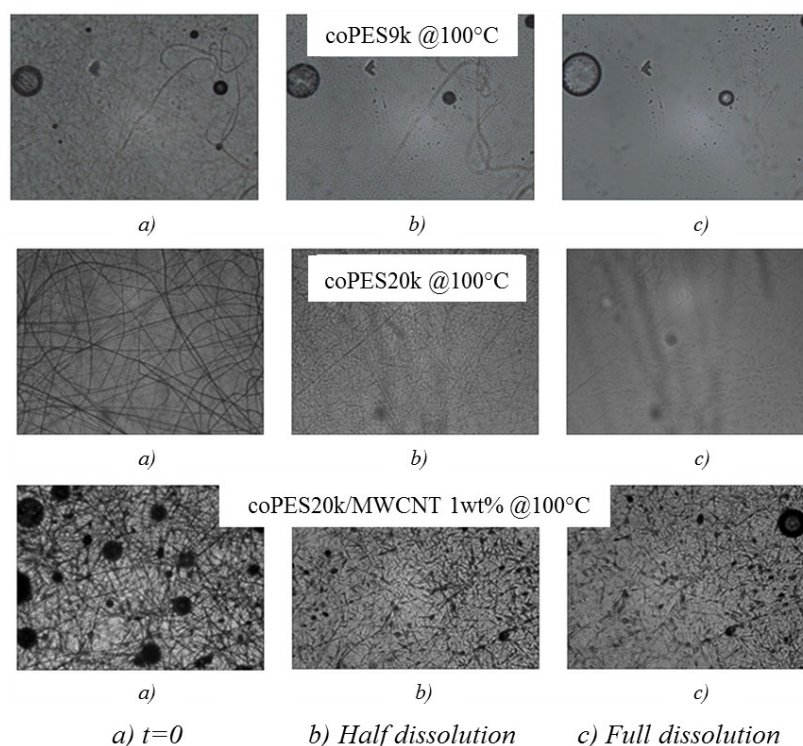
Figure 6:32 Dissolution study by Hot-Stage Microscopy

Data at all temperature are reported in figure 6:33. Note that coPES20k shows longer dissolution times than PES9k due to the higher molecular weight of its chains that makes diffusion phenomena more difficult. Furthermore, in samples with MWCNTs an increased dissolution time can be observed. This may be coming from the fact that the addition of MWCNTs hinders polymeric chains diffusion thus increasing the fibres' dissolution behavior.

Same effect of nanofillers on dissolution times is reported in figure 6:34 foe coPES9k veils filled with MWCNTs, SiO_2, CB and ZnO.

In figure 6:35 a comparision between resins DGEBA and TGAP is reported. It is evident that TGAP, thanks to its major functionality, acts as a better solvent for coPES9k with respect to DGEBA.
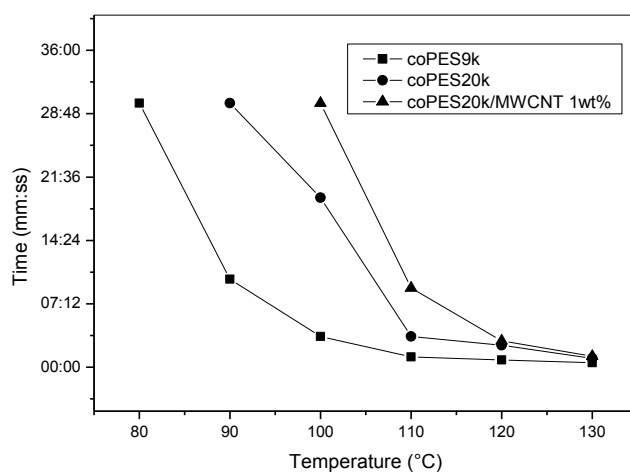
Figure 6:33 Dissolution curves of electrospun coPES9k, coPES20k and coPES20k/MWCNT 1wt%
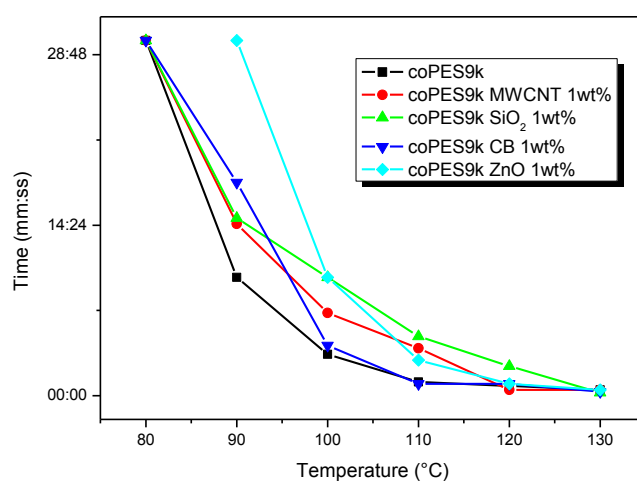
Figure 6:34 Dissolution curves of electrospun coPES9k filled with MWCNTs, SiO2, CB and ZnO
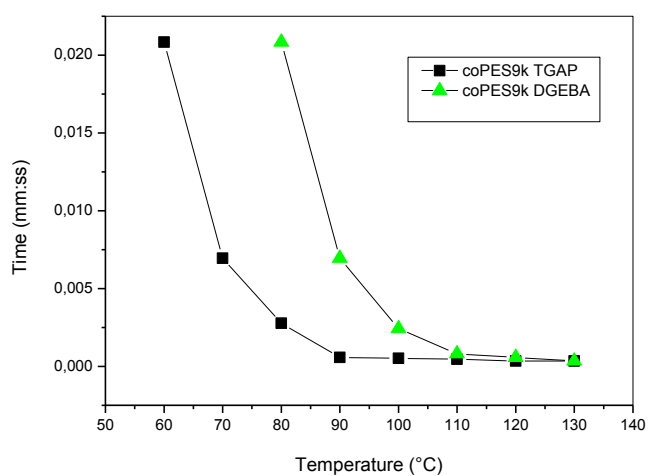
Figure 6:35 Dissolution curves of electrospun coPES9k: DGEBA vs TGAP

121

Scale-up of the electrospinning process

In order to scale up the project, it was necessary to move to commercially available thermoplastics. Two polyethersulfones sold by Solvay were the choice: Virantage® 30500 RP and Viratange® 10200 RP. Both of them are PESs but differ for the average molecular weight and for chemistry of the reactive end-groups. Main properties are reported in table 6:7.

Table 6:7 Main properties of Viratange® polymers

Virantage® Grade	M_{GPC} [g/mol *1000]	End Groups
30500 RP	45	$-NH_2$
10200 RP	14	$-OH$

The scale up of the electrospinning process was performed at Elmarco facilitiy placed in Liberec, Czech Republic. Elmarco machines work with the needle-less technology. In this specific electrospinning process, the needle is not expected to be used. Instead, there is a wire which act as positive electrode which is constantly wet with the polymer solution by a basket that moves back and forward (figure 6:36). This kind of machine electrospins with higher voltages applied, and allow continuous and, as a consequence, bigger production volumes.
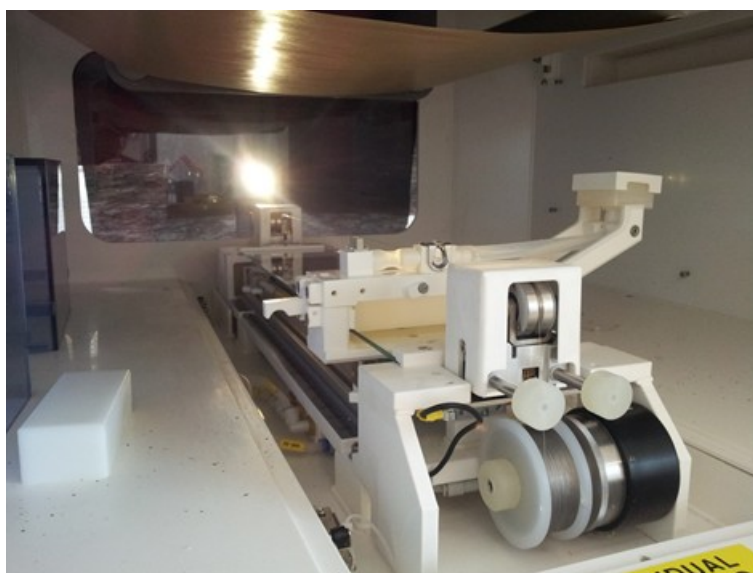
Figure 6:36 Needle-less technology of Elmarco machines

A first set-up was done with a laboratory machine in order optimize the process because of the needle-less technology (figure 6:37). The polymers were electrospun on both antistatic PP and silicon paper in order to facilitate the subsequent peel of the veils.

Figure 6:37 NanoSpider NS 1WS500U by Elmarco

Figure 6:38 reports the SEMs of the electropun Virantage 30500. SEM analysis showed fibers with more defects with respect to needle machine, with a bead-on-string morphology. Instead, the fibers diameter analysis revealed a lower value, with an average of 380 nm.
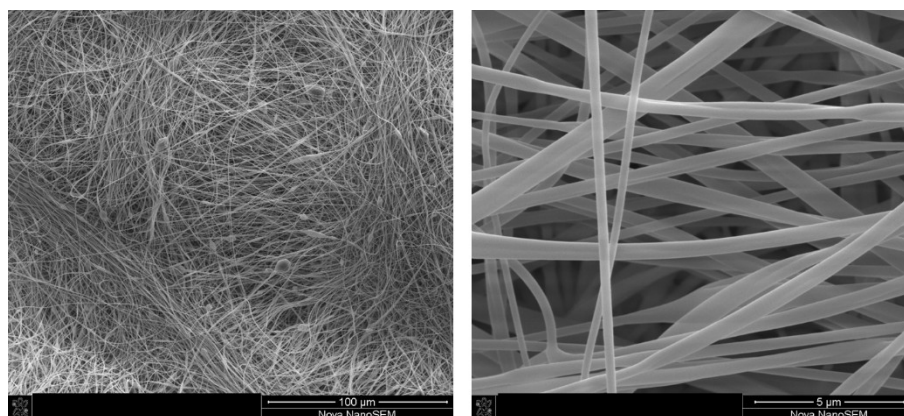
Figure 6:38 SEM images of electrospun Virantage 30500 by NanoSpider NS 1WS500U

Once all the conditions were set up, the process was transferred to the industrial production machine shown in figure 6:39. This machine works with four wire at the same time.

Figure 6:39 NanoSpider NS 4S1000U by Elmarco

Figure 6:40 reports the SEMs of the electropun Virantage 30500 with the NS 4S1000U machine. SEM analysis showed fibers with less defects with respect to the lab machine, with reduced bead-on-string morphology. Instead, the fibers diameter analysis revealed a bigger value, with an average of 504 nm.
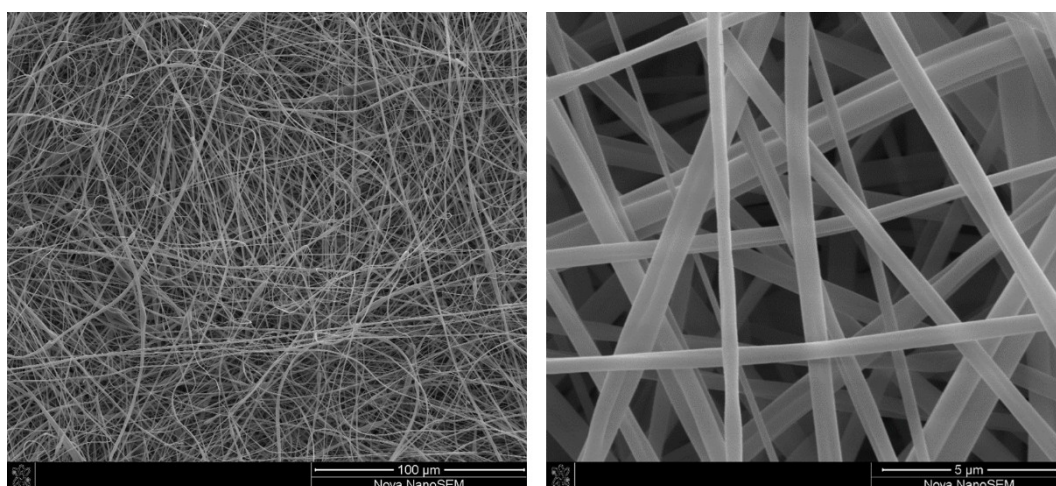
Figure 6:40 SEM images of electrospun Virantage 30500 by NanoSpider NS 4S1000U

6.4.2 Neat resins characterization

DGEBA neat resins

Figure 6:41 reports the tan δ-versus-temperature curves for the neat matrices prepared with veils and prepreg route at 10wt% of coPES9k in comparison to the unmodified epoxy resin. The tan δ curves for the sample of coPES9k veil is also reported. The neat matrices containing the thermoplastic showed two peaks in the tan δ curves. This behavior is typical of micro-phase separated epoxy/blends cured by MDEA [6]. The lower tan δ peaks of modified blends (162°C and 165°C for prepreg and veil, respectively) were at higher temperatures than the single peak of the unmodified epoxy resin (158°C). The higher tan δ peaks (206°C and 197°C for prepreg and veil, respectively) were at lower temperatures than the tan δ peak shown by coPES9k veil (209°C). These tan δ peaks were due to the glass transition relaxations of epoxy-rich and thermoplastic-rich phase domains at low and high temperatures, respectively.
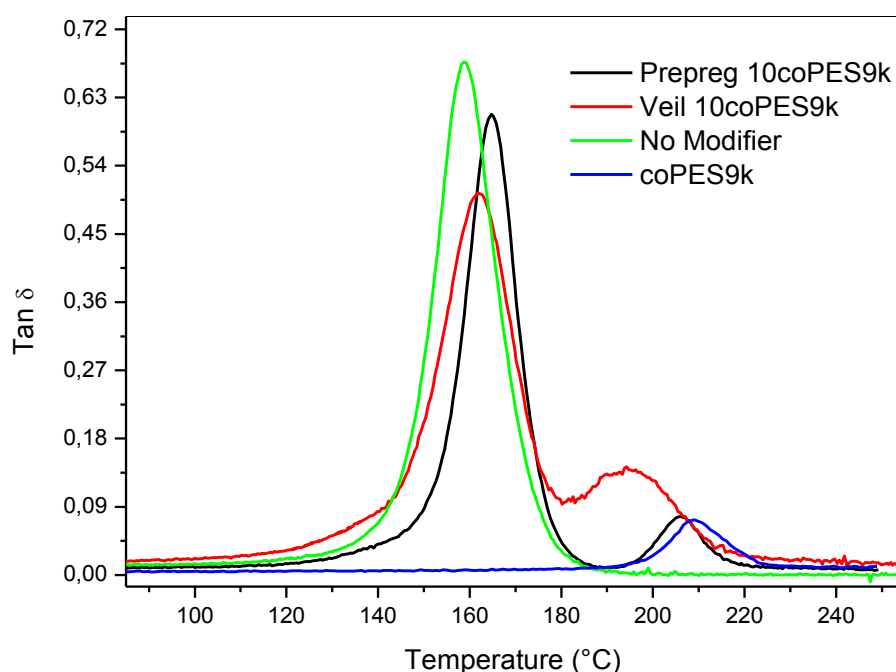
Figure 6:41 Comparison of Tan δ curves for three neat cured DGEBA matrices: prepreg, veil-modifier and no-modifier. The graph reports the Tan δ for the coPES9k veil analyzed with pocket tool

These results suggest the presence of incomplete phase separation of the two phases with one component of each phase dissolved in the other phase. Van Overbeke et al [7] explained, by the use of micro-Raman spectroscopy, that each phase tends to purify itself during curing.

However, the increasing viscosity of epoxy-amine network during curing hinders diffusional process and stops the purifying process thus resulting into an incomplete separation process. The presence of two well separated tan δ peaks for both the veil and prepreg samples confirmed that the veils were dissolved undergoing phase separation during curing. However, the two samples differed for slight shifts in temperature and height of the tan δ peaks. These differences can be ascribed to the different processing route as shown schematically in figure 6:42. The prepreg sample was prepared by predissolving the thermoplastic powder in the uncured resin. Therefore, when the prepreg is cured, the epoxy/thermoplastic is a homogenous blend experiencing curing and phase separation. The veil system, in its initial state, presents thermoplastic veils undissolved. This means that when the heating started, the thermoplastic veils were dissolved while the resin was curing thus resulting in a different diffusional process for the prepreg and veil system that caused a different viscoelastic behavior for the cured samples.
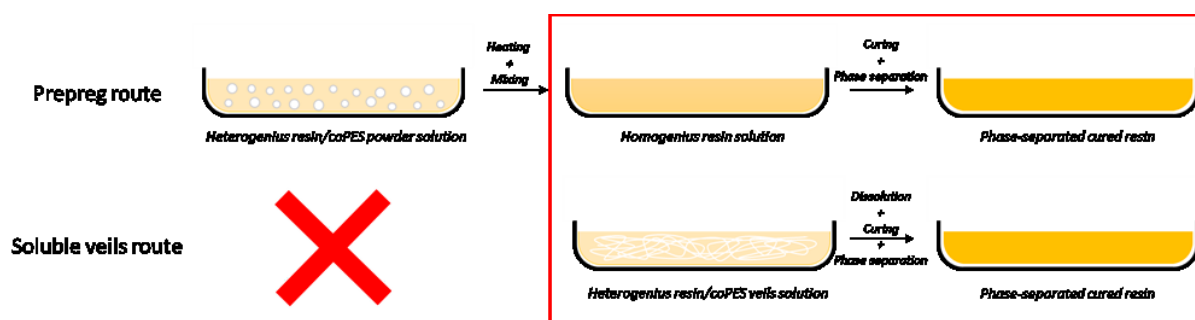
Figure 6:42 Schematics of the process differences between the prepreg and soluble veil routes

The Scanning Electron Microscopic (SEM) analyses (figure 6:43) confirmed the DMA data. SEM showed particulate morphology for the modified samples, prepreg (figure 6:43a) and veil (figure 6:43b), with particles having a diameter of 2-5µm, uniformly distributed. No sign of undissolved fibers was found in the veil sample. Similar results were found for the samples with 15wt% and 20wt% of coPES9k veil.
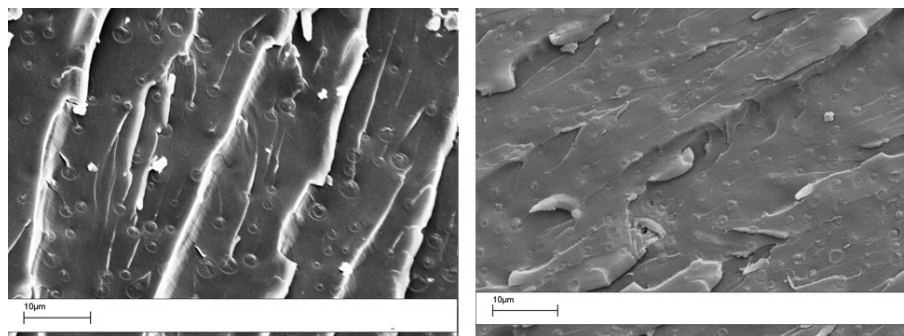
Figure 6:43 SEM images of the modified DGEBA samples: prepreg (left), veil-modified (right)

Figure 6:44 shows the comparison between the Tgs of the prepreg and veil samples with a different modifier's content. Differences between Tgs for prepreg and veil samples were small (less than 10°C) for all the samples. The phase-separated domains showed differences compared to the pure blend components (159°C and 205°C for pure epoxy and coPES9k, respectively). This result has been seen in previous papers and is explained by the presence of a minor epoxy in the thermoplastic-rich phase and thermoplastic in the epoxy-rich phase [7]. This phenomenon is seen also in prepreg samples and it is typical of the phase separation process of epoxy/thermoplastic blends. Therefore, for coPES9k samples, the veil dissolution step had only a minor effect on the residual presence of minor components in phase-separated domains.
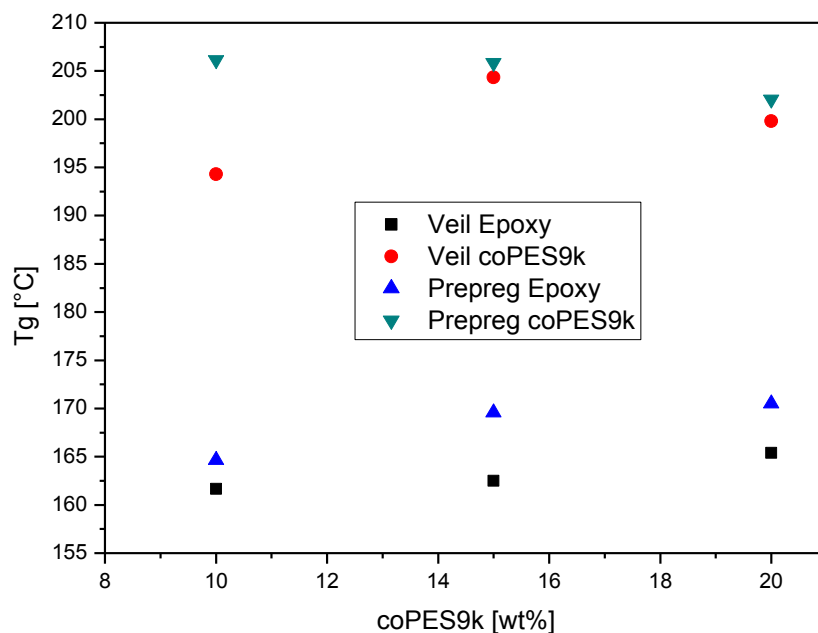
Figure 6:44 Glass transition temperatures (Tgs) versus coPES9k content for neat DGEBA resin samples

SEM analysis (figure 6:45) showed similar morphologies for both prepreg and veil samples at the respective coPES9k percentages.
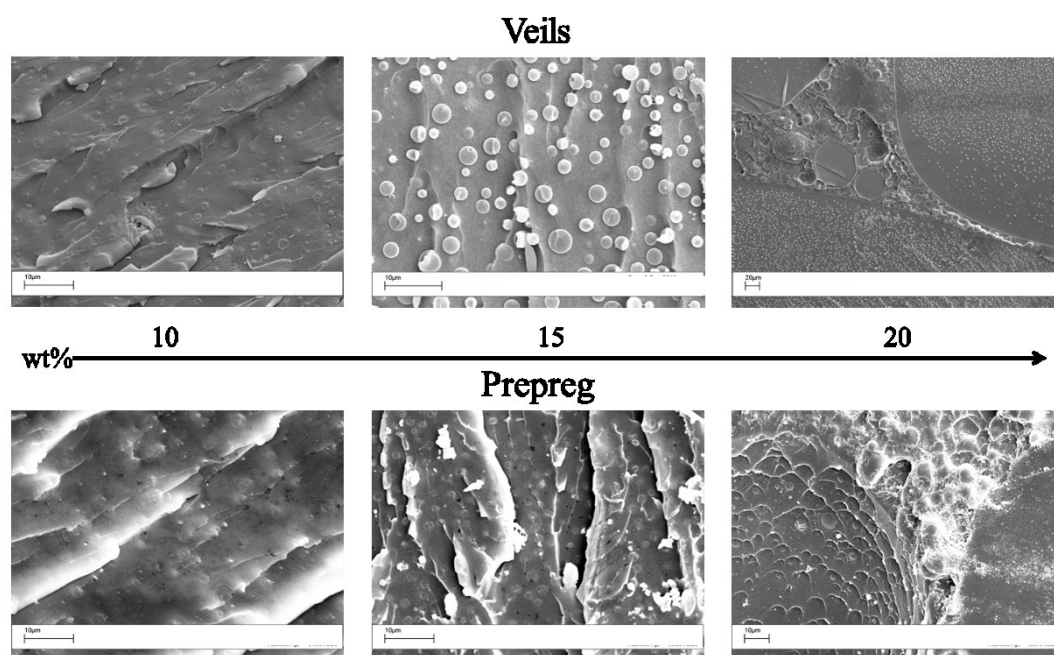
Figure 6:45 SEM images of the TGAP-modified samples: prepreg (down), veil-modified (up) at different percentages

128

The coPES20k veils were dissolved in the epoxy resin, as reported above. The polymer powder did not dissolve, so prepreg samples were not prepared. The results of the formulation at 10wt% of the coPES20k veil are detailed in figure 6:46. The DMA analysis revealed for the veil sample two distinct peaks respectively for the epoxy-rich and the thermoplastic-rich phases, as seen for the coPES9k samples. The two peaks are in between the peaks of the pure phase, indicating once again the incomplete purification during the phase separation.
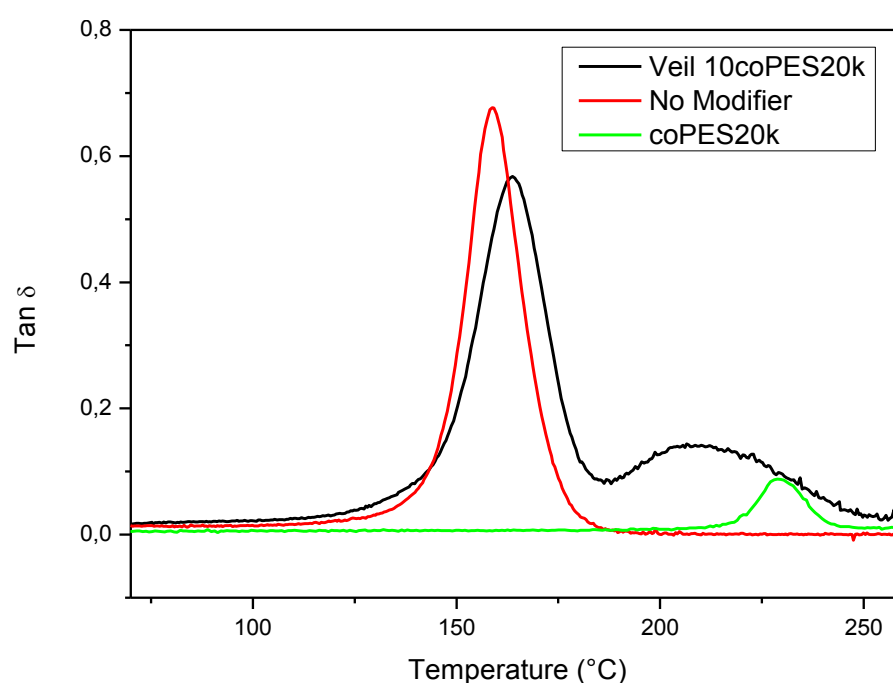
Figure 6:46 Comparison of Tan δ curves for two neat cured DGEBA matrices:veil-modifier and no-modifier. The graph reports the Tan δ for the coPES20k veil analyzed with pocket tool

Figure 6:47 shows the SEM analysis, where the presence of undissolved fibers was confirmed. SEM analysis showed also the presence of inhomogeneous phase separation (figure 6:47c) with the coexistence of particulate and sea-island morphology as well. Recently, similar results were obtained by Rico et al [8] using an epoxy system modified with low and high molecular weight polystyrene.
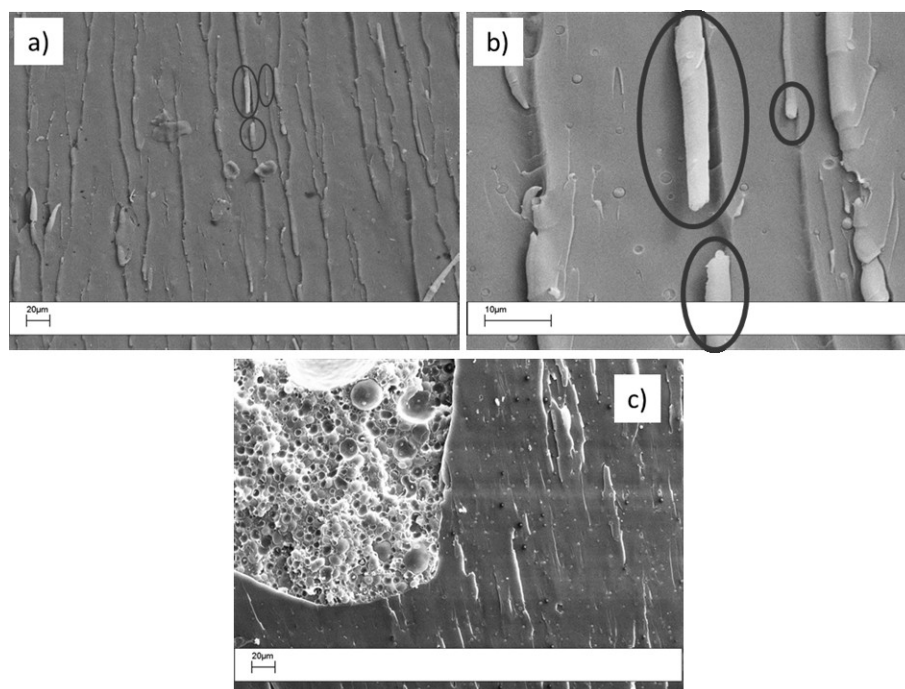
Figure 6:47 SEM images of 10wt% coPES20k modified system with unidissolved fibres (a, b) and complex morphology (c)

This result, which somehow contrasts with the dissolution trials, is explained as the result of the dense packing of thermoplastic veils in this particular preparation method that, combined with the higher molecular mass of coPES20k, limited the dissolution of the veil. Naffakh et al [9] showed that increasing the thickness of PEI film delays its dissolution rate in epoxy/amine systems. They found that a film thickness as low as 20μm was necessary to ensure complete dissolution. Our veils were porous and this allowed lay up of veil with a thickness greater than 20μm to be soluble. However, the results reported in figure 6:47 show that the neat resin sample procedure has some limits with coPES20k. The samples with coPES20k prepared with this procedure were not further analyzed.

Nanofilled DGEBA neat resins

In figure 6:48 and 6:49 the comparisons of nanoparticle-filled electrospun coPES9k veils are reported. Tan δ curves show again two distinct peaks for filled salmples, with slight enhancements of the Tg of the epoxy-rich phases. In particular, increases of +4°C and +6°C

130

were observed when adding respectively 1wt% of MWCNTs and 1wt% of POSSs, while for

SiO$_2$-filled veils (1wt%) it remained quite the same with just +1°C. The higher increase for

the POSS-filled sample is due to the characteristic of POSS particle to interact with molecule

of both resin and thermoplastic, acting as a kind of chain-extensor increasing the Tg of

polymers.
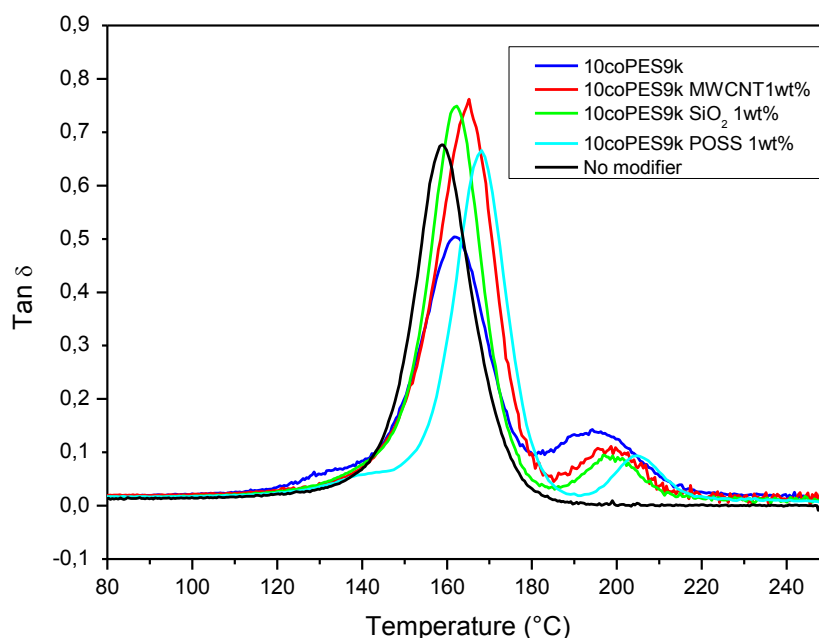
Figure 6:48 Comparison of Tan δ curves for neat cured DGEBA veil-modified matrices:10wt% coPES9k, 10wt% coPES9k +1wt%MWCNT, 10wt% coPES9k +1wt%SiO$_2$, 10wt% coPES9k +1wt%POSS, no modifier

The addition of nanoparticles also enhanced the values of elastic moduli for filled samples

(figure 6:49). MWCNT-filled sample showed an increase of +60,2% with respect to the

simple coPES9k toughened sample and of +190,8% with respect to the unmodified sample.

On the other hand, the addition of 1wt% of SiO$_2$ led to increases of respectively +11,0% and

101,5% POSS-filled sample act very similar to the simple coPES9k-modified sample, with

increases only with respect to the unmodified system.
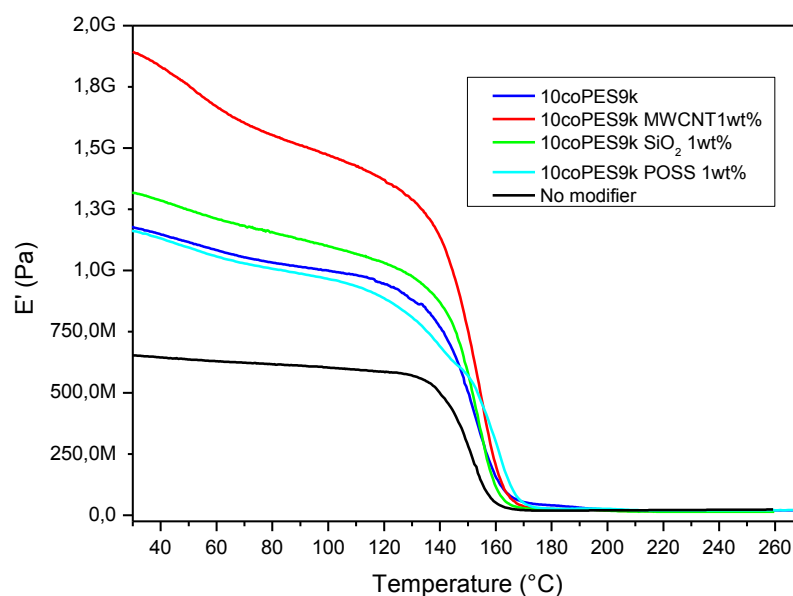
Figure 6:49 Comparison of elastic moduli curves for neat cured DGEBA veil-modified matrices:10wt%coPES9k, 10wt%coPES9k +1wt%MWCNT, 10wt%coPES9k +1wt%SiO$_2$, no modifier

For all veil-modified samples, the presence of nanofiller did not change the final morphology (particulate) with respect unfilled coPES veils sample, as shown in figure 6:50. TEM analysis revealed that MWCNTs are mostly in the thermoplastic-rich phase as shown in figure 6:51.
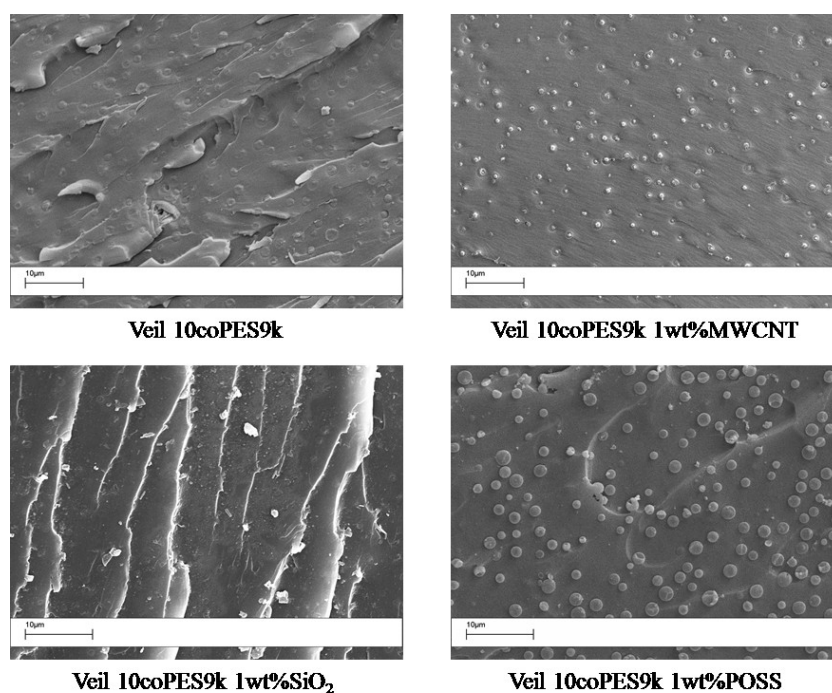
Figure 6:50 SEM images of the filled-veils modified DGEBA samples

132
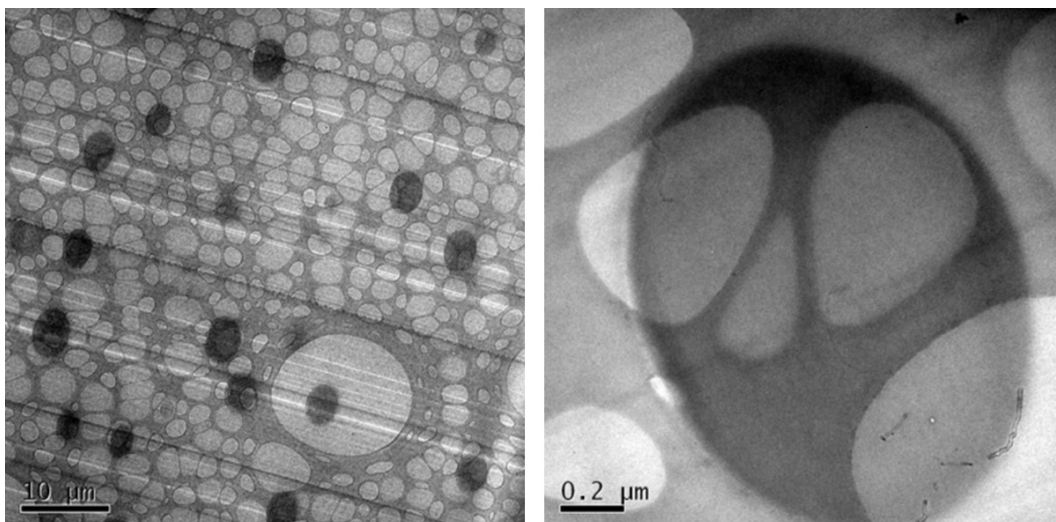
Figure 6:51 TEM images of the cured neat DGEBA resin modified with MWCNT-filled veils

TGAP neat resins

Neat-resin samples were prepared also by using the TGAP epoxy. As seen above for DGEBA samples, comparisons of prepreg and veil routes are reported in figure 6:52, analyzing coPES9k at 10wt%. A big difference in the Tgs of the two modifying routes is observable. In both cases, the addition of the coPES led to decreases of Tgs, with a major impact of veils (almost -60°C) with respect to the unmodified samble. To better understand this effect, SEM analysis was carried out (figure 6:53). The lower Tg of the veil sample with respect the prepreg sample can be due to the different final morphologies: 10wt% coPES9k prepreg was co-continuous while 10wt% coPES9k veil showed particulate morphology. As seen in figure 6:53, the different morphologies are a consequent of the different thermodynamic status of the samples in the first step when curing starts.
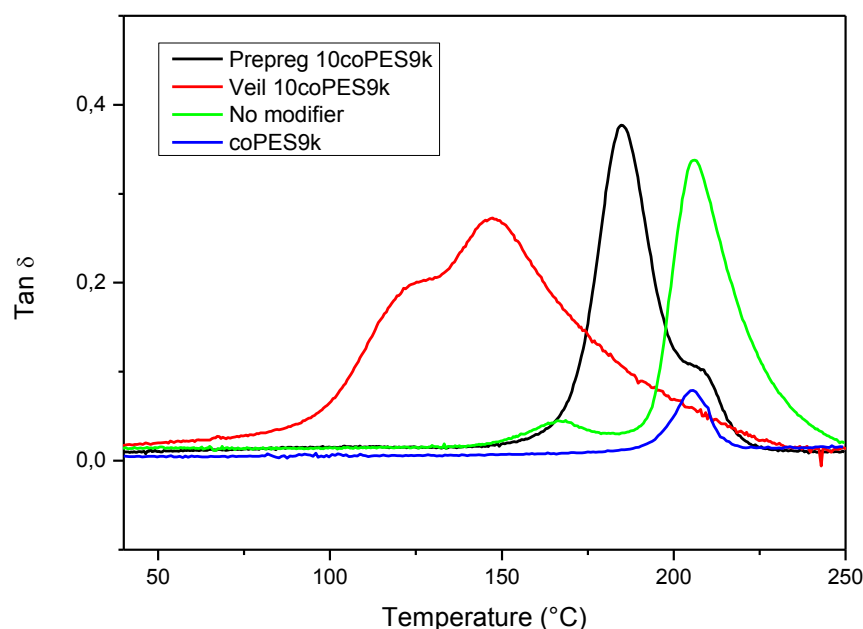
Figure 6:52 Comparison of Tan δ curves for three neat cured DGEBA matrices: prepreg, veil-modifier and no-modifier. The graph reports the Tan δ for the coPES9k veil analyzed with pocket tool
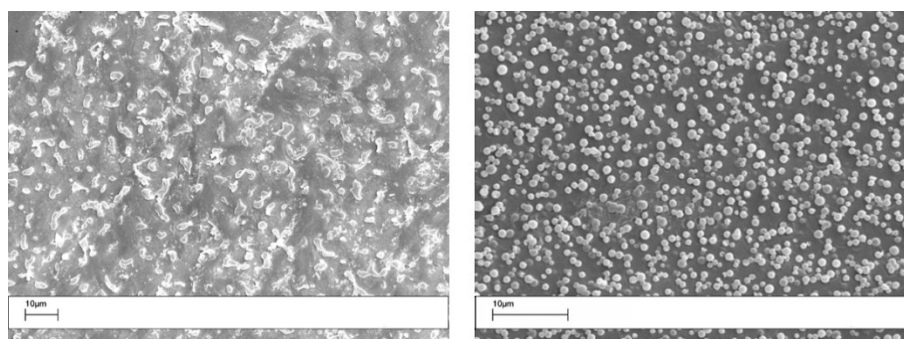
Figure 6:53 SEM images of the TGAP-modified samples: prepreg (left), veil-modified (right)

Other amounts (15 and 20wt%) of coPES9k were examined. Figure 6.54 shows the Tan δ curves for all the percentages of coPES in prepregs (left) and veils (right). In both routes there is a trend indicating an increase of Tgs when coPES9k amount increases as well. SEM analysis (figure 6:55) confirmed differences between the two routes: prepreg showed always co-continuous morphologies, while veils more complex one, going from particulate at 10wt% to double morphology (particulate + phase inversion) at 20wt%.
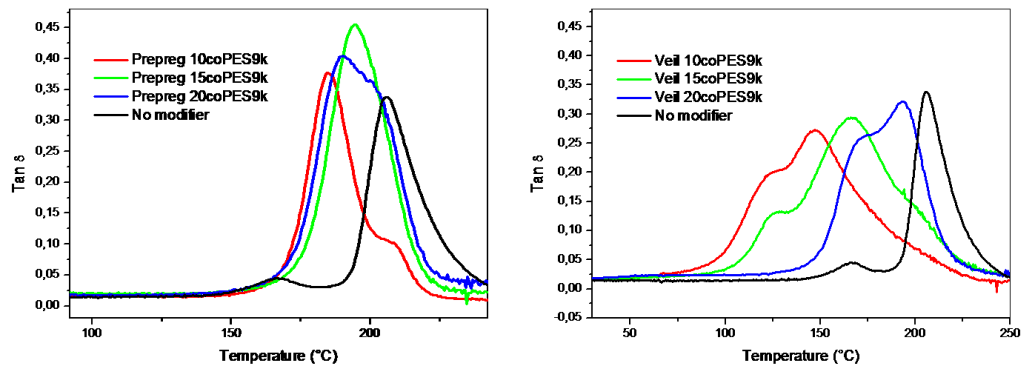
Figure 6:54 Comparison of Tan δ curves for neat cured TGAP matrices: prepregs (left) and veils (right)
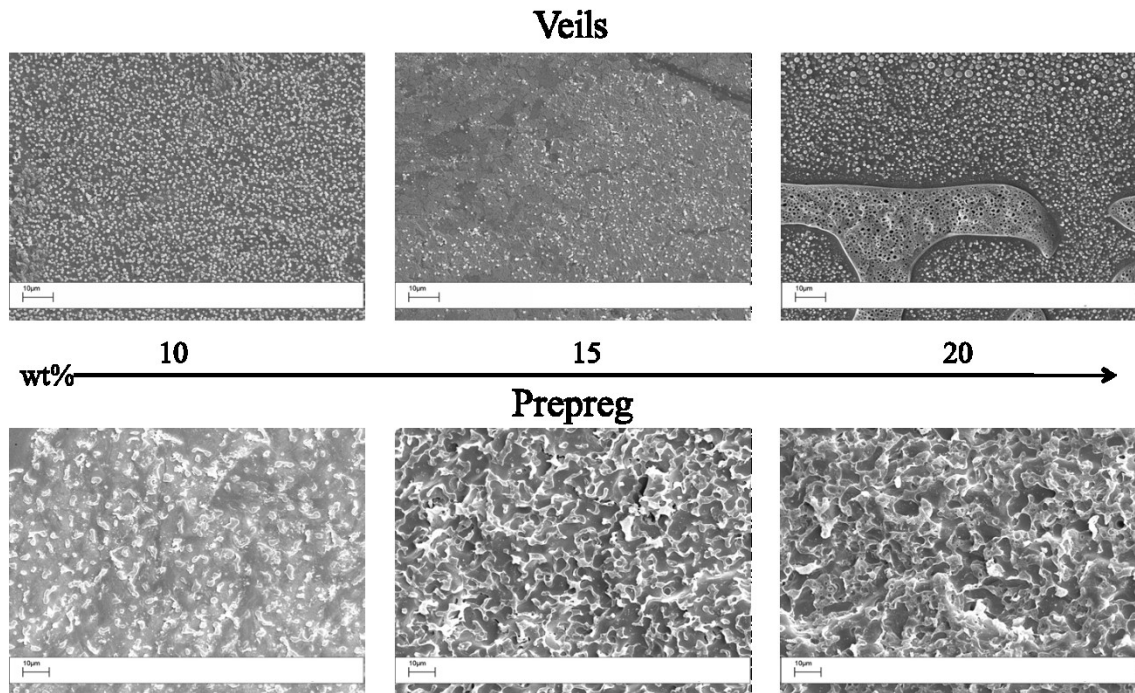
Figure 6:55 SEM images of the TGAP-modified samples: prepreg (down), veil-modified (up) at different percentages

6.4.3 Composite laminates characterization

Hybrid carbon fabrics with electrospun veils deposited onto were prepared to produce by infusion technique composite laminates as detailed in the experimental section. In this case unmodified epoxy resin was used for the infusion trials. The areal weight of the veil was balanced against the areal weight of the carbon fabric to obtain the desired amount of

thermoplastic in the interlaminar region. The thermoplastic content varied between 10wt% and 20wt% for coPES9k veils and 5wt% and 10wt% for coPES20k veils. For comparison purposes, prepreg resins with predissolved coPES were used to impregnate carbon fabrics which were then cured.

Figure 6:56 reports the Tan δ-versus-temperature curves for the composite laminates prepared with veils and prepreg route at 10wt% of coPES9k in comparison to the unmodified epoxy resin. The tan δ curves for the sample of coPES9k veil is also reported as well. As already seen for the neat resins, the samples containing the thermoplastic showed two peaks in the tan δ curves. The lower tan δ peaks of modified blends (166°C and 164°C for prepreg and veil, respectively) were at higher temperatures than the single peak of the unmodified epoxy resin (158°C). The higher tan δ peaks (197°C and 194°C for prepreg and veil, respectively) were at lower temperatures than the tan δ peak shown by coPES9k veil (209°C). These tan δ peaks were due to the glass transition relaxations of epoxy-rich and thermoplastic-rich phase domains at low and high temperatures, respectively.
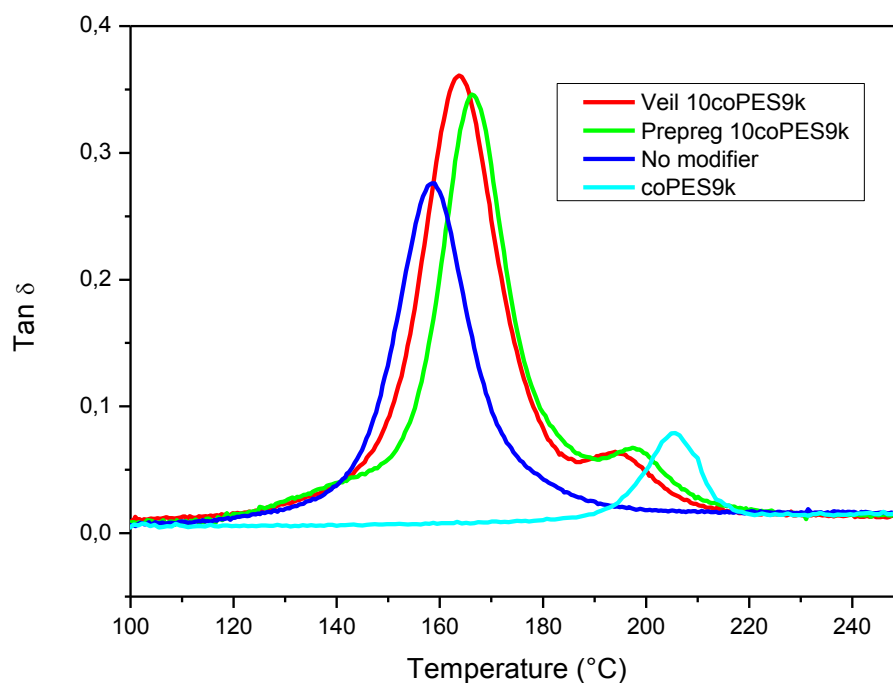
Figure 6:56 Comparison of Tan δ curves for three cured DGEBA composite laminates: prepreg, veil-modifier and no-modifier. The graph reports the Tan δ for the coPES9k veil analyzed with pocket tool

Figure 6:57 shows the comparison between the Tgs of the prepreg and veil composite laminates with a different modifier's content. A similar trend to neat resin sample shown in figure 6:44 is found. Differences between Tgs for prepreg and veil samples were smaller as coPES9k amount increased. The phase-separated domains showed differences compared to the pure blend components (159°C and 205°C for pure epoxy and coPES9k, respectively). This result, again, is in accordance with has been reported in literature [7].
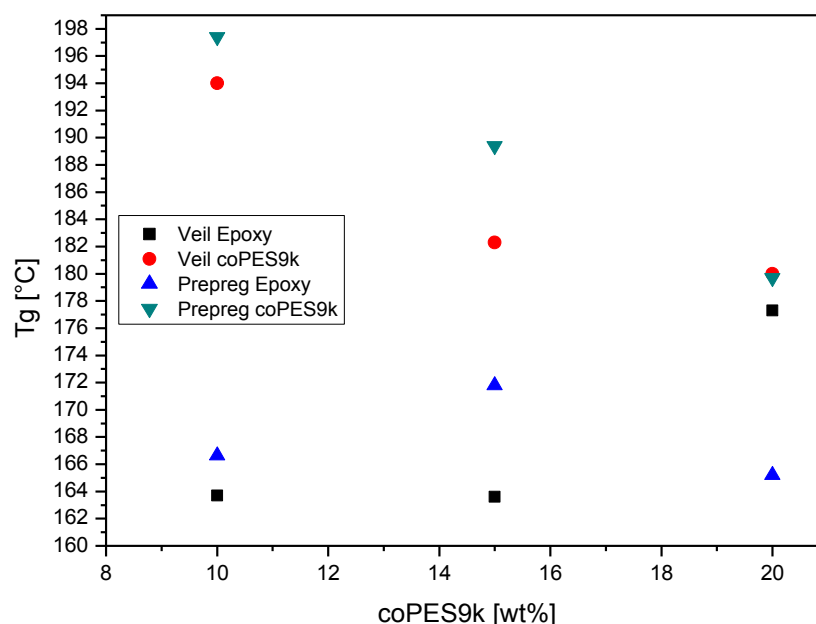
Figure 6:57 Glass transition temperatures (Tgs) versus coPES9k content for DGEBA composite laminates

Figure 6:58 shows the comparison between the interlaminar regions for the samples modified with the coPES9k veils and the predissolved coPES9k (i.e. prepreg). No undissolved veil was observed for all the percentages analyzed for the infused specimens. The morphology of the samples loaded with 10wt% of coPES9k was very similar for the prepreg and the veil samples. When the thermoplastic content raised to 15wt%, the prepreg sample showed smaller thermoplastic particles compared to the veil sample. Finally, the sample at 20wt% of coPES9k showed a morphology that became a combination of particulate and phase inverted for both the prepreg and the veil samples. However, the prepreg sample (at 20wt%) showed a predominant presence of particulate morphology over the veil sample, which showed an even presence of phase-inverted morphology.
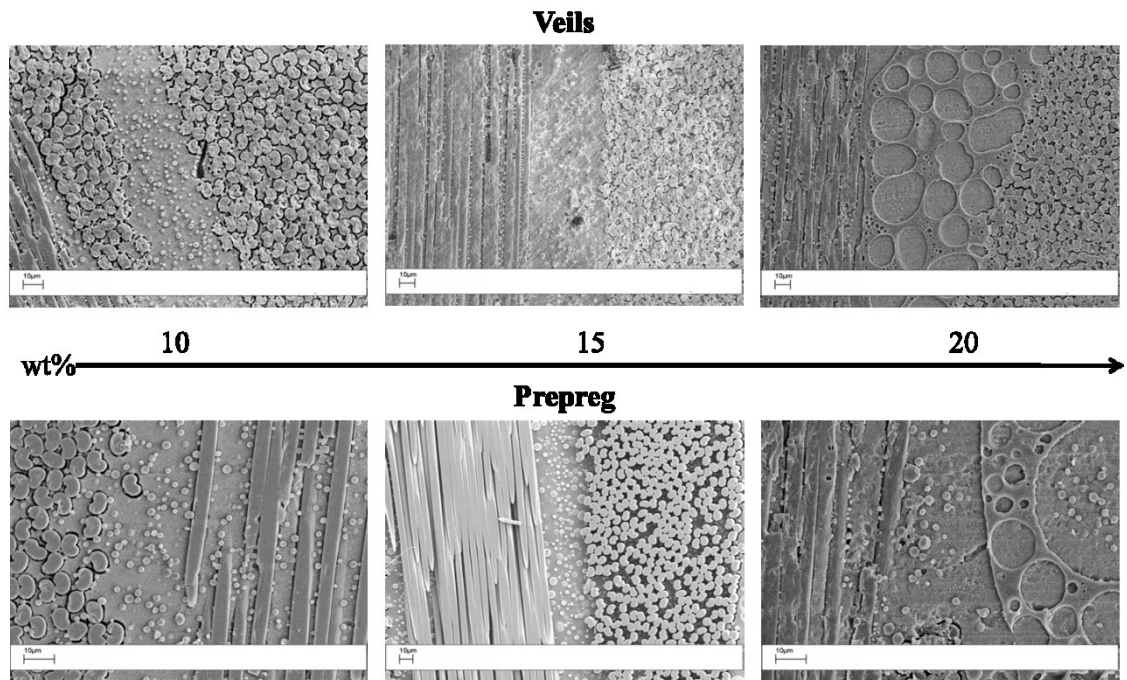
Figure 6:58 Interlaminar regions of coPES9k modified laminates (prepreg down, veil up) for different coPES9k contents

Figure 6:59 reports a SEM analysis for fractured veil samples with 10wt% of coPES9k. These pictures confirm the presence of particulate morphology both in the interlaminar region and between the carbon fibers. These results suggest the complete dissolution of the veil with a diffusion of the dissolved thermoplastic across the laminate during curing.
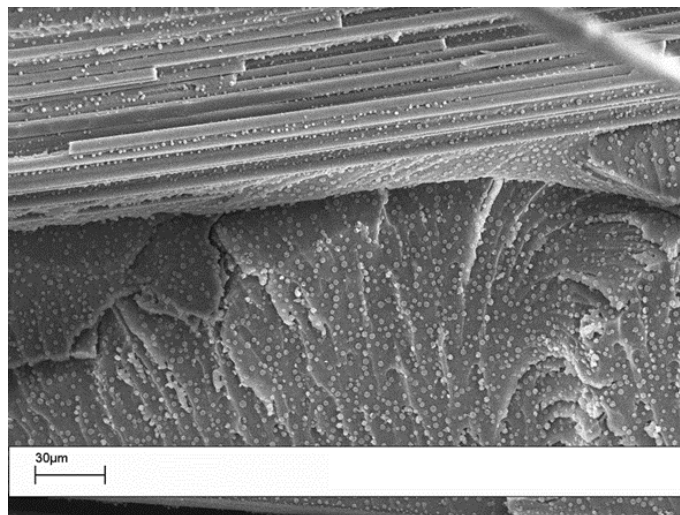

Figure 6:59 SEM images of fractured surfaces obtained from 10%wt coPES9k veil modified laminates

To further assess the thermoplastic diffusion, a sample with the veil placed in the middle layers only was prepared (figure 6:60a). SEM analysis of the laminate thickness showed the presence of particulate morphology both in the middle and external layers of the laminate (figure 6:60b). However, the thermoplastic-rich particle density was lower for the external layers than for the middle layers. This finding can be explained by the filtering effect of the carbon fibers, which limited the complete diffusion of the polymer from the central veil to the external layers of the laminates.
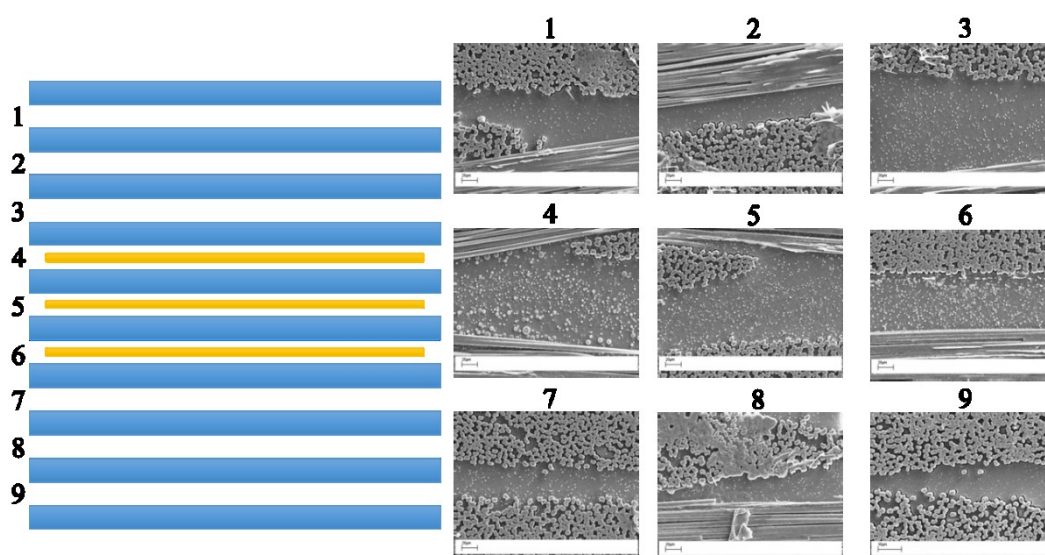
Figure 6:60 a) Scheme of the laminate with veils (green) placed in the middle layers only and b) SEM images of the interlaminar region in different positions for the laminate a)

Figures 6:61a and 6:61b show the DMA results for samples cut from prepreg and veil laminates. Figure 6:62 summarizes the Tg of the epoxy-rich domains for the samples analyzed in figure 6:61. The samples with a thermoplastic content up to 15wt% showed similar two-peak behavior. The samples at 20wt% differed showing two overlapping peaks for the prepreg and one broad peak for the veil sample. These differences, with an increase in the thermoplastic concentration, are summarized in figure 6:48 where the Tgs for the epoxy-rich domains are compared. These differences were the results of the dissimilar diffusion path for the prepreg and the veil samples which was highlighted by the experiment described in figure 6:60. Interestingly, the veil sample with 20wt% of coPES9k showed a peak shift of 13°C

compared to the prepreg. This shift was due to the different phase morphology. The veil sample presented a predominant phase inversion, which led to the complete overlap of the thermoplastic-rich and epoxy-rich relaxation peak, resulting in one broad peak centered at 178°C. The prepreg sample (at 20wt%) showed two peaks at 165°C and one broad shoulder between 170 and 180°C. This behavior was the result of the complex coexistence of two morphologies.
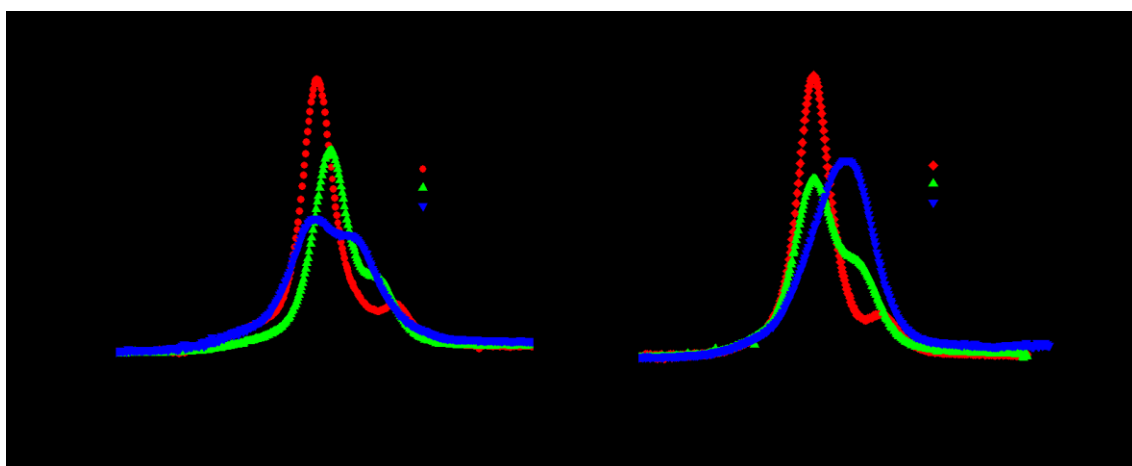

Figure 6:61 DMA curves for laminates with different coPES9k content: a) prepreg route, b) veil route
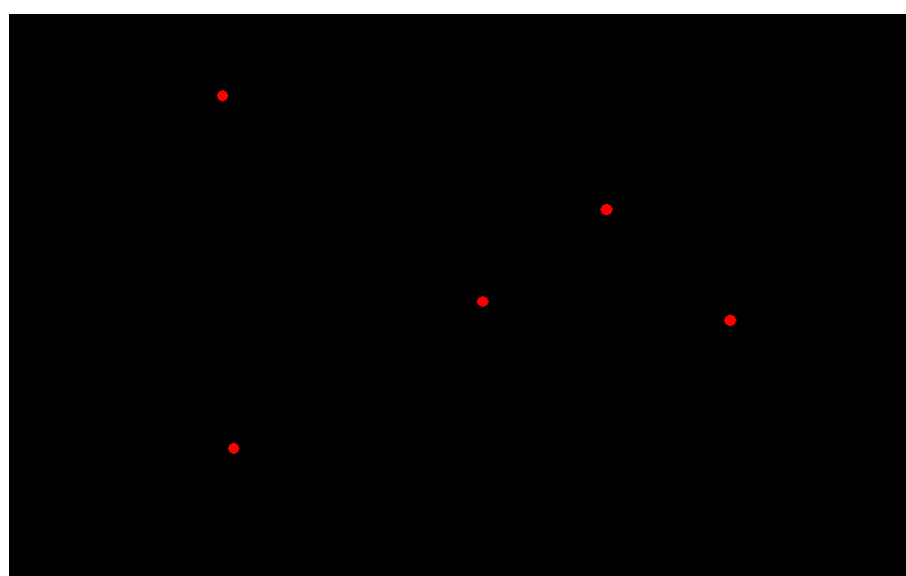
Figure 6:62 Comparison of Tgs for veil and prepreg laminate systems

141

A detailed explanation of the contribution of each morphology to the relaxation behavior would require micro-thermal characterization, which is beyond the scope of the present project.

Laminates with coPES20k veils were prepared and analyzed even if their prepared neat resin samples showed the presence of undissolved fibers. Figure 6:63 reports the SEM for the 10wt% sample. The microscopic analysis showed no undissolved fiber across the specimen thanks to the improved wetting of the veils in the laminate construction compared to neat resin. However, even if the thermoplastic content was 10wt%, clear phase-inverted domains were observed in the interlaminar regions. This behavior was a consequence of the low diffusion of the coPES20k, which resulted in a higher local concentration of dissolved thermoplastic polymer. This in turn resulted in phase inversion rather than particulate morphology for the coPES9k veil.
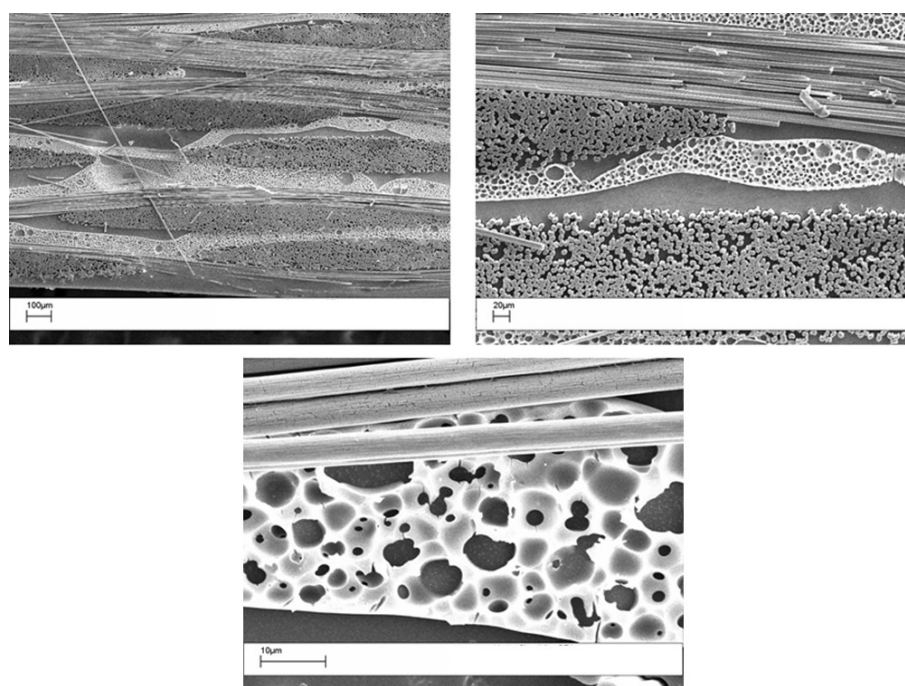

Figure 6:63 SEM images of laminate modified with 10wt% coPES20k at different magnifications

For comparison purposes, laminates with 5wt% of coPES20k veil were prepared. Figure 6:64 shows the SEM analysis of this sample. At this low coPES20k percentage the veils likewise dissolved, mainly forming phase-inverted domains.
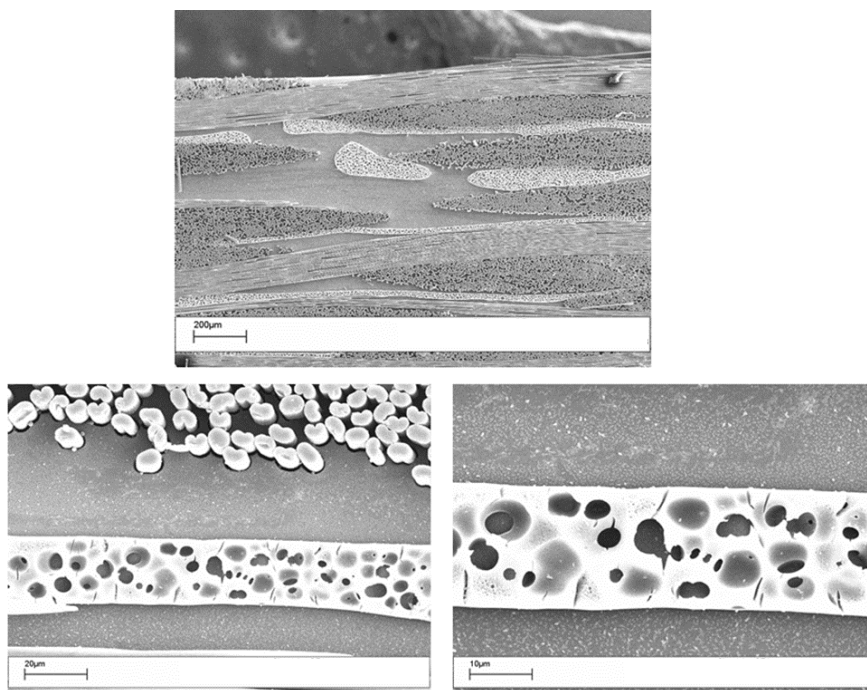

Figure 6:64 SEM images of laminate modified with 5wt% coPES20k at different magnifications

Laminates modified with Solvay's Virantage® PESs were manufactured following the scale-up process. Figure 6:65 shows the comparison of the Tan δ curves of Vir10200 and Vir30500 at 10wt%. Both of them show increases of Tg with respect to the unmodified system: +6°C for Vir 30500, +9°C for Vir10200, due to its higher molecular weight. It has to be noted that for Vir30500 there seems not to be phase separation. SEM analysis was carried out in order to better study these systems. Figure 6:66a show a phase-inverted morphology for the sample with 10wt% of veils of Vir10200, due to its higher molecular weight that confirms a behavior similar to the coPES20k. Vir30500 showed a very fine particulate morphology (figure 6:66b), with dimensions of the particle less than 1 μm. This can justify the apparent single peak tan δ curve.
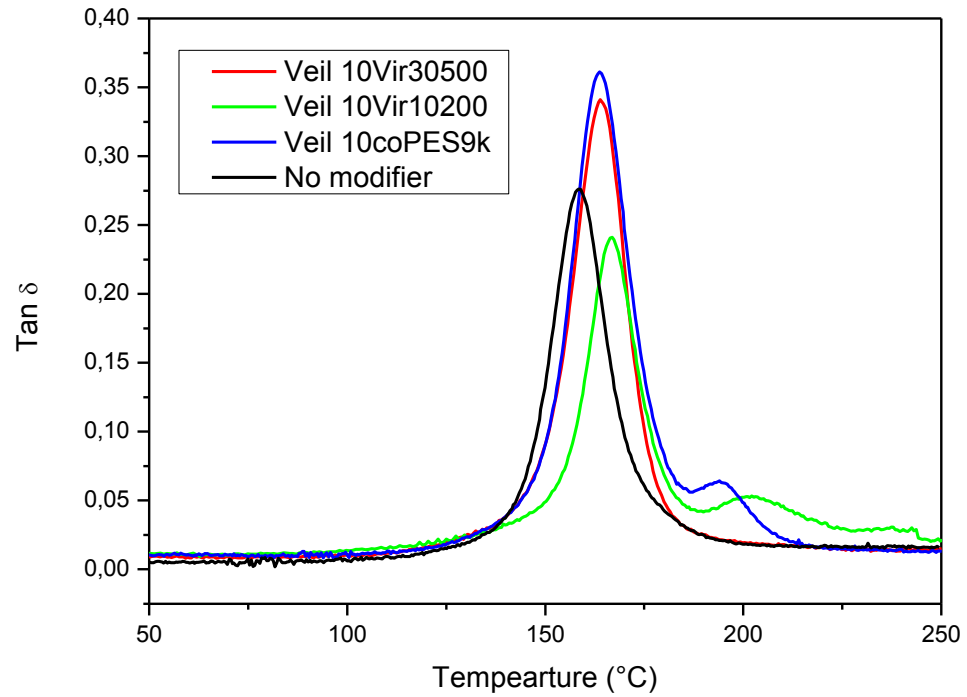
Figure 6:65 Comparison of Tan δ curves for four cured DGEBA composite laminates: Veil 10Vir30500, Veil 10Vir10200prepreg, Veil 10coPES9k and no-modifier.
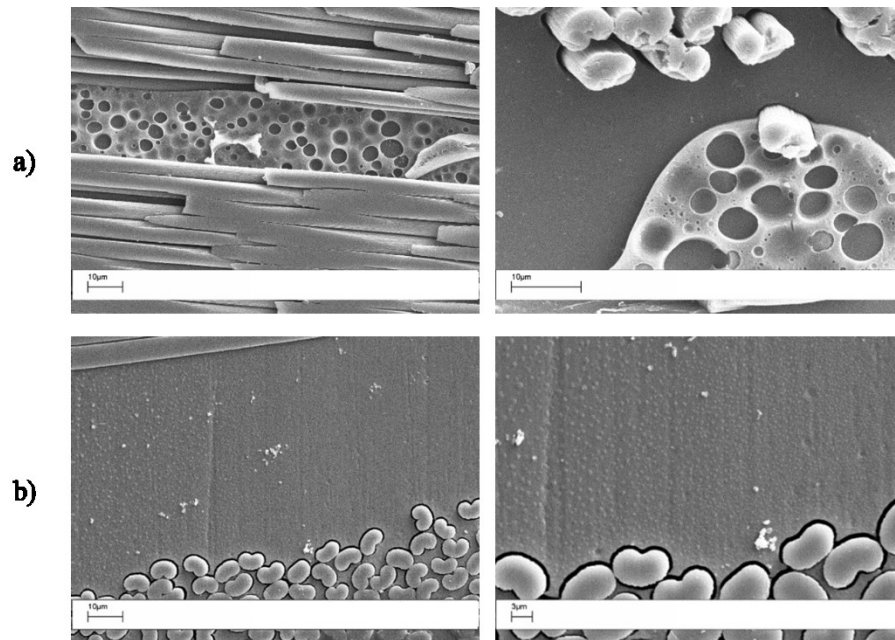

Figure 6:66 SEM images of interlaminar regions of laminates modified with 10wt% of (a) Veil 10Vir10200 and (b)Veil 10Vir30500

Figure 6:67 shows the mode I failure curves of the samples in the DCB testing. Data are reported in table 6:8. All of the systems showed instable crack propagations, with increased

values of fracture toughness G_{ic} for the veil-modified samples with respect to the unmodified laminate, by +47,96% and +39,09% respectively for Vir10200 and Vir30500. These results are very promising since at the same level of what is reported in literature. Magniez et al [10] used phenoxy electrospun veil as toughening agents obtaining same results, but it must be said that the use of a low-Tg polymer like phenoxy leads to overall decreases in Tgs of epoxies. On the contrary, PESs does not thanks to their high Tg values.
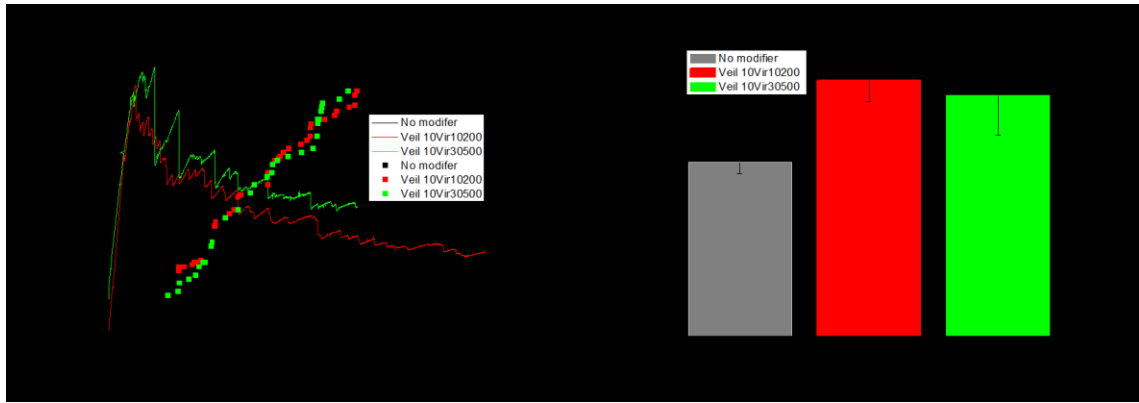

Figure 6:67 DCB results of mode I failures for veil-modified Vir10200 and Vir30500 samples

Table 6:8 DCB data of mode I failures for veil-modified Vir10200 and Vir30500 samples

Sample	Max Load/Width [N/mm]	S_{n-1} [N/mm]	%Δ	Max G_{ic} [J/m^2]	S_{n-1} [J/m^2]	%Δ
No modifier	1,79	0,10		544,70	35,27	
Veil 10Vir10200	2,82	0,15	+57,54% -6,93%	805,96	67,12	+47,96% +6,38%
Veil 10Vir30500	3,03	0,57	+69,27% +7,45%	757,65	125,74	+39,09% -5,99%

By comparing two amounts of Vir30500 veils (figure 6:68), it can be seen that the single-peak behavior appears again also for the system modified with 20wt% of polymer veils. At this modification percentage, there is a slight increase of +2°C compared to the 10wt% sample

and +7°C compare to the unmodified sample. From SEM analysis (figure 6:69), very fine particles rich of Vir30500 were found again in the morphology for the 20wt% sample
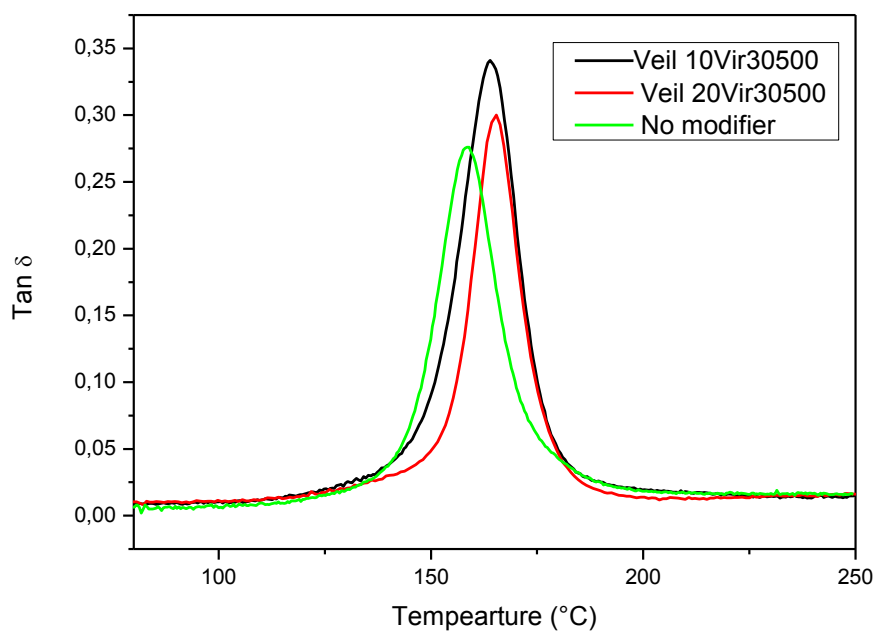

Figure 6:68 Comparison of Tan δ curves for four cured DGEBA composite laminates: Veil 10Vir30500, Veil 20Vir30500prepreg and no-modifier
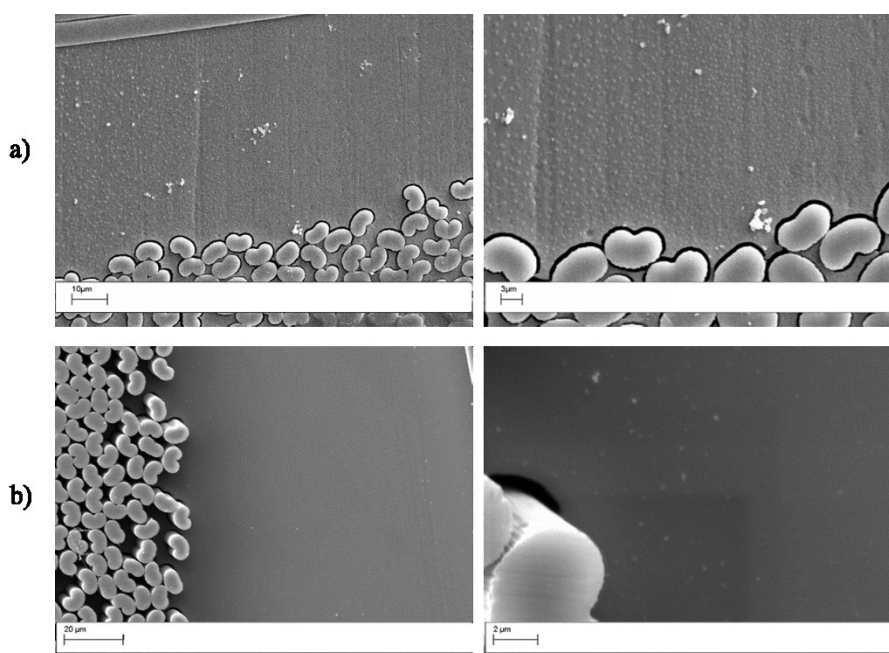

Figure 6:69 SEM images of interlaminar regions of laminates modified with Vir30500 veil: (a) 10wt% and (b) 20wt%

Figure 6:70 shows the mode I failure curves of the samples in the DCB testing. Data are reported in table 6:9. Both systems showed again instable crack propagations, with increased values of fracture toughness G_{ic} with respect to the unmodified laminate, +39,09% and +15,39%respectively for 10 and 20wt%.
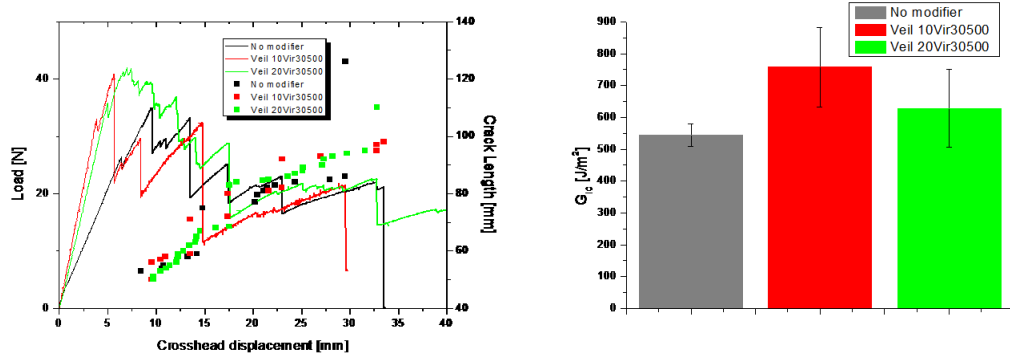

Figure 6:70 DCB results of mode I failures for veil-modified Vir30500 at 10 and 20wt%

Table 6:9 DCB data of mode I failures for veil-modified Vir30500 at 10 and 20wt%

Sample	Max Load/Width [N/mm]	S_{n-1} [N/mm]	%Δ	Max G_{ic} [J/m^2]	S_{n-1} [J/m^2]	%Δ
No modifier	1,79	0,10		544,70	35,27	
Veil 10Vir30500	3,03	0,57	+69,27% +35,27%	757,65	125,74	+39,09% +20,55%
Veil 20Vir30500	2,24	0,16	+25,14% -26,07%	628,51	122,70	+15,39% -17,04%

A comparison for the Vir30500 PES was carried out by using the two epoxy resins: DGEBA and TGAP. Table 6:10 puts on evidence the better thermal properties of TGAP resin thanks to its larger cross-link density with respect to the difunctional epoxy DGEBA. SEM analysis showed similar very fine particulate morphology for both of them (figure 6:71). On the

contrary, the larger cross-link density of the epoxy TGAP led to lower fracture toughness values: DGEBA resin performed +55,60% better (figure 6:72 and table 6:11).

Table 6:10 DMA data for 10wt% Vir30500 veils in DGEBA and TGAP

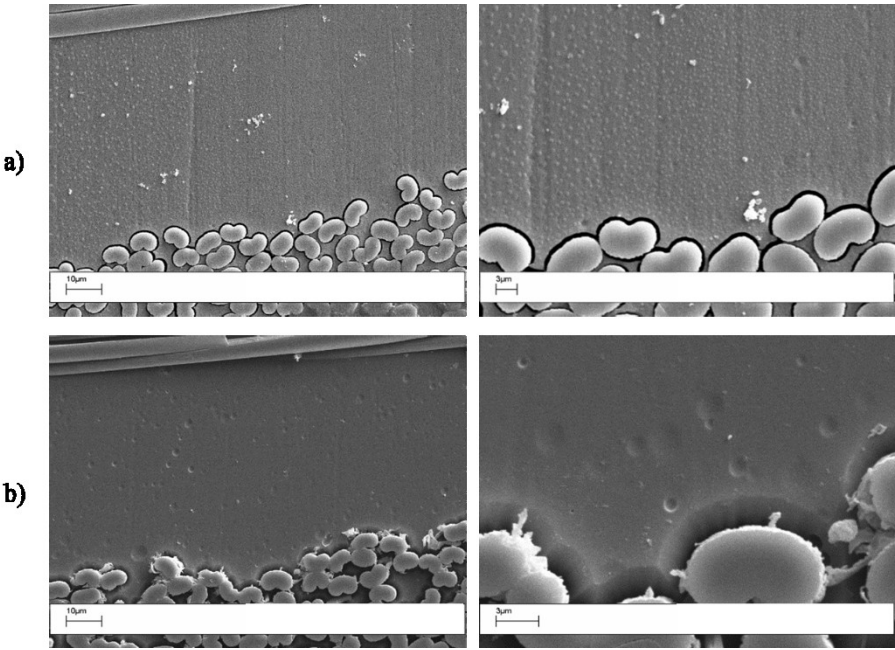| Sample	T_g Epoxy [°C]	%Δ
Veil 10Vir30500 DGEBA	164	-17,17%
Veil 10Vir30500 TGAP	198	+20,73%

Figure 6:71 SEM images of interlaminar regions of DGEBA (a) and TGAP (b) laminates modified with 10wt% of Vir30500
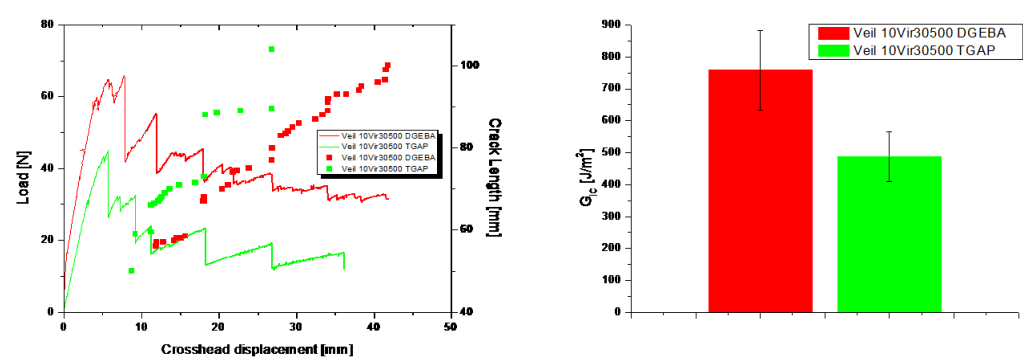

Figure 6:72 DCB results of mode I failures for DGEBA and TGAP laminates modified with 10wt% of Vir30500

Table 6:11 DCB results of mode I failures for DGEBA and TGAP laminates modified with 10wt% of Vir30500

Sample	Max Load/Width [N/mm]	S_{n-1} [N/mm]	%Δ	Max G_{ic} [J/m^2]	S_{n-1} [J/m^2]	%Δ
DGEBA-MDEA-10NANOVIR30500	3,03	0,57	+56,99%	757,65	125,74	+55,60%
TGAP-MDEA-10NANOVIR30500	1,93	0,16	-36,30%	486,93	77,13	-35,73%

Other trials with non-soluble electrospun veils were performed. Samples were prepared by placing one ply of veil in the mid-plane of the composite laminate. The systems used are commercially available from Revolution Fibers. The ones used were AP1500 and AP4500. In addition, carbon nanofibers were used as non-soluble veils as well. SEM analysis showed the undissolved nanofibers between the interlaminar region of the mid-plane (6:73).

a)   b)
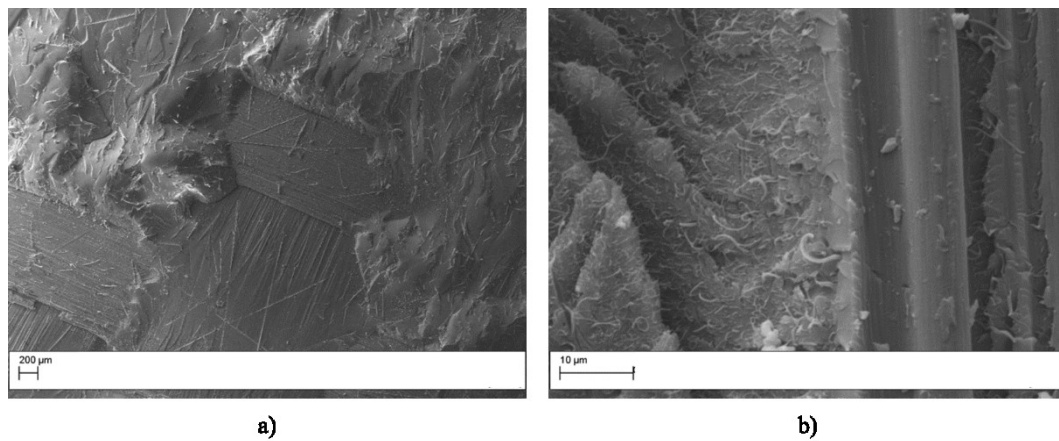
Figure 6:73 SEM images of fractured composite laminates with carbon nanofibers (a) and Revolution Fibers AP1500 (b)

DCB testing showed very high increases in fracture toughness values of G_{ic} for the non-soluble veils by Revolution Fibers up to +78,40%, as shown in figure 6:74 and table 6:12. This result for non-soluble veil is in accordance compared to what is reported in literature by

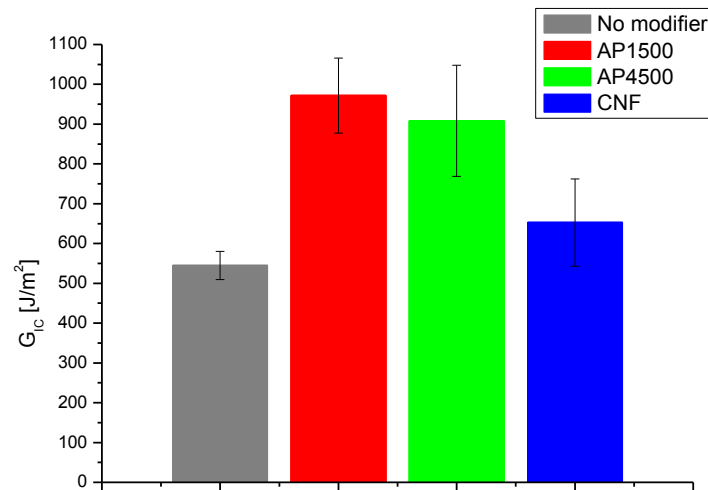Harmer at al. [11]. Carbon nanofibers did not perform so well with respect to Revolution Fibers' veils.

Figure 6:74 DCB results of mode I failures for composite laminates toughened by AP4500, AP1500, CNF

Table 6:12 DCB data of mode I failures for composite laminates toughened by AP4500, AP1500, CNF

Sample	Max Load/Width [N/mm]	S_{n-1} [N/mm]	%Δ	Max G_{ic} [J/m^2]	S_{n-1} [J/m^2]	%Δ
No modifier	1,79	0,10		544,70	35,27	
AP1500	1,80	0,16	0,56%	971,73	94,13	+78,40%
AP4500	1,83	0,16	+2,23%	908,58	139,61	+66,80%
CNF	2,14	0,06	+19,55%	652,78	109,55	+19,84%

Nanofilled composite laminates

Nanofilled composite laminates were manufactured by using MWCNTs and POSS particles.

Figure 6:75 reports the Tan δ curves for samples modified with 1wt% of MWCNTs and POSS

150

with respect to the thermoplastic content. A strange behavior was brought in by MWCNTs, since the sample showed a broad peak. This is a consequence of MWCNTs' interaction with both the epoxy-rich phase and the coPES-rich phase, activating the glass transition at an earlier stage. A narrower peak was observed for the POSS-filled veils. On the contrary of the neat resin results, the Tg was lowered by -11°C, this may come from a bad distribution of the particle, like for MWCNTs, in the matrix. Figure 6:76 reports the elastic moduli curves. It can be seen that there is a drop-off of the elastic modulus for the phase-separated coPES9k cured sample with respect to the unmodified one. E' is recovered when coPES9k veils are filled with nanoparticles.

SEM images are reported in figure 6:77 and 6:78 for MWCNT- and POSS-filled samples. MWCNTs tend to stay in the thermoplastic-rich phase, even though there is also some evidence in the epoxy phase. As for POSS, cubic agglomerates are evident in some points of the epoxy-rich phase. Furthermore, it is clear how the interactions of POSS particle with both thermoplastic and epoxy modify the final morphology from particulate to a more complex one, which is particulate plus phase inversion.
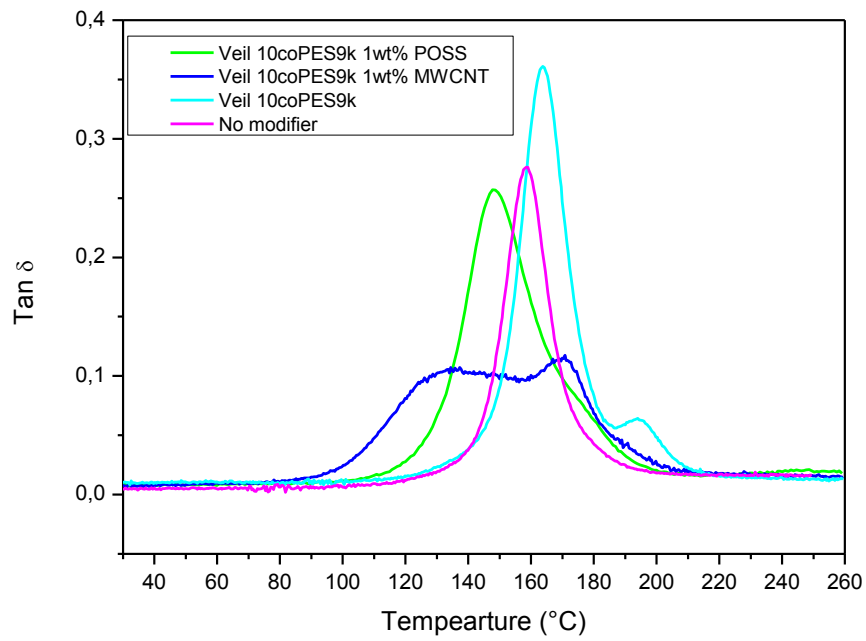
Figure 6:75 Comparison of Tan δ curves for cured DGEBA veil-modified composite laminates: 10wt%coPES9k +1wt%MWCNT, 10wt%coPES9k +1wt%POSS, 10wt%coPES9k no modifier
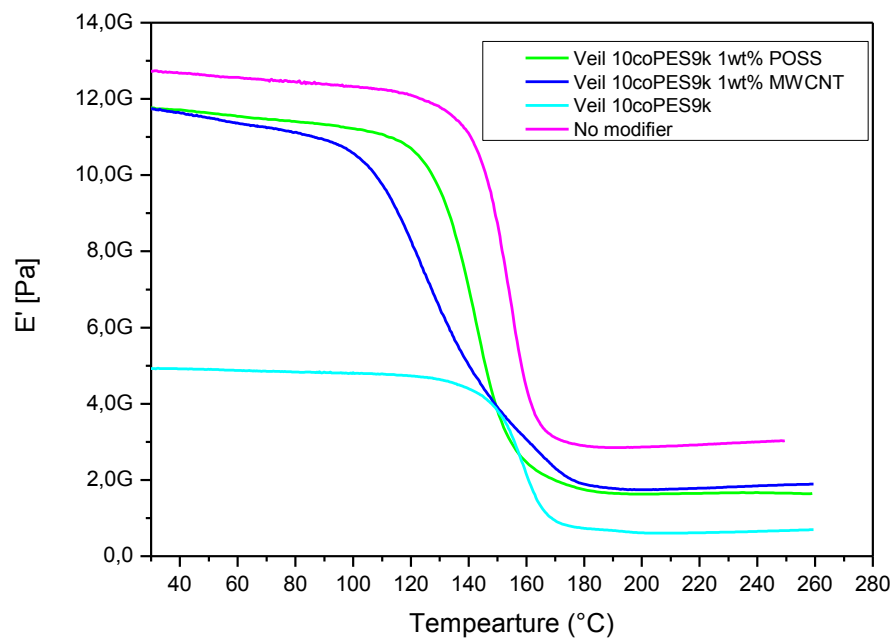

Figure 6:76 Comparison of elastic moduli curves for cured DGEBA veil-modified composite laminates: 10wt%coPES9k +1wt%MWCNT, 10wt%coPES9k +1wt%POSS, 10wt%coPES9k no modifier
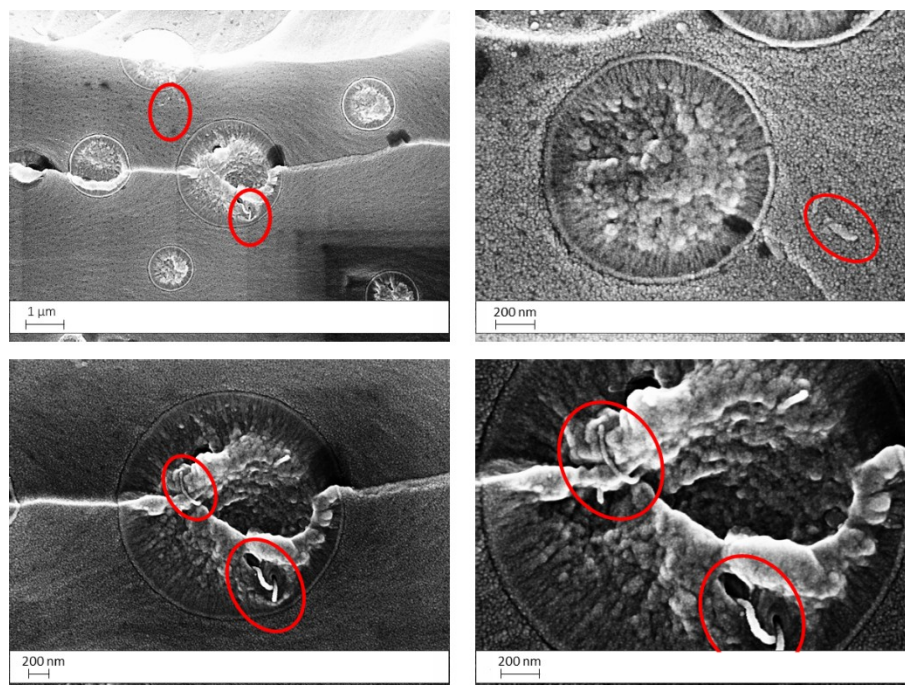
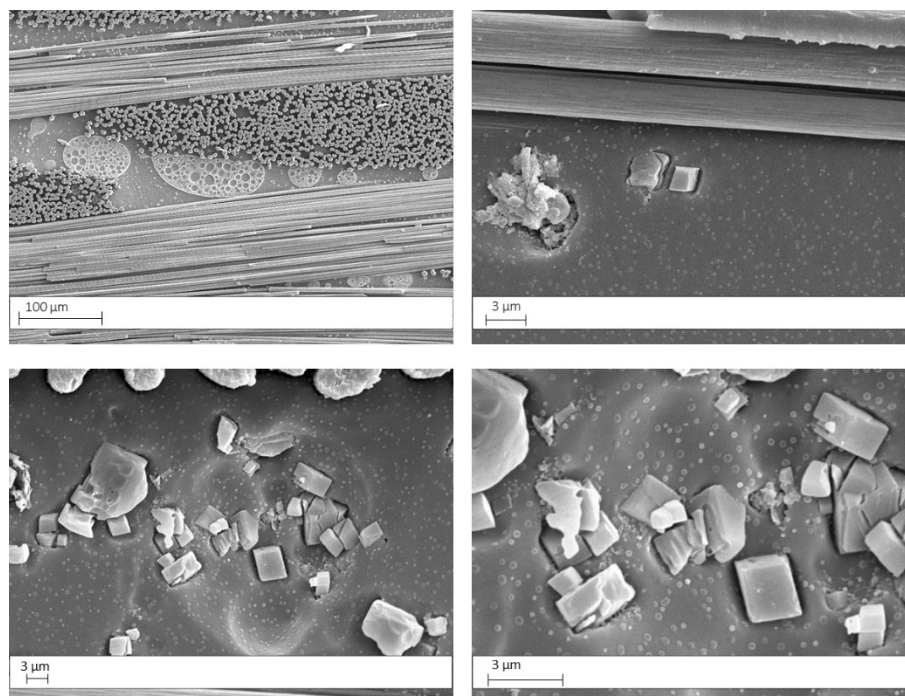**Figure 6:77** SEM images of 1wt% MWCNT-filled sample

Figure 6:78 SEM images of 1wt% POSS-filled sample

A composite laminate was prepared by following the scheme reported in figure 6:79 with the compound OpteSTAT PES/MWCNT provided by OVATION Polymers. The idea was to put

153

a large excess of thermoplastic/MWCNT on one surface in order to achieve phase separation and percolation for carbon nanotubes. This was confirmed by SEM analysis reported in figure 6:80.

It is evident the phase inversion that occurred in the outer surface due to the large excess of polymer with respect to the resin. In this way, percolation of CNTs was achived, as shown by the greater SEM magnification where it is possible to observe most of CNTs in the thermoplastic-rich phase and a few in the epoxy-rich phase as well. This CNT-percolated morphology was wanted in order to ensure an improved electrical conductivity on the outer surfaces of the composite laminate.

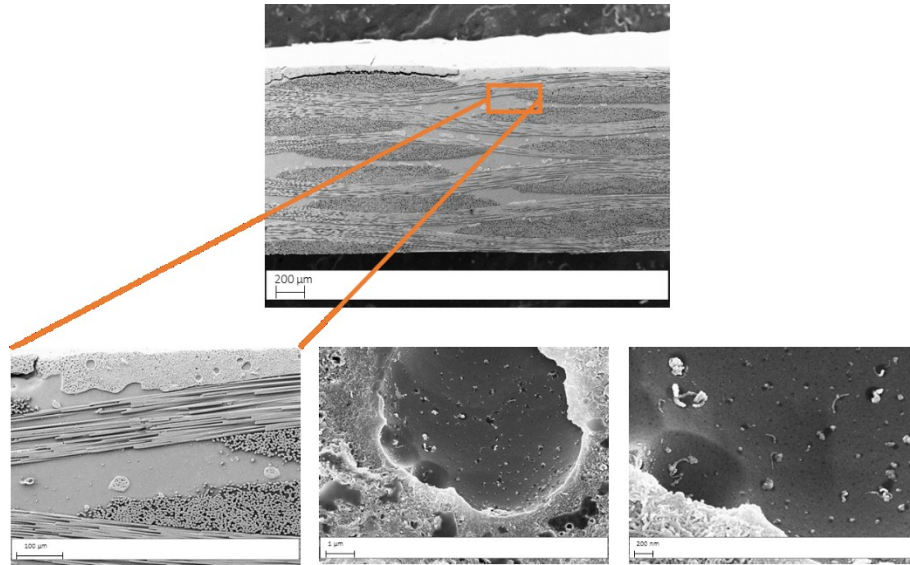**Figure 6:79** Schematics of the composite laminate prepared with OPTEStat elctrospun nanofibers

Figure 6:80 SEM images of OPTEStat-veil modified composite laminate reproducing the sheme shown in figure 6:66. MWCNTs coming out from the epoxy-rich phase and percolation in the thermoplastic-rich phase are evident

6.5 Chapter 6 References

[1] C. Puglisi, F. Samperi, G. Cicala, A. Recca, C.L. Restuccia, *Combined MALDI–TOF MS and NMR characterization of copoly(arylen ether sulphone)s,* Polymer Elsevier, (**2006**).

[2] Blanco, L. Abate, F. A. Bottino, P. Bottino and M. A. Chiacchio, J. Therm. Anal. Calorim. 107, 1083-1091 (2012)

[3] Narain, *Chemistry of Bioconjugates Synthesis, Characterization, and Biomedical Applications,* John Wiley & Sons Inc, Hoboken, New Jersey, 2014, pp. 348-351

[4] B. Alvarado-Tenorio, A. Romo-Uribe and P. T. Mather, *Macromolecules* **44**, 5682–5692 (2011)

[5] Blanco I., Cicala G., Motta O., Recca A., Influence of a selected hardener on the phase separation in epoxy/thermoplastic polymer blends, Journal of Applied Polymer Science,**94**, 361 (2004).

[6] O'Brien, T. K., and Martin, R. H., Journal of Composites Technology and Research, Vol 15, No. 4, Winter 1993 (also in NASA TM 104222, 1992).

[7] Overbeke E. van, Devaux J., Legras R., Carter J.T., McGrail P.T., Carlier V, Phase separation in epoxy-copolyethersulphone blends: morphologies and local characterisation by micro-Raman spectroscopy, Polymer, **44**, 4899 (2003).

[8] Rico M., López J., Montero B., Bouza R., Díez F. J., Influence of the molecular weight of a modifier on the phase separation in an epoxy thermoset modified with a thermoplastic, European Polymer Journal, **58**, 125 (2014).

[9] Naffakh M., Dumon M., Gerard J.F., Study of a reactive epoxy–amine resin enabling in situ dissolution of thermoplastic films during resin transfer moulding for toughening composites, Composites Science and Technologies, **66**, 1376, (2006)

[10] Magniez K., Chaffraix T., Fox B., Materials, 2011, **4**, 1967-1984

[11] Hamer S., Leibovich H., Green A., Avrahami R., Zussman E., Siegmann A., Sherman D.,Composites Science and Technology, 90 (2014) 48–56

7.Conclusions and Recommendations for Future Work

The choice of coPESs as thermoplastic polymers to electrospin turned out to work well. The electrospinning process did not show any difficulties in particular boh for the neat coPES and the nanoparticle-filled ones. MWCNT were more difficult to disperse with respect to SiO_2 and POSS particle because of MWCNTs tendency to stay agglomerated.

The molar mass of the coPES showed a significant effect on the dissolution behavior of the veils studied. Larger masses led to longer dissolution time s. The addition of nanofiller increased dissolution times as well. Their presence inside electrospun nanofibers was confirmed by SME, EDX and TEM analysis.

coPES9k veils were fully dissolved in epoxy resins, resulting in a homogenous morphology. In contrast, increasing the coPES molar mass from 9k to 20k resulted in traces of undissolved fibers for neat resin samples. Veil dissolution for coPES20k appeared better for carbon fiber reinforced samples but phase-inverted domains were observed due to a lower diffusion of the coPES20k even at a low modifier content (5wt% of coPES20k).

Veil route versus prepreg route was also analyzed. This comparison outlined only irrelevant differences in morphology and dynamic mechanical properties for DGEBA neat resins modified with coPES9k. On the contrary, differences were observed for TGAP neat resins, where morphologies turned from co-continuous to very fine particulate. The addition of nanofillers affected positively the Tgs of neat resins and also the elastic moduli for nanofilled-coPES9k veils.

A higher Tgs difference for samples prepared with coPES9k veil and their prepreg counterpart were observed for carbon-reinforced samples. The filtering effect of carbon fibers, which altered the diffusion path of coPES9k, explained these differences. The diffusion of coPES9k across the laminate thickness was qualitatively assessed by placing coPES9k in middle layers only.

Commercial PESs by Solveay, Virantage® 30500 and Virantage® 10200 were able to be electrospun in the same conditions of coPES9k and 20k. Vir30500 acted similar to coPES9k, Vir10200 acted similar to coPES20k. they both were totally dissolved in the epoxies, neat resins and composite laminates., increasing the Tg of the epoxy-rich phase. DCB tests confirmed the their ability to toughen the interlaminar regions, leading to higher fracture toughness values of G_{ic} with respect to the unmodified resin. DGEBA resin performed better compared to TGAP resin in terms of fracture toughness. Trials with composite laminated toughened by non-soluble electrospun veil confirmed very high value of fracture toughen G_{ic}, as reported in literature.

The results presented are relevant for the correct design of electrospun veils for the toughening of epoxy resin composites.

Recommendations for future work are:

- better dispersion of nanoparticles in polymer solutions thus increasing the mass fraction in the elctrospun veil, in order to achieve higher percentages in the finale epoxy matrix

- to explore the comparison between prepreg and veil routes with blends of more epoxies together

- to evaluate the functionalities given by the presence of nanoparticles to the final composite laminate

- to optimize the hybrid-fabrics concept for very fast processing techniques such as High Pressure Resin Transfer Molding, allowing to manufacture toughened systems not only for the aerospace sector but also for the automotive field where larger production volumes are required.

"Confidence allows you to progress in something you're attempting to accomplish, whether it's playing basketball or baseball, or whether it's trying to succeed in business"

Michael J. Jordan